The ACS Fornax Cluster Survey: The Nuclei of Early-Type Galaxies

by

Monica Turner
B.Sc., McGill University, 2009

A Thesis Submitted in Partial Fulfillment of the
Requirements for the Degree of

MASTER OF SCIENCE

in the Department of Physics & Astronomy

The ACS Fornax Cluster Survey: The Nuclei of Early-Type Galaxies

by

Monica Turner
B.Sc., McGill University, 2009

Supervisory Committee

Dr. Patrick Côté, Supervisor
(Department of Physics & Astronomy, University of Victoria)

Dr. Jon Willis, Departmental Member
(Department of Physics & Astronomy, University of Victoria)

Supervisory Committee

Dr. Patrick Côté, Supervisor
(Department of Physics & Astronomy, University of Victoria)

Dr. Jon Willis, Departmental Member
(Department of Physics & Astronomy, University of Victoria)

ABSTRACT

The Advanced Camera for Surveys (ACS) Fornax Cluster Survey is a *Hubble Space Telescope* programme that imaged 43 early-type galaxies in the Fornax cluster, using the ACS F475W ($\approx g$) and F850LP ($\approx z$) bandpasses. We use this data set, which spans a range of ~ 600 in blue luminosity down to $M_B \sim -16$, to study and characterize the properties of central galactic nuclei by fitting ellipses to the galaxy isophotes and examining their 1-dimensional surface brightness profiles. To test the robustness of this method, we perform a similar analysis with 2-dimensional surface brightness profile fitting using GALFIT, and find acceptable agreement between the derived structural parameters from the two techniques. We determine 72% of our sample (31 galaxies) to be nucleated, a significant increase from 28% found in the ground-based study of Ferguson et al. (1989). This high frequency of nucleation suggests that the creation of a compact nuclear component is a common outcome in early-type galaxy formation. Only three of the nuclei (10%) are observed to be significantly offset (by $\gtrsim 0\farcs5$) from their host galaxy photocentres, and a trend of increasing offset in fainter galaxies is observed, which indicates that nucleus formation timescales and/or pathways may vary with host luminosity. The nuclei are found to be larger and approximately $50\times$ brighter than typical globular clusters from our Fornax sample, and to follow different half-light surface brightness versus magnitude scaling relations. The colours of the nuclei are characteristic of intermediate to old stellar populations, and those residing in galaxies with $B_T \gtrsim 13$ are observed to correlate with the nucleus luminosities. Both nucleus and galaxy colours become redder with increasing host luminosity, although the trend with the nuclei is steeper, and the

nuclei in the brightest galaxies are found to be redder than their hosts. However, the majority of nuclei are bluer than their hosts, having an average colour difference of 0.27 ± 0.25 mag. Comparison of our results to the complementary ACS Virgo Cluster Survey (ACSVCS) study of nuclei (Côté et al., 2006), which examined 100 early-type galaxies in the Virgo cluster, yields strikingly similar results. Both samples show similar frequency of nucleation (68% in the ACSVCS), a constant nucleus-to-galaxy luminosity ratio (with a mean value of $\langle \eta \rangle = 0.41\% \pm 0.04\%$ derived from the combined samples), as well as excellent agreement in the nucleus luminosity functions and sizes (with median values of 6 pc in g and 7 pc in z in both studies). Since the Fornax cluster presents a much denser environment than Virgo, such consistency between the properties of the nuclei indicates that their formation and evolution may be influenced by local factors more than environmental ones. In particular, a constant η suggests that a host galaxy's luminosity (or, more likely, mass) may be a key element in determining the properties of its nucleus. Since simulations have found the two main theorized nucleus formation pathways to be effective on different mass scales (with dissipationless infall of star clusters being more efficient in lower-mass galaxies, and in-situ gas accretion in higher-mass hosts), we propose that both processes may both in fact be responsible for nucleus formation, but varying in relative importance along the galaxy luminosity function.

Contents

List of Tables

List of Figures

ACKNOWLEDGEMENTS

I would like to thank Pat Côté for providing funding, support, and many hours of help. I would also like to acknowledge Chien Peng, Laura Ferrarese, Andrés Jordán, Lisa Glass, Kaushi Bandara, Hannah Broekhoven-Fiene, and Albert Santoni, for their valuable help and discussions.

Finally, thanks to everyone who drove me up and down Observatory Hill, particularly Andy Pon, and also Pat Côté, Chien Peng, Kaushi Bandara, Lisa Glass, Alex Parker, Ben Hendricks, James DiFrancesco, Stephen Gwynn, and Matt Penrice.

DEDICATION

To my Děda and Babička.

Chapter 1

Introduction

With current cosmological models favouring hierarchical clustering as the formation mechanism for early-type galaxies (e.g., White & Rees, 1978; Searle & Zinn, 1978; White & Frenk, 1991; Kauffmann & Haehnelt, 2000; Cole et al., 2000; Springel et al., 2005; Bower et al., 2006), these historically straightforward objects are believed to be more complex than previously thought. A key feature of early-type galaxies is that they appear to have formed the majority of their stars at high redshift ($z > 1$) and on short timescales (< 1Gyr) (e.g., Bower et al., 1992; Franx, 1993; Thomas et al., 1999; Trager et al., 2000; Wake et al., 2006). This effect can be attributed to feedback from active galactic nuclei (AGN), which produce the jets and outflows necessary to blow away gas and subsequently suppress star formation (e.g., Silk & Rees, 1998; King, 2003; Murray et al., 2005; Fabian et al., 2006; Robertson et al., 2006). The discovery of the $\mathcal{M}_{\rm BH} - \sigma$ relation (Ferrarese & Merritt, 2000; Gebhardt et al., 2000) points to a fundamental connection between the central black hole powering these AGN, and the dynamical properties of the host galaxy. Indeed, there are several other properties of galaxies that have been found to scale with black hole mass, including luminosity (e.g., Kormendy & Richstone, 1995; Ferrarese & Merritt, 2000), light concentration (e.g., Graham et al., 2001), global velocity dispersion (e.g., Ferrarese & Merritt, 2000; Gebhardt et al., 2000; Gültekin et al., 2009), bulge mass (e.g., Magorrian et al., 1998; Marconi & Hunt, 2003; Häring & Rix, 2004), and total gravitational mass of the host (Bandara et al., 2009). Thus, it has become clear that an understanding of black holes and AGNs is essential if we are to gain insight into galaxy formation and evolution.

However, black hole formation remains highly uncertain, with proposed mechanisms ranging from the collapse of either Population III stars, dense protogalactic cores, or star clusters, to primordial black hole remnants from the Big Bang (Djor-

govski et al., 2008). Recently, the relationship between the virial mass of a host galaxy and the mass of its central black hole was proposed to extend down to central nuclear star clusters found in lower-luminosity galaxies (Ferrarese et al., 2006a; Wehner & Harris, 2006). Similar scaling relations between a galaxy's black hole or nucleus and the host bulge luminosity, mass, and Sérsic index have also been found (Rossa et al., 2006; Balcells et al., 2007; Graham & Driver, 2007), implying a global relationship between galaxies and their central massive objects (CMOs) of both types. Moreover, some intermediate luminosity galaxies (Filippenko & Ho, 2003; González Delgado et al., 2008; Seth et al., 2008; Graham & Spitler, 2009) as well as dwarfs (Barth et al., 2004; Reines et al., 2011) were found to contain both a central stellar nucleus and a black hole. This connection has lead to proposals of galaxy evolution models involving both types of CMO; for example, models in which the nuclei are black hole progenitors (Devecchi et al., 2010), where competitive feedback with both objects shapes the fate of the host galaxy (Nayakshin et al., 2009), or where merging galaxies dynamically heat the clusters such that they can be tidally destroyed (Bekki & Graham, 2010). The study of nuclei is therefore integral to our understanding of how galaxies evolve.

Although dwarf galaxies have long been known to contain nuclei, complete studies of galaxy clusters in which the frequency of this phenomenon within a population could be robustly quantified did not appear until Binggeli et al. (1987) published the Virgo Cluster Catalogue (VCC). This program observed 1277 members and 574 probable members of the Virgo cluster using the 2.5 m Las Campanas telescope; about 25% of all dwarf galaxies in the VCC sample were found to be nucleated. Shortly thereafter, a similar survey of the Fornax galaxy cluster by Ferguson (1989), which constitutes the Fornax Cluster Catalogue (FCC), found 30% of galaxies to contain nuclei. However, due to both the faintness and compact nature of these nuclei, the inferred frequency of nucleation from these studies is likely limited by the shallow depth and moderate spatial resolution of ground-based surveys.

Lotz et al. (2004) then used the WFPC2 to observe 69 dwarf elliptical galaxies in both Virgo and Fornax, and found 6 additional nuclei in galaxies which were previously classified as non-nucleated in the VCC and FCC. Renewed scrutiny of early-type galaxies with high-resolution instruments was further motivated by subsequent studies of late-type galaxies that often found a frequency of nucleation of $\approx 70\%$ (e.g., Carollo et al., 1998; Matthews et al., 1999; Böker et al., 2004; Walcher et al., 2005; Seth et al., 2006).

The first study to find a similar frequency of nucleation of early-type galaxies in Virgo was conducted by Côté et al. (2006, hereafter C06) with the Advanced Camera for Surveys (ACS) onboard the Hubble Space Telescope, known as the ACS Virgo Cluster Survey (ACSVCS). In addition to finding a high frequency of nucleation for early-type galaxies (at least 66% for galaxies brighter than $M_B \approx -15$), the high resolution images of the survey have offered new insight into the properties of the nuclei themselves, such as their luminosity function, structural properties, colour-magnitude relation, and nucleus-to-galaxy luminosity ratio. The study presented in this dissertation, which is part of the ACS Fornax Cluster Survey (ACSFCS), examines the properties of nuclei belonging to galaxies in the Fornax Cluster, at a distance of $D = 20 \pm 0.3 \pm 1.4$ Mpc (Blakeslee et al., 2009, hereafter Paper V). This cluster is smaller, denser, more dynamically evolved, and more regular in shape than the Virgo cluster, and therefore allows us to study the properties of the nuclei of galaxies residing in a considerably different environment.

Other papers in the ACSFCS series have described the data reduction procedures used in the survey (Jordán et al., 2007, hereafter Paper I), the scaling relations of the central regions of galaxies (Côté et al., 2007, hereafter Paper II), the logarithmic slope of the galaxy central surface brightness profiles (Glass et al., 2011, hereafter Paper IV), and the use of surface brightness fluctuations as a distance indicator (Paper V). Papers studying the properties of globular clusters (GCs) in ACSFCS galaxies have examined their half-light radii (Masters et al., 2010, hereafter Paper VII), luminosity function (Villegas et al., 2010, hereafter Paper VIII), colour-magnitude relation (Mieske et al., 2010, hereafter Paper IX), and colour gradients (Liu et al., 2011, hereafter Paper X).

The outline of this dissertation is as follows: in Chapter 2 we describe the observations and the analysis that allows us to extract the nucleus structural parameters; in Chapter 3 we examine the nucleus properties, such as frequency of nucleation, luminosity function, size, brightness, and colour; in Chapter 4 we put our results into the context of current formation scenarios; and in Chapter 5 we summarize the main results.

Chapter 2

Observations and Analysis

The ACSFCS sample was constructed by selecting galaxies from the FCC using a faint-end cutoff of $B_T \leq 15.5$ and choosing morphological types E, S0, SB0, dE, dE,N and dS0,N, as classified by Ferguson (1989). These classifications were based on the system of Sandage & Binggeli (1984): dwarfs were distinguished from giants by their relatively low surface brightness and flat surface brightness profiles; S0s were identified through evidence of a disk, either from visual inspection of the image or the presence of an exponential component in the surface brightness profile; and nucleation was defined as the existence of a point source near a galaxy's photocentre. In addition to 42 FCC galaxies, two ellipticals that lie just beyond the FCC survey region (NGC 1340 and IC 2006) were added, giving a total of 44 proposed programme galaxies. For all galaxies in this sample, membership in the cluster is confirmed through previously available radial velocity measurements. Unfortunately, due to a shutter failure during execution, no images were obtained for FCC 161 (NGC 1379). Our final sample therefore consists of 43 early-type galaxies, which is complete (apart from FCC 161) down to a limiting magnitude of $B \approx 15.5$ mag ($M_B \approx -16.0$ mag). A more detailed description of the Fornax sample selection can be found in Paper I. In this thesis, we will often refer to the sample of galaxies and nuclei from the ACSVCS, which is comprised of 100 early-type members of the Virgo Cluster; by contrast, the ACSVCS is magnitude-limited down to $B \approx 12$ mag ($M_B \approx -19$ mag) and 44% complete down to its limiting magnitude of $B \approx 16$ mag ($M_B \approx -15$ mag). Both the Fornax and Virgo objects were observed with the ACS using Wide Field Channel (WFC) mode with the F475W and F850LP filters, which correspond closely to the g- and z-band filters in the Sloan Digital Sky Survey (SDSS) system (see, e.g., Fukugita et al., 1996; York et al., 2000; Sirianni et al., 2005).

Basic data for the ACSFCS galaxies and their nuclei are presented in Table 2.1. Each galaxy's identification number, FCC number from Ferguson (1989), and alternate name are reported in columns 1, 2, and 3, respectively. The table is ordered by increasing FCC blue magnitude (i.e., decreasing luminosity), B_T, which is given in column 4. In calculating absolute magnitudes, we used the individual surface brightness fluctuation (SBF) distances measured in Paper V. Beginning in Chapter 3, all reported magnitude are extinction corrected, using dust maps from Schlegel et al. (1998), with the ratios of total-to-selective absorption in the WFC filters taken from Sirianni et al. (2005); the adopted B-band extinctions are shown in column 5. The galaxy g- and z- band surface brightness at $1''$ geometric mean radius are given in columns 6 and 7.

The remaining parameters in Table 2.1, which are derived from our surface-brightness profile analysis, will be discussed in § 2.3. Additional information about our program galaxies, such as coordinates and morphological classifications, can be found in Paper I.

Table 2.1. Basic Data for Nuclei of Program Galaxies

ID	FCC	Other	B_T (mag)	A_B (mag)	$\mu_g(1'')$ (mag/$\Box''$)	$\mu_z(1'')$ (mag/$\Box''$)	Class (FCC)	Class (ACS)	$g_{\rm AB}$ (mag)	$z_{\rm AB}$ (mag)	$(g-z)_{\rm AB}$ (mag)	$(g-z)^a_{\rm AB}$ (mag)	$r_{h,g}$ ($''$)	$r_{h,z}$ ($''$)	$\log M$ ($M_\odot$)
(1)	(2)	(3)	(4)	(5)	(6)	(7)	(8)	(9)	(10)	(11)	(12)	(13)	(14)	(15)	(16)
1..	21	N1316	9.06	0.090	15.61	14.12	N	cS	...	...	...	...	...	...	...
2..	213	N1399	10.04	0.056	16.78	15.17	N	cS	...	...	...	...	...	...	...
3..	219	N1404	10.96	0.049	16.45	14.88	N	cS	...	...	...	...	...	...	...
4..	1340	E418-G005	11.23	0.077	17.00	15.56	N	cS	...	...	...	...	...	...	...
5..	167	N1380	10.84	0.075	16.88	15.32	N	S1	...	...	...	...	...	...	...
6..	276	N1427	11.79	0.048	17.07	15.59	N	S1	...	...	...	...	...	...	...
7..	147	N1374	11.95	0.060	17.14	15.58	N	S1	...	...	...	...	...	...	...
8..	2006	E359-G007	12.59	0.048	17.72	16.18	N	S2	18.17	16.35	1.82	1.66	0.132	0.139	8.245
10.	83	N1351	12.33	0.061	17.35	15.83	N	S1	...	...	...	...	...	...	...
9..	184	N1387	11.77	0.055	16.70	15.05	N	S1	...	...	...	...	...	...	...
11.	63	N1339	12.77	0.057	17.13	15.56	N	S2	15.22	13.53	1.70	1.49	0.889	0.927	9.298
12.	193	N1389	12.59	0.046	17.34	15.88	N	S2	17.97	16.54	1.43	1.41	0.100	0.097	8.129
14.	170	N1381	12.91	0.058	17.12	15.62	N	S2	19.06	18.29	0.77	0.64	0.153	0.153	7.166
13.	153	I1963	13.55	0.062	18.32	16.91	N	S2	17.26	15.82	1.45	1.43	0.228	0.207	8.454
15.	177	N1380A	13.60	0.063	18.83	17.58	N	S2	17.76	16.95	0.82	0.84	0.130	0.099	7.736
16.	47	N1336	13.34	0.049	18.50	17.11	N	S2	16.09	14.86	1.24	1.33	0.750	0.612	8.651
19.	43	I1919	13.82	0.062	19.99	18.83	Y	S2	19.67	18.64	1.03	0.96	0.129	0.121	7.108
17.	190	N1380B	13.79	0.074	19.32	17.89	N	S2	18.64	17.29	1.35	1.37	0.359	0.328	7.763
18.	310	N1460	13.68	0.047	19.32	17.96	N	S2	21.57	20.05	1.52	0.88	0.039	0.127	6.498
21.	249	N1419	13.61	0.056	17.68	16.25	N	S2	16.38	15.69	0.70	0.70	0.270	0.233	8.191
20.	148	N1375	13.39	0.063	18.20	17.02	N	S2	20.08	19.22	0.85	0.99	0.038	0.018	6.988
22.	255	E358-G50	13.99	0.025	19.50	18.26	Y	S2	20.22	19.14	1.08	0.95	0.028	0.023	6.891
23.	277	N1428	14.01	0.044	18.84	17.45	N	S2	20.08	18.75	1.33	1.32	0.089	0.082	7.195
24.	55	E358-G06	14.23	0.043	19.68	18.41	Y	S2	20.16	18.98	1.18	1.05	0.064	0.057	7.025
25.	152	E358-G25	14.13	0.044	20.44	19.25	N	S1	...	...	...	...	...	...	...
26.	301	E358-G59	14.22	0.039	18.61	17.31	N	S2	20.32	19.29	1.03	0.87	0.016	0.015	6.792
27.	335	E359-G02	14.90	0.063	20.40	19.27	N	S2	19.95	18.81	1.14	1.19	0.094	0.066	7.079
28.	143	N1373	14.19	0.061	18.39	16.96	N	S1	...	...	...	...	...	...	...
29.	95	G87	15.01	0.064	20.16	18.83	N	S2	21.25	20.10	1.15	1.12	0.035	0.013	6.550
30.	136	G99	15.00	0.069	20.73	19.39	Y	S2	20.38	19.31	1.07	0.95	0.055	0.042	6.778
31.	182	G79	15.01	0.057	19.61	18.18	N	S2	22.15	21.62	0.53	0.38	0.038	0.038	5.695
32.	204	E358-G43	15.33	0.045	20.50	19.23	Y	S2	20.00	18.86	1.13	1.00	0.092	0.093	7.064
33.	119	G26	15.44	0.060	21.35	20.10	N	S1[a]	20.20	19.56	0.63	0.58	0.025	0.030	6.620
35.	90	G118	15.10	0.052	19.55	18.76	N	S2	21.28	20.31	0.97	0.84	0.073	0.066	6.368
34.	26	E357-G25	15.26	0.067	19.80	19.39	N	S1	...	...	...	...	...	...	...
36.	106	G47	15.34	0.046	19.89	18.62	Y	S2	20.69	19.54	1.15	1.08	0.042	0.036	6.768
37.	19	E301-G08	15.81	0.085	21.56	20.49	Y	S2	20.86	20.02	0.85	0.78	0.042	0.032	6.500
38.	202	N1396	15.50	0.057	20.71	19.41	Y	S2	20.57	19.64	0.94	0.88	0.053	0.047	6.674
39.	324	E358-G66	15.83	0.042	22.16	21.01	N	S2	22.92	22.13	0.79	0.70	0.040	0.028	5.620

2.1 Parameterization of Surface Brightness Profiles

Since stellar nuclei, which are the focus of this study, are obviously found in the luminous central regions of their host galaxies, accurately modelling the underlying galaxy surface brightness is necessary to measure their photometric and structural parameters. Indeed, for the faintest nuclei, or for some nuclei embedded in high surface brightness galaxies with steeply rising brightness profiles, this can be important for even identifying the central stellar component (Côté et al., 2006). Using the IRAF task `ellipse`, which is based on the algorithm of Jedrzejewski (1987), elliptical isophotes with logarithmically increasing fixed semi-major axis length were fitted to the galaxies. In most cases, all ellipse parameters (centre, ellipticity, and position angle) were allowed to vary throughout the fit. However, to achieve convergence, the galaxies with large amounts of central dust required the ellipse centres to be held fixed throughout the fit (FCC 335, FCC 119, FCC 90), as well as the position angles and ellipticities while fitting the innermost areas (FCC 119 and FCC 90), where the fixed parameter values were determined by ellipse fits to the outer regions ($R_e \gtrsim 5''$). For more details on the fitting procedures, see § 3.2 of (Ferrarese et al., 2006b). The results from the `ellipse` isophote analysis were used to derive azimuthally-averaged radial surface brightness profiles, which were then fitted using one of three different parameterizations for the global surface brightness profile.

The first parameterization is the well known Sérsic profile (Sersic, 1968), a three parameter model which has the form

$$I_{\rm S}(R) = I_e \exp\left\{ b_n \left[\left(\frac{R}{R_e} \right)^{1/n} - 1 \right] \right\}, \tag{2.1}$$

where I_e is the intensity at the effective radius, R_e; the constant b_n is defined such that $\Gamma(2n) = 2\gamma(2n, b_n)$, where Γ and γ are the complete and incomplete gamma functions, respectively (Ciotti, 1991); and the Sérsic index n characterizes the shape of the light profile. For lower values of n, the Sérsic profile is shallow in the inner regions and steep in the outer regions; $n = 1$ produces a pure exponential profile, which generally provides a reasonable fit to the brightness profiles of dwarf galaxies. Conversely, higher values of n give profiles with similar inner and outer slopes; these generally fit the profiles of bright ellipticals quite well (i.e., $n = 4$ reduces to a

Table 2.1 (continued)

ID	FCC	Other	B_T (mag)	A_B (mag)	$\mu_g(1'')$ (mag/$\square''$)	$\mu_z(1'')$ (mag/$\square''$)	Class (FCC)	Class (ACS)	$g_{\rm AB}$ (mag)	$z_{\rm AB}$ (mag)	$(g-z)_{\rm AB}$ (mag)	$(g-z)^a_{\rm AB}$ (mag)	$r_{h,g}$ ($''$)	$r_{h,z}$ ($''$)	$\log M$ ($M_\odot$)
(1)	(2)	(3)	(4)	(5)	(6)	(7)	(8)	(9)	(10)	(11)	(12)	(13)	(14)	(15)	(16)
40.	288	E358-G56	15.82	0.025	21.03	19.85	Y	S2	21.32	20.41	0.91	0.82	0.081	0.075	6.414
42.	203	E358-G42	15.82	0.051	21.50	20.28	Y	S2	21.01	20.10	0.91	0.75	0.072	0.071	6.471
43.	303	NG47	15.74	0.046	21.63	20.49	Y	S2	21.78	20.92	0.86	0.78	0.051	0.040	6.156
41.	100	G86	15.75	0.062	22.18	21.08	Y	S2	19.72	18.77	0.96	0.83	0.079	0.078	6.973

Column key:
(1) Identification number;
(2) Fornax Cluster Catalog (FCC) number (Ferguson, 1989));
(3) Alternative names in the NGC, ESO or IC catalogs;
(4) Total blue magnitude from ACSFCS;
(5) A_B from Schlegel et al. (1998);
(6)-(7) g- and z-band surface brightness measured at a geometric radius of $1''$;
(8) Nuclear classification in FCC;
(9) Nuclear classification in ACSFCS (S1=Sérsic, cS=core-Sérsic, S2=double-Sérsic);
(10)-(11) g- and z-band magnitudes for nucleus;
(12) Integrated colour of nucleus;
(13) Nucleus colour within a 4-pixel aperture;
(14-15) Double-Sérsic model half-light radius in the g- and z-bands;
(16) Nucleus mass using mass-to-light ratios from Bell et al. (2003).

[a]Due to the offset of the nucleus and the amount of central dust, the nucleus parameters for FCC 119 were derived using a King profile fit to the ACS image.

classical de Vaucouleurs profile). Historically, these two types of profiles have been used to separately parameterize dwarfs and giants. However, more complete studies of galaxies have found that n actually varies steadily with galaxy luminosity (e.g., Graham & Guzmán, 2003; Gavazzi et al., 2005; Ferrarese et al., 2006b). In what follows, we will refer to these single component parameterizations as S1 models.

Although the Sérsic profile describes the outer surface brightness component of galaxies remarkably well — a consequence of the wide range in range of concentration, spatial extent, and global surface brightness available by varying n, R_e and I_e, respectively — there can be variations in the *central* structure that cannot be accounted for in this simple model (see, e.g., Figure 1 of Côté et al. (2007)). Specifically, the brightest ellipticals tend to show a *luminosity deficit* in their central regions; for these objects, the six-parameter Core-Sérsic model (Graham et al., 2003) provides a good description of their surface brightness profiles. The core-Sérsic model, referred to hereafter as cS, can be written as

$$I_{\rm cS}(R) = I' \left[I + \left(\frac{R_b}{R} \right)^{\alpha} \right]^{\gamma/\alpha} \exp \left[-b_n \left(\frac{R^{\alpha} + R_b^{\alpha}}{R_b^{\alpha}} \right)^{1/\alpha n} \right], \tag{2.2}$$

where

$$I' = I_b 2^{-\gamma/\alpha} \exp \left[b_n \left(2^{1/\alpha} R_b / R_e \right)^{1/n} \right]. \tag{2.3}$$

This parameterization consists of the usual Sérsic profile in the outer region, with effective radius R_e and Sérsic index n, going inwards until the "break" radius R_b is reached (at which point the intensity is I_b). At R_b, the profile transitions to the core component according to the "sharpness" parameter α (where smaller values translate to smoother transitions), yielding an inner slope of γ.

Meanwhile, most of the less-luminous galaxies in our sample show evidence for a *luminosity excess* in their cores which is, by definition, the signature of a central nucleus (see Appendix A of Côté et al., 2006). The central excess in the surface brightness profile can be modelled by adding a second Sérsic component. This double-Sérsic profile (which we denote hereafter as an S2 profile) has the form

$$\begin{aligned} I_{\rm S2}(R) = & I_{e,1} \exp \left\{ b_{n,1} \left[\left(\frac{R}{R_{e,1}} \right)^{1/n_1} - 1 \right] \right\} \\ & + I_{e,2} \exp \left\{ b_{n,2} \left[\left(\frac{R}{R_{e,2}} \right)^{1/n_2} - 1 \right] \right\} \end{aligned} \tag{2.4}$$

where the enumerated subscripts indicate the Sérsic parameters for the outer and inner components.

It should be noted that in C06, double-Sérsic profiles were not used to fit the nucleated galaxies. Instead, the central nuclei were modelled by King profiles (Michie, 1963; King, 1966), while the outer component was represented by either a core-Sérsic or Sérsic profile. Our decision to use a double-Sérsic parameterization in the ACSFCS analysis is motivated by two considerations. Firstly, modelling the inner component with the Sérsic profiles allows for a large diversity of possible physical systems, due to the range of the Sérsic parameter (see above). For $n \sim 1$, the profile is a pure exponential and is suitable for embedded disks, whereas $n \sim 2$ parameterizes Galactic GCs quite well, and presumably, nuclear star clusters. Secondly, the use of Sérsic profile for both the inner and outer components allows for comparisons of their respective structural properties.

2.2 Fitting Procedure

As described in Paper I, the ACSFCS uses the *Lanczos3* kernel for drizzling rather than the *Gaussian* kernel which was used for the ACSVCS. Due to the slightly larger distance of the Fornax cluster – 20.0 vs. 16.5 Mpc (Mei et al., 2007, Paper V) – and the fact that some of the Virgo nuclei were only marginally resolved in the ACSVCS (C06, Ferrarese et al., 2006b,a), the sharper point-spread function (PSF) possible with the *Lanczos3* kernel was determined to be more important for the ACSFCS than the *Gaussian* kernel's ability to repair bad pixels.

New PSFs for the ACSFCS were constructed using $\gtrsim 1000$ stars from the GO-10048 and GO-10375 programme photometric calibration observations of the Galactic GC 47 Tucanae. Using multiple observations allowed the the derived PSFs to be extracted from data that was acquired no more than two months away from the ACSFCS observation times – this proved to be important since on 2004 December 20, the secondary mirror on the HST was moved by 4.6 μm.

After running KINGPHOT (Jordán et al., 2005) on the GC candidates identified in the ACSFCS images,[1] it was found that the mean half-light radius for some GC candidates in the ACSFCS was significantly larger in the g-band than in the z-band: i.e., roughly 0.5 pixels in F475W, which is much larger than the differences of $\lesssim 0.1$

[1]KINGPHOT fits two-dimensional, PSF-convolved King models to candidate GCs in the ACS images.

pixels found in the ACSVCS. Anderson & King (2006) discovered the WFC PSF exhibited unpredictable variations on orbital timescales, particularly in the bluer filters, with differences in flux values of up to $\sim 10\%$ in central regions. To correct the seven galaxies whose imaging suffered from this variabillity (FCC 213, IC 2006, FCC 193, FCC 249, FCC 277, FCC 19, and FCC 202), stellar objects from the individual images were used to empirically adjust the 47 Tucanae derived PSFs. Complete details on this procedure are given in Paper I.

Azimuthally averaged one-dimensional surface brightness profiles were fitted using a χ^2 minimization scheme to determine the use of either a Sérsic or core-Sérsic model. If visual inspection of the images or surface brightness profiles revealed the presence of a nucleus, then the S2 profile was used. All models used were convolved with the PSF before fitting. As in Byun et al. (1996), each point along the profile was weighted equally, since the low signal-to-noise ratio of the outer regions is offset by the fact that there are more points along these isophotes.

All profile parameters, save for intensity, were first fit to both bandpasses simultaneously. These preliminary values were then used as initial guesses for the independent fits for most of the galaxies, with the exception of those with high central surface brightness that appear to be nucleated. In these galaxies, the nuclei are quite extended, and difficult to differentiate from the underlying galaxy light; thus, only the intensity parameters were allowed to vary between the two bands.

A conservative resolution limit of $0\farcs025$ was deduced in C06, by using half light radii of King models fit to stars classified as unresolved by KINGPHOT, as well as using the size of the central non-thermal point source found in VCC 1316, which is only resolved in one of the two bands. C06 also showed that most of the detected nuclei were more extended than point sources, by fitting point source profiles in a addition to King profiles, and comparing the residuals.

2.3 Identification and Classification of the Nuclei

The classification of a galaxy as nucleated or non-nucleated in the ACSFCS was performed in the following way. The programme galaxies were all fitted with pure Sérsic profiles outside of a geometric mean radius of $0\farcs5$. The geometric mean radius was derived from the fitted elliptical isophotes, and is thus defined as $R \equiv a(1-\epsilon)^{1/2}$, where a is the semi-major axis, and ϵ is the ellipticity. If an inward extrapolation of this profile revealed an excess of light in the centre, then the full profile was refitted

by adding a second Sérsic component, and the galaxy was thus considered nucleated and classified as S2. The significance of the nucleation was generally greater in the g-band, as the nuclei are often found to be slightly bluer than their host.

One of our programme galaxies, FCC 119, appears to have a distinct nucleus offset from its photocentre by $\sim 0\farcs7$. However, due to large amounts of dust in the central regions, the ellipse centres were held fixed to the photocentre throughout the fit, and the nucleus is not apparent in the 1D surface brightness profile. We therefore use parameters derived from a KINGPHOT fit to this object, and consider it to be nucleated for the remainder of this analysis.

Galaxy classifications as nucleated or non-nucleated in the FCC, and our revised classification, are given in columns 8 and 9 of Table 2.1 We also present the g- and z-band integrated nucleus magnitudes (columns 10 and 11), integrated and 4-pixel aperture nucleus colours (columns 12 and 13), g- and z-band nucleus half-light radii (columns 14 and 15), and nucleus masses derived using mass-to-light ratios from Bell et al. (2003) (column 16). Although the measured half-light radii in a handful of the nuclei were found to be significantly larger in the g-band than in the z-band (i.e. FCC 310, FCC 177, FCC 95), we note that these nuclei are not present in the galaxies that suffered from the variable PSF (discussed in § 2.2); rather, the size difference is caused by the tendency for nuclei to be bluer than their host galaxy. On average, we obtain only a $0\farcs018 \pm 0\farcs028$ difference in measured nucleus sizes between the two bands.

F475W images of the central $10'' \times 10''$ region of the program galaxies, where a distinct nuclear component is often discernible, are shown in Figure 2.1. The FCC number of the galaxy is labelled in each of the panels, along with the type of profile fitted; S2 therefore indicates that the galaxy was considered to be nucleated (that is, fitted with a double-Sérsic profile). Individual fits to the azimuthally averaged F475 surface brightness profiles are shown in Figure 2.2.

2.4 Comparison with 2-Dimensional Surface Brightness Profile Fitting

Up to now, we have discussed the procedures for measuring photometric and structural parameters for the nuclei by using one-dimensional (1D) fitting of the azimuthally averaged brightness profiles. In this section, we examine our choice of

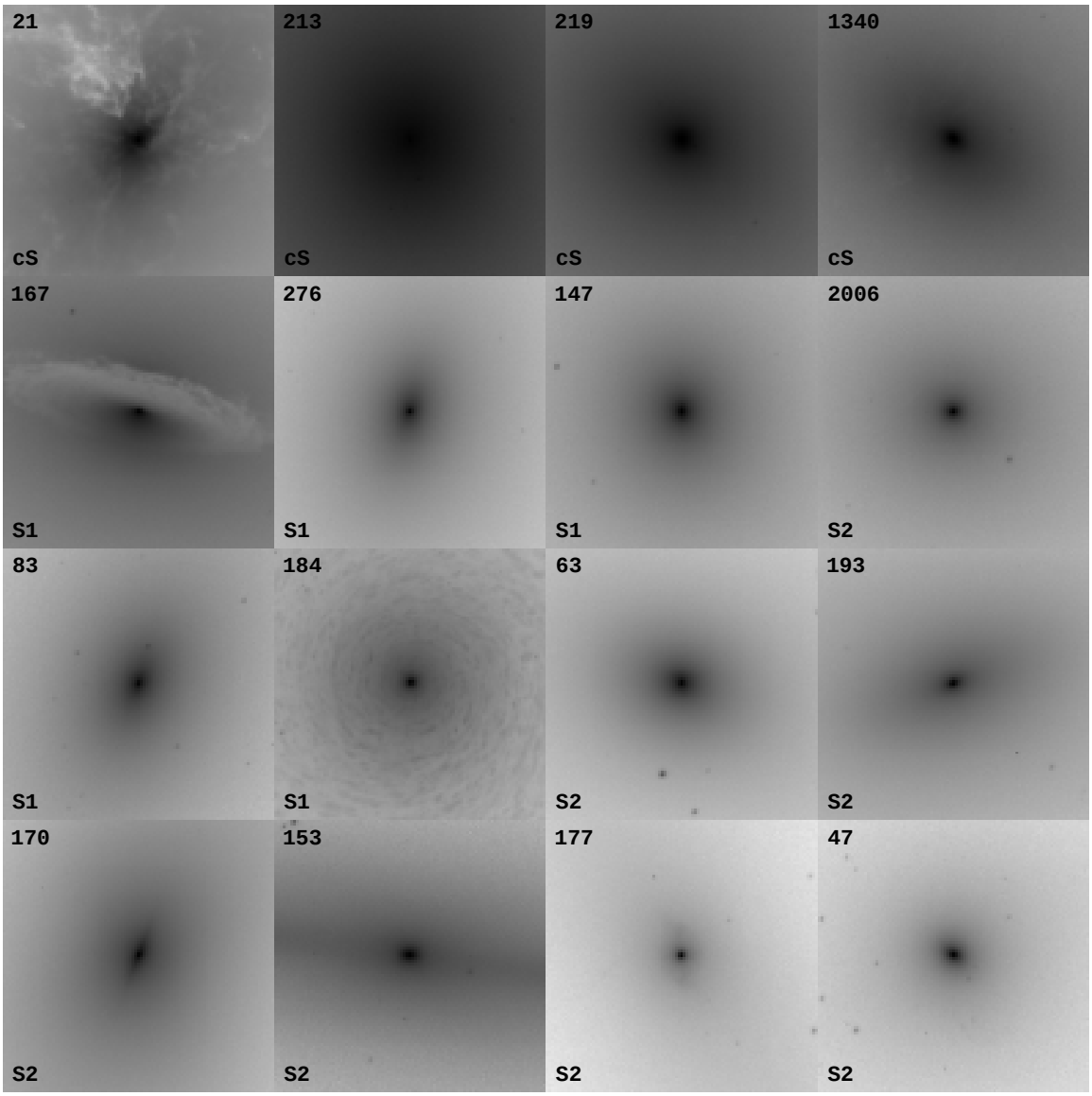

(a)

Figure 2.1 F475W (g-band) images of the inner $10'' \times 10''$ ($\approx$ 0.97kpc $\times$ 0.97kpc) regions of the ACSFCS galaxies. The galaxies are arranged in order of increasing blue magnitude (i.e., decreasing luminosity) from left to right and top to bottom. Each galaxy's FCC number is displayed in the top left, and the bottom left denotes the model used to fit the galaxy, either S1 (Sérsic), cS (core-Sérsic), or S2 (double-Sérsic).

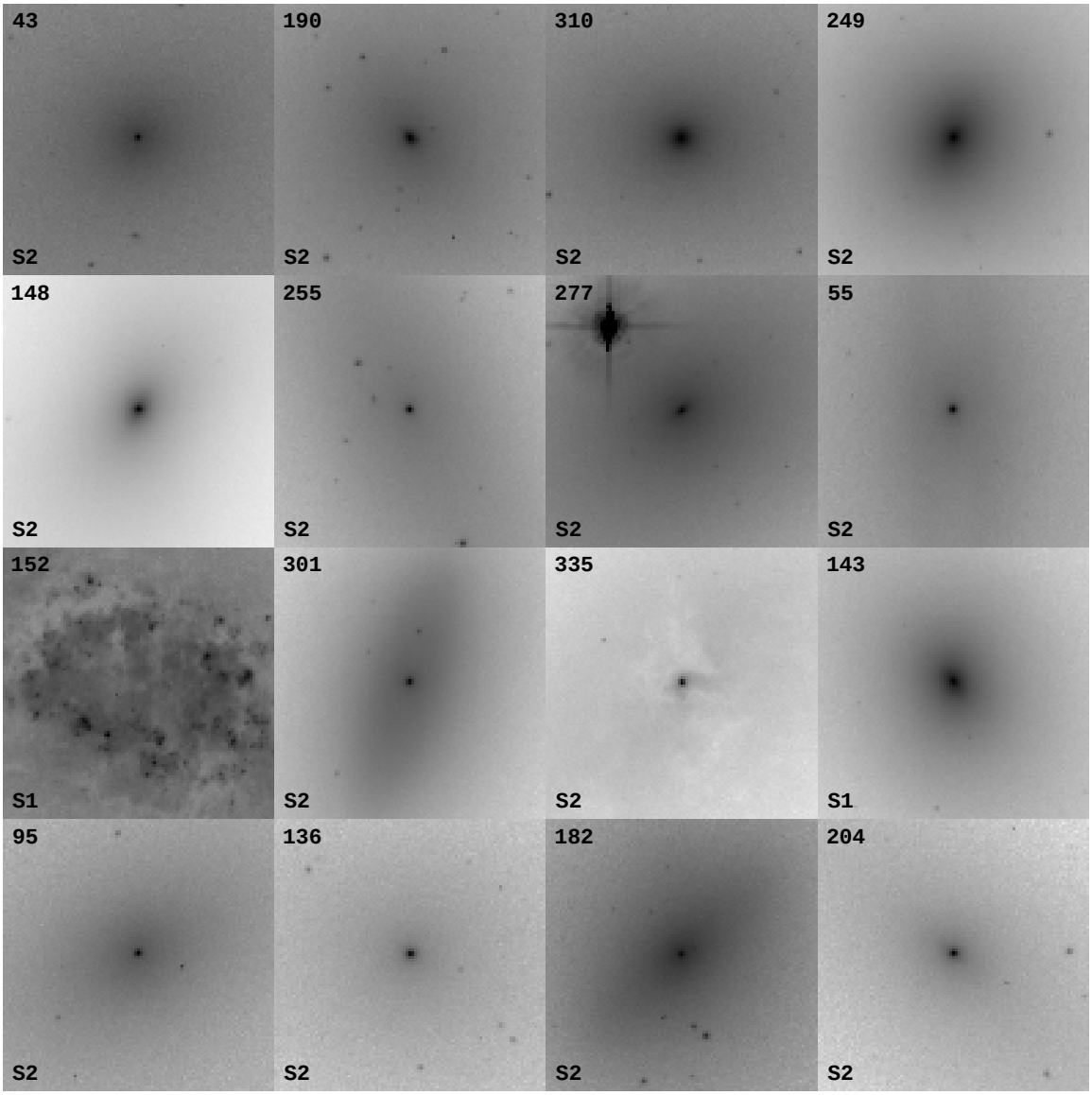

(b)

Figure 2.1 *Continued*

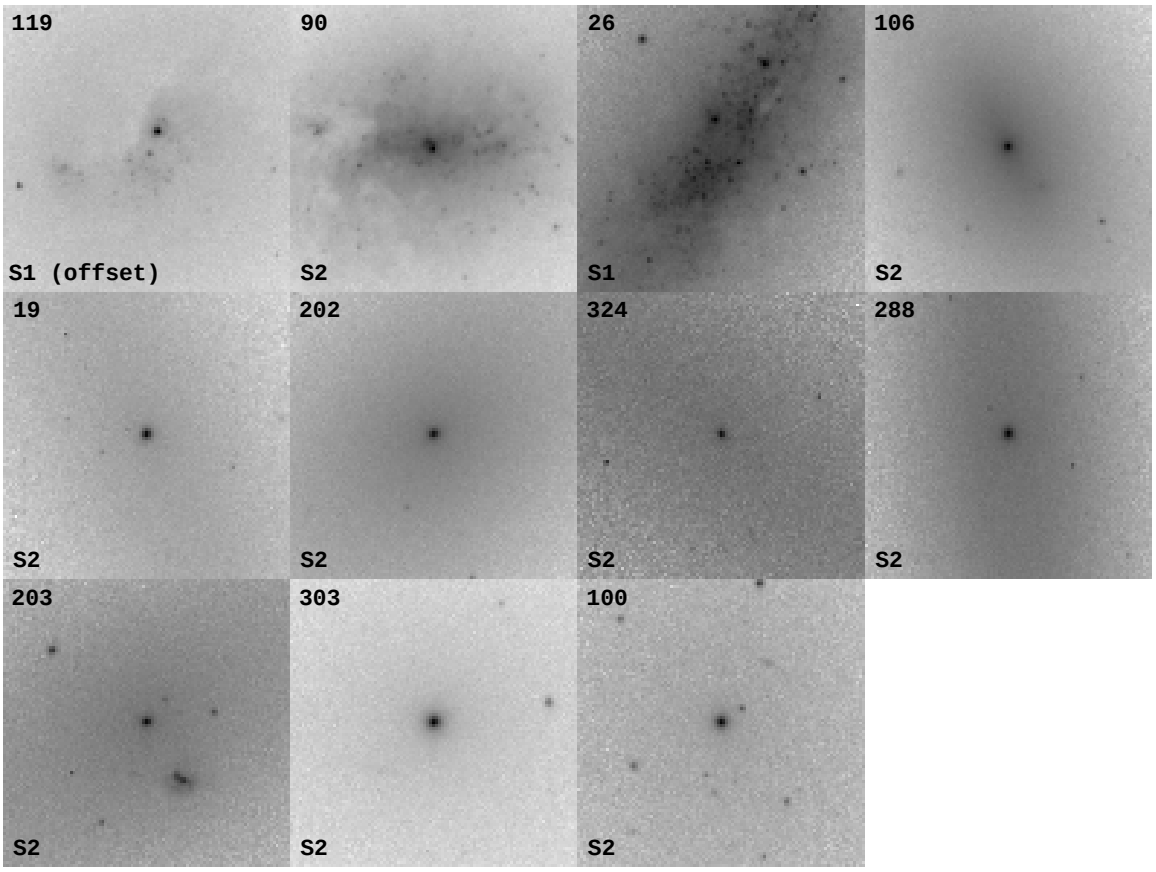

(c)

Figure 2.1 *Continued*

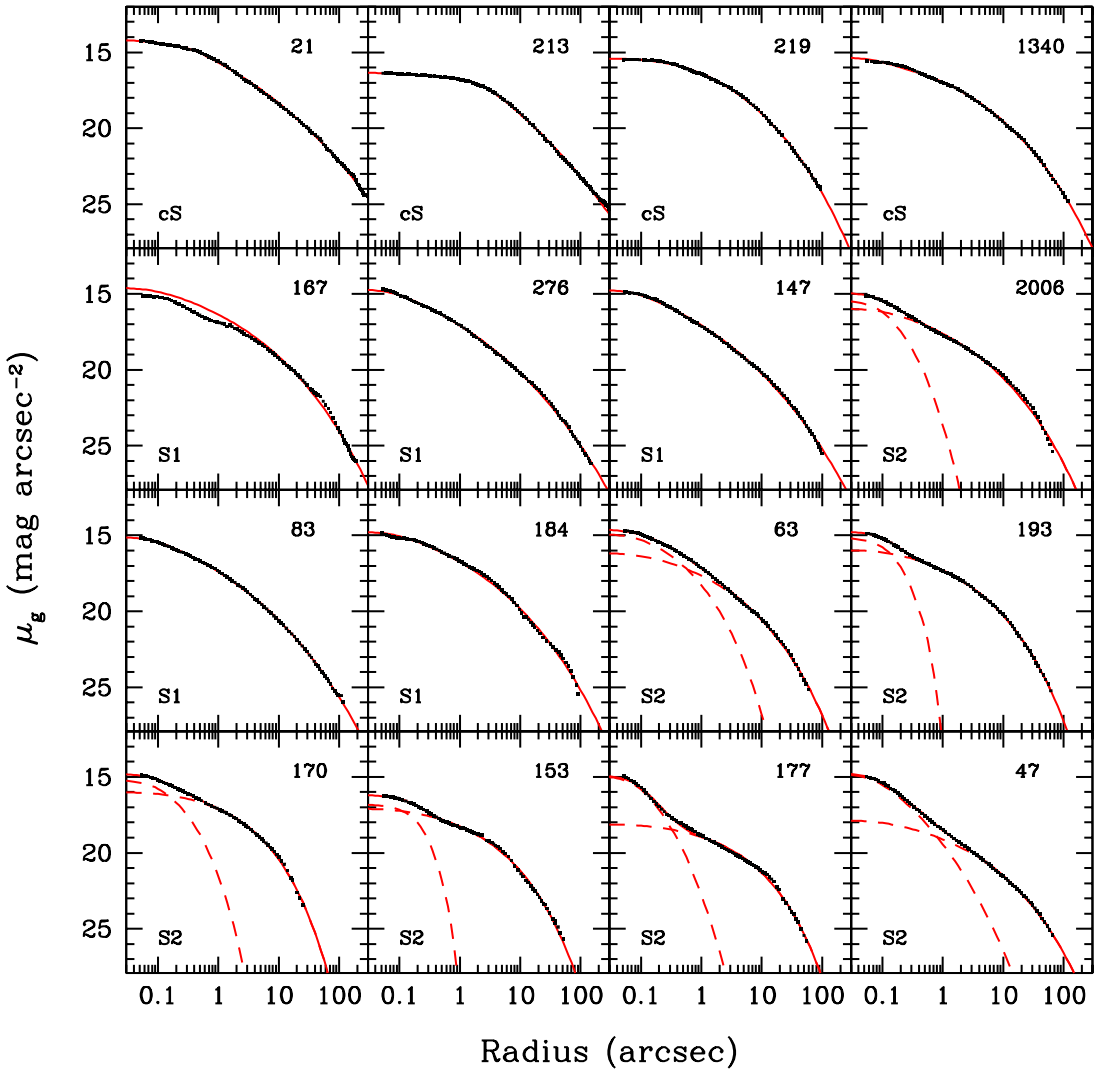

(a)

Figure 2.2 Azimuthally-averaged g-band surface brightness profiles for the ACSFCS galaxies, ranked by increasing blue magnitude (or decreasing luminosity) from left to right and top to bottom, as in Figure 2.1. The black points correspond to the the observed profiles, while the red solid and dashed lines represent the fitted models. The top right label denotes the galaxy FCC number, and the three types of fitted models are denoted in the bottom left, by S1 (Sérsic), cS (core-Sérsic), or S2 (double-Sérsic).

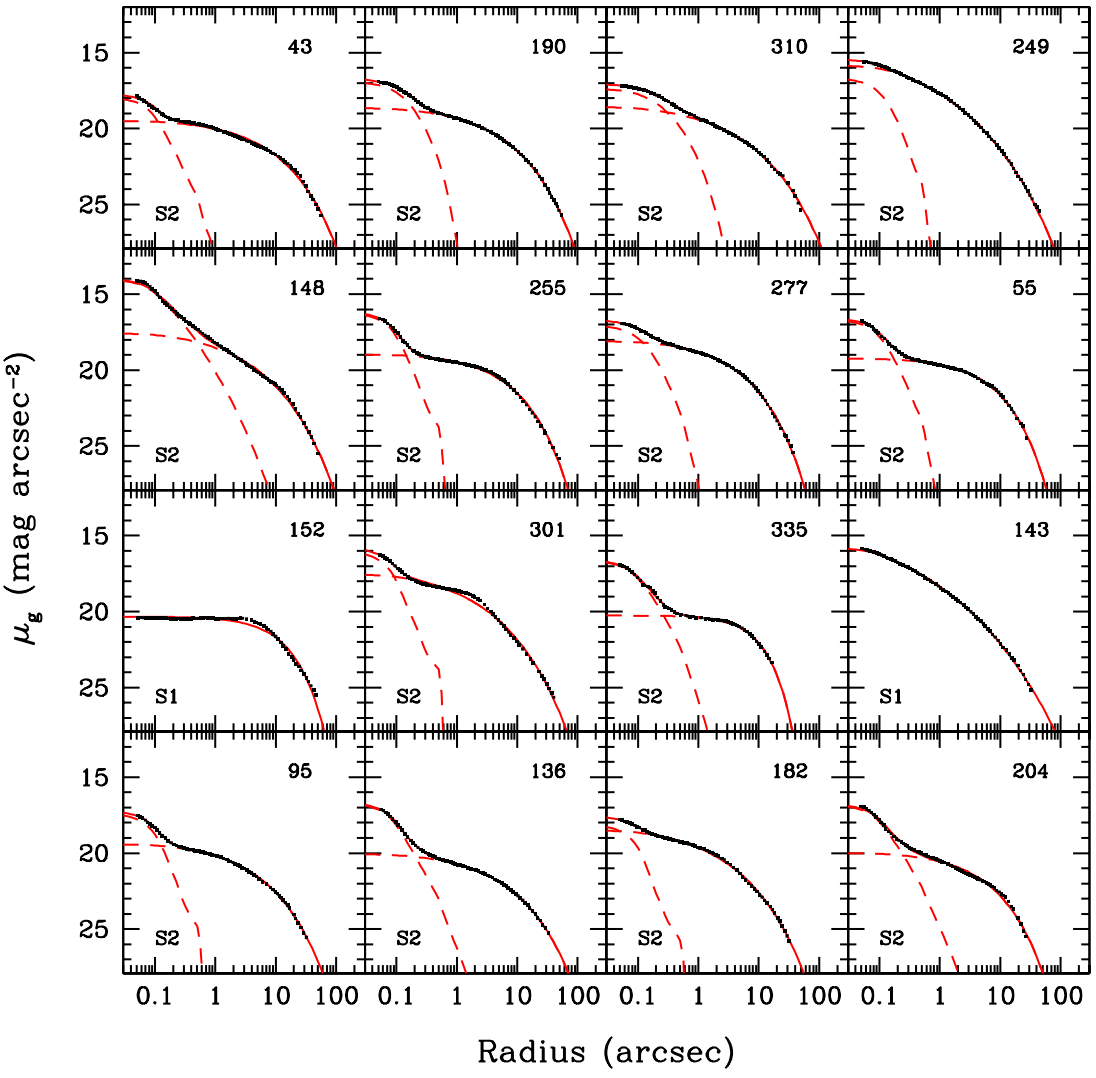

(b)

Figure 2.2 *Continued*

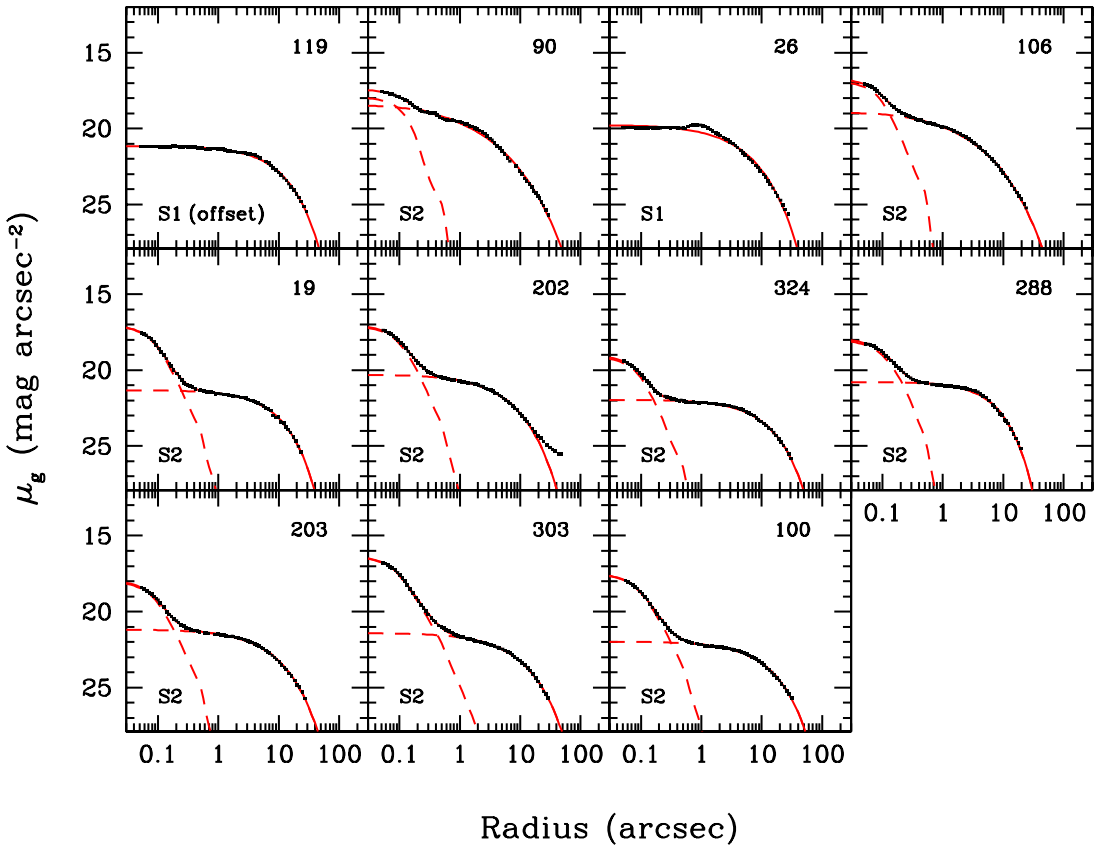

(c)

Figure 2.2 *Continued*

implementing 1D versus two-dimensional (2D) surface brightness profile fitting when extracting the structural parameters.

In general, the decision to use a 1D or 2D analysis is dependent on the science goals. If a galaxy has multiple components (e.g., combinations of bulges, large-scale disks, embedded disks, bars, shells, and even dust patches or faint spiral arms), then, by using 2D decomposition, individual structure can, in principle, be fitted with separate profiles, and the details of the galaxy's composition examined in detail. The 2D fitting algorithm GALFIT (Peng et al., 2002, 2010) allows the implementation of many surface brightness profile modifications, such as variability of their diskyness/boxyness, or the addition of spiral arms and non-axisymmetric bending modes, an attractive advantage of the 2D method. However, in practice, full galaxy decomposition is not always straightforward – in many situations, it is not clear how many components are needed to fully fit a galaxy, and the physical origin of each component may not be obvious. For example, sometimes multiple surface brightness profiles are required to fit what may be the same photometric component (see examples from Peng et al. (2002)), due to the fact that the models used in 2D methods have fixed centre, ellipticity, and position angle, and have difficulty characterizing a galaxy profile in which these parameters are not intrinsically constant on all scales.

The method of 1D profile fitting used in this work, however, allows the aforementioned parameters to vary, and we are therefore often able to cleanly fit an entire galaxy well with a 1D model. A demonstration of this is shown in Figure 2.3, where we examine the structure of FCC 190 (panels A–C), and plot the model derived from our fitted elliptical isophotes (panels D–E). This figure illustrates the striking difference in the shape of this galaxy's isophotes when transitioning from small to large scales, and how this effect is well-captured by the model. The residuals of the fit (panel F) are relatively clean, and reveal a weak ($\mu_g \sim 23.8$ mag arcsec^{-2}) central bar. To compare to a 2D fit, the inner $10 \times 10''$ residuals from fitting 1S and 2S profiles to FCC 190 using GALFIT are shown in Figure 2.6a. Clearly, two Sérsic profiles with fixed ellipticity and position angle are unable to fully parameterize this galaxy. However, the disadvantage to the 1D approach is that the information about the shapes, sizes, and relative position angles of various galaxy components is lost, as their surface brightness profiles blend together into a single model.

Our study is concerned with the properties of the nuclei in comparison to their host galaxies, and with the global trends in these properties as a function of galaxy luminosity or mass. Thus, we are not interested in a full decomposition of any large-

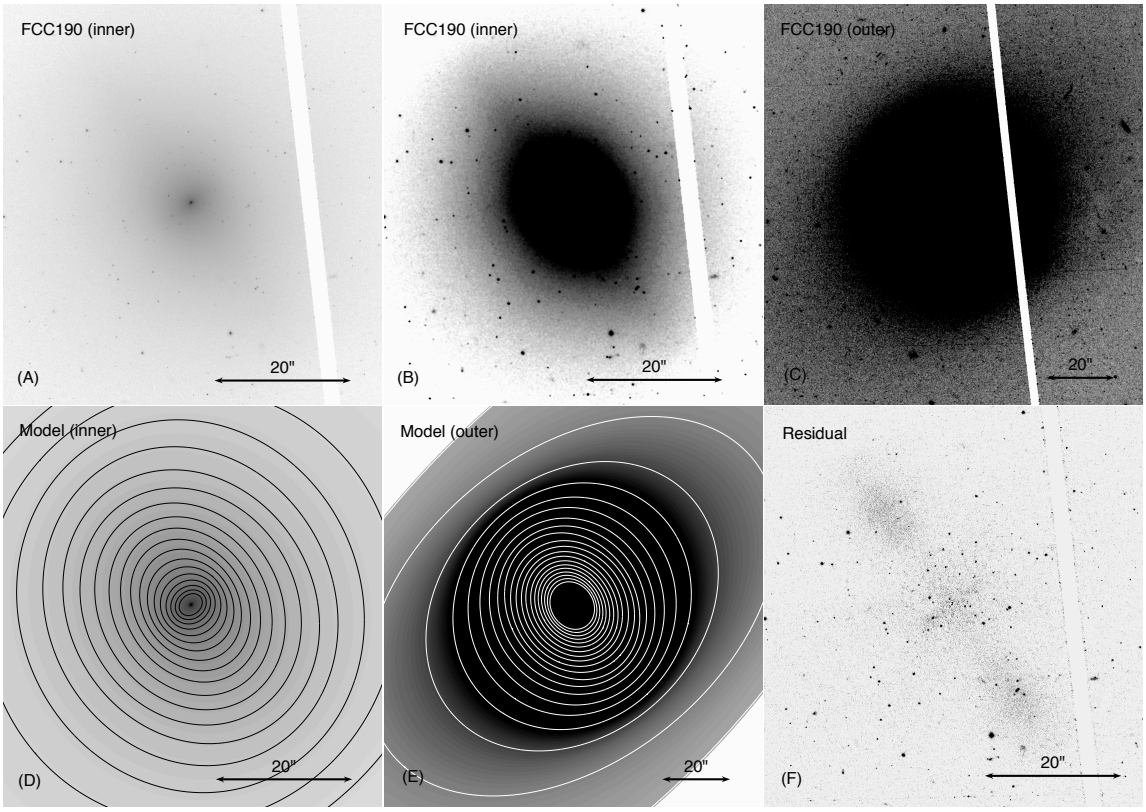

Figure 2.3 *Upper row*: F475W image for FCC 190 displayed at three different intensity stretches (A, B and C) and two different magnifications (A/B vs. C). Note the prominent nucleus visible in *panel (A)*, and the dramatic changes in ellipticity and position angle with radius. *Panels (D) and (E)*: Galaxy model constructed using , with contours overlaid to illustrate the gradual changes in galaxy flattening and orientation. *Panels (D) and (E)*: Residual image (observed − model) showing a weak residual bar, with a peak intensity of ~ 0.02 e pixel^{-1}, corresponding to $\mu_g \sim$ 23.8 mag arcsec^{-2}.

scale galaxy structure; rather, we are seeking to characterize the main galactic body component as a whole, and believe that 1D techniques are more appropriate for our particular objectives. However, it is important to ensure that the nucleus structural parameters extracted using 1D methods are robust. To test this, we perform surface brightness profile fitting in 2D, and compare the results from both techniques.

2.4.1 Procedure

To perform our 2D analysis, we use GALFIT (Peng et al., 2002, 2010), a program that fits galaxy images using multi-component 2D intensity profiles, using an iterative downhill gradient Levenberg-Marquardt algorithm. This 2D analysis is performed on all galaxies in our sample with $B_T \geq 13.5$, a cutoff which was chosen to include most of the nucleated galaxies, while avoiding those that are much more challenging to fit in either 1D or 2D. Galaxies brighter than this are known to often show a complex structure, regardless of their classification as Es, S0s, dEs or dS0s. For instance, the brightest dEs are known to show a significant amount of substructures including disks, spiral arms, and bars (Lisker et al., 2006b, 2007). Likewise, somewhat more massive galaxies, often classified as Es and S0s, frequently show similar morphological complexities (see, e.g., Bender & Moellenhoff, 1987; Combes et al., 1990; Nieto et al., 1992; Scorza et al., 1998; Ferrarese et al., 2006b; Krajnovic et al., 2011). The substructures identified in these early-type galaxies could either be a sign that they are intrinsically more complex objects, or a selection effect arising from their higher luminosities and surface brightnesses, which aid in the detection of these distinct components. In any case, the sample of galaxies used in our 2D analysis consists of 27 galaxies, 24 of which are found to be nucleated in our 1D analysis. This sample includes roughly equal numbers of galaxies listed in Table 2 of Paper I as "giants" (E/S0) or "dwarfs" (dS0, dE, etc), although such classifications such be viewed with some caution since there can be significant discrepancies among classifiers: see, e.g, Chen et al. (2010) and Côté et al. (2011) where issues relating to the morphology of ACSVCS and ACSFCS galaxies will be explored in more detail.

Our analysis proceeded by first measuring the background sky value. To do so, we used *SExtractor* to mask out any background sources, and then convolved this mask with a gaussian in order to thoroughly cover any diffuse outer edges. The galaxy was then masked out with an ellipse of geometric radius length between five and six effective radii (as determined from the 1D analysis). We then took the biweight of the

remaining pixels as the sky value for each of the four ACS chips. Although the sky value between different chips was found to vary up to ~ 1 count, we found that such a count difference in the sky value used for the GALFIT fitting procedure resulted in no more than 5% difference in any of the fitted parameters. Thus, we adopted the average of the biweight estimates for each of the four chips as the sky value.

We began by fitting each galaxy with a single Sérsic (S1) profile. We then attempted to fit each of the 24 galaxies classified as nucleated in 1D by adding a second Sérsic component. In 13 cases, it was possible to fit the nucleus with a Sérsic profile while having all fit parameters for the nucleus allowed to vary, while five more galaxies required a prior on the nucleus Sérsic index (which was fixed at $n = 2$ in analogy with Galactic GCs). For the six remaining nucleated galaxies, GALFIT was not able to converge on a nucleus with only one Sérsic profile fitted to the galaxy main body. At least one other large-scale component needed to be added for before a satisfactory fit to the nucleus could be achieved.

The results of the above procedure are shown in Fig 2.4, where we have plotted the 1D versus 2D magnitudes, Sérsic indices, and effective radii for the galaxies and nuclei from our sample. For the galaxies that require more than two Sérsic components to fit the nucleus, we use the parameters from our S1 fit to plot the galaxy portion. The galaxy main body (filled black circles) parameters are in good agreement from both techniques, however, we note a slight offset in effective radius, where those obtained from the 2D fits are usually somewhat smaller than in 1D (by a factor of 0.94 ± 0.02, derived from least-squares fit, with a fixed line slope of 1, to the galaxy main body effective radii in the log). The S2 nuclei (filled blue squares) are also relatively consistent between techniques, although with some notable outliers that will be discussed. Finally, the non-S2 nuclei (magenta open squares) appear to have the most scatter. We note that the scatter in nucleus magnitudes appears to be the most significant for the brightest nuclei, most likely due to the increased difficulty of extracting nucleus parameters from complex galaxies. We now now discuss findings for galaxies in these different categories.

2.4.2 Non-Nucleated Galaxies (S1)

There are three galaxies in our 2D sample where we do not find a nucleus in our 1D analysis, a result with which we find full agreement in 2D. It is interesting to examine the residuals of a single-Sérsic fit to these objects individually to determine why they

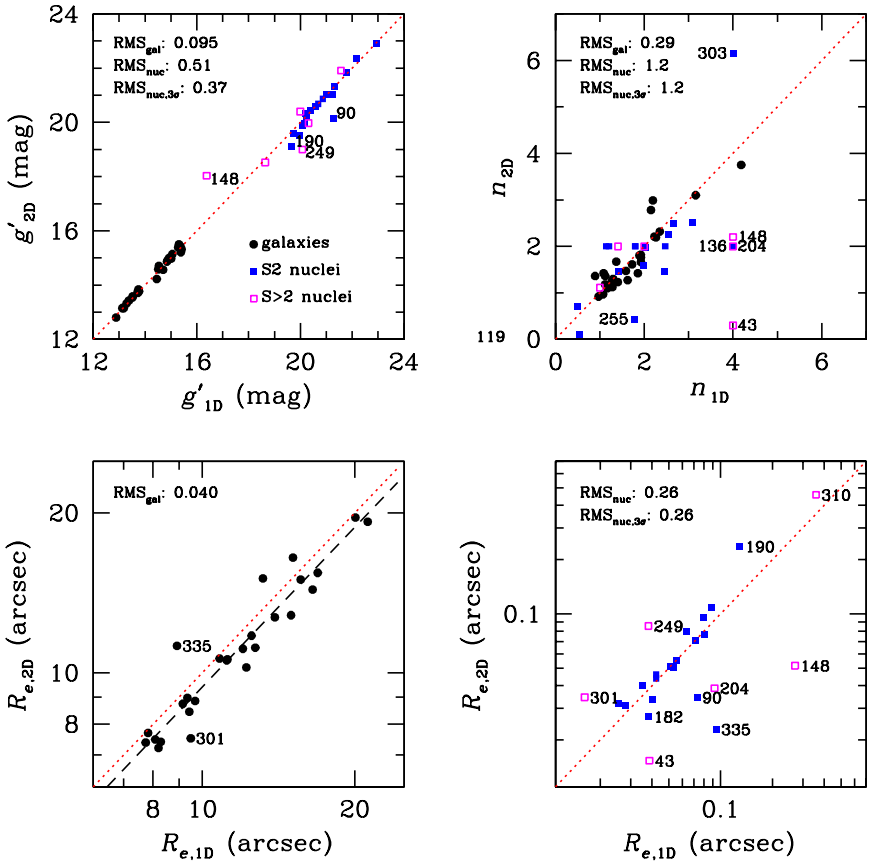

Figure 2.4 *Top left*: Values for nucleus g-band luminosity obtained from 1D (ordinate) and 2D (abscissa) fits. The filled black circles show the host galaxies, the filled blue squares indicate the nuclei from galaxies fit well by a S2 profile in 2D, and the magenta open squares represent the nuclei in galaxies where more than two Sérsic profiles (S>2) were required to fit the galaxy and nucleus in 2D. The dotted red line marks where the parameters obtained from both methods are equal. Galaxies and nuclei where the measured magnitudes differ by more than 0.5 mag between methods are labelled. The root mean squared (RMS) error around the magnitude sample mean is shown for the galaxies, nuclei, and nuclei again after applying 3σ-clipping. *Top right*: Same as the top left, except for Sérsic indices. Galaxies and nuclei where the measured Sérsic indices differ by more than 1.0 between methods are labelled. We note that labels for the blue filled squares are to the left of the points, while those for the magenta open squares are to the right. *Bottom*: Same as top, except for galaxy (*left*) and nucleus (*right*) geometric mean effective radii. Galaxies and nuclei where the measured effective radii in 1D and 2D differ by more than 0.1 in the log are labelled. The black dashed line shows the best-fit line to the galaxy effective radii, with a fixed slope of 1.

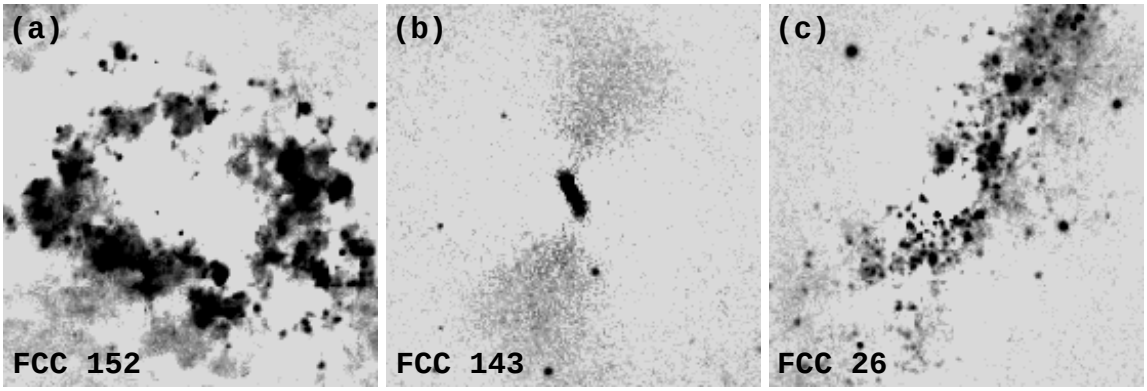

Figure 2.5 *(a)*: GALFIT residuals from an S1 profile fit to FCC 152, showing the inner $10'' \times 10''$ region. *(b)–(c)*: Same as for (a), but for the galaxy labelled.

are not found to be nucleated, since we find the lack of a nucleus to be unusual for galaxies in our sample.

The residuals of FCC 152 (Figure 2.5a) reveal large amounts of dust, but with no nucleus-like object present in the central regions. FCC 143 (Figure 2.5b) shows a small bar in the residuals, which appears to have a bright excess in the centre. Nevertheless, even with the addition of one or two more large-scale Sérsic profile components, GALFIT is unable to fit a central nucleus. Finally, the low-mass galaxy FCC 26 (Figure 2.5c) has two bright compact objects located $0\farcs95$ and $1\farcs37$ away from the galaxy photocentre. However, it is unclear if either of these objects in this actively star-forming, "dE/dIrr" transition galaxy can unambiguously called a true "nucleus".

2.4.3 Nucleated Galaxies Fit With Double-Sérsic Profiles (S2)

Of the 23 nucleated galaxies in our 2D sample, we are able to fit the galaxy and nucleus using an S2 profile for 18 systems. The residuals from the S1 and S2 fits to these galaxies are shown in Figure 2.6, where the galaxies are displayed in order of increasing blue magnitude from the FCC. This figure illustrates how the structural complexity of galaxies seems to diminish as their luminosity decreases, with the residuals for the faintest galaxies appearing much cleaner. Of course, part of this apparent simplicity is likely related to the lower S/N of the available imaging for the faintest and lowest surface brightness systems.

For five of the S2 galaxies, the Sérsic index of the nucleus needed to be held fixed during the fit. FCC 190 (Figure 2.6a), FCC 55 (Figure 2.6d), FCC 95 (Figure 2.6e),

and FCC 136 (Figure 2.6g), all have substructure such as bars that overlap with the nuclear region which the second Sérsic component attempts to fit. Fixing the nucleus Sérsic index at 2 (typical for Galactic GCs) allows GALFIT to fit the nucleus, with the resulting magnitude and effective radius of the nucleus is in agreement with the 1D results in all cases except for FCC 190, which is discussed below. The other galaxy that requires a fixed nucleus Sérsic index, FCC 335, contains a large amount of dust in the central regions, and if the nucleus Sérsic index is allowed to vary, then the nucleus effective radius and Sérsic index converge to very small values, which are deemed unreliable by GALFIT. The differences between the 1D and 2D results for this galaxy are also discussed below, where we describe nuclei that are notable outliers in Fig 2.4. Specifically, the nuclei of FCC 190, FCC 335,and FCC 90 have 1D and 2D magnitude differences of > 0.4 mag and fractional differences in their effective radii of > 0.5.

FCC 190: This nucleus is 0.55 mag brighter and twice as large in effective radius in the 2D fit than in 1D. The host galaxy exhibits a distinct peanut-shape in the residual, shown in Figure 2.6a. It should be noted that after fitting a both a bulge and a disk component along with the nucleus, the nucleus magnitude and radius are still notably disparate.

FCC 335: The nucleus is 0.42 mag brighter, but four times smaller in the 2D than in the 1D fit. The 2D residuals are shown in Figure 2.6e. This galaxy has a large amount of dust, and the centre was held fixed during the ellipse fitting for the 1D analysis. However, the position of the 1D fit ellipse centre is actually ~ 0.5 pixels away from the nucleus (as determined by GALFIT and confirmed by eye). This would cause the 1D analysis to overestimate the nucleus effective radius and underestimate the magnitude, as the light from the nucleus effectively becomes smeared out.

FCC 90: This nucleus is 1.12 mag brighter in 2D than in 1D. The residuals of a single-Sérsic fit (Figure 2.6j) show a bright central nucleus as well as a secondary fainter object $\sim 0\farcs25$ away. This second object may be what causes the secondary bump in the 1D surface brightness profile (see Figure 2.2). After simultaneously fitting this secondary object, the nucleus is still found to be 1.08 mag brighter in 2D than in 1D. Similar to FCC 90, there are large amounts of dust in the centre of this galaxy, and the centre was held fixed for the 1D ellipse fitting, at a point ~ 1 pixels away from the 2D nucleus centre, which may account for the more compact and brighter nucleus found in 2D.

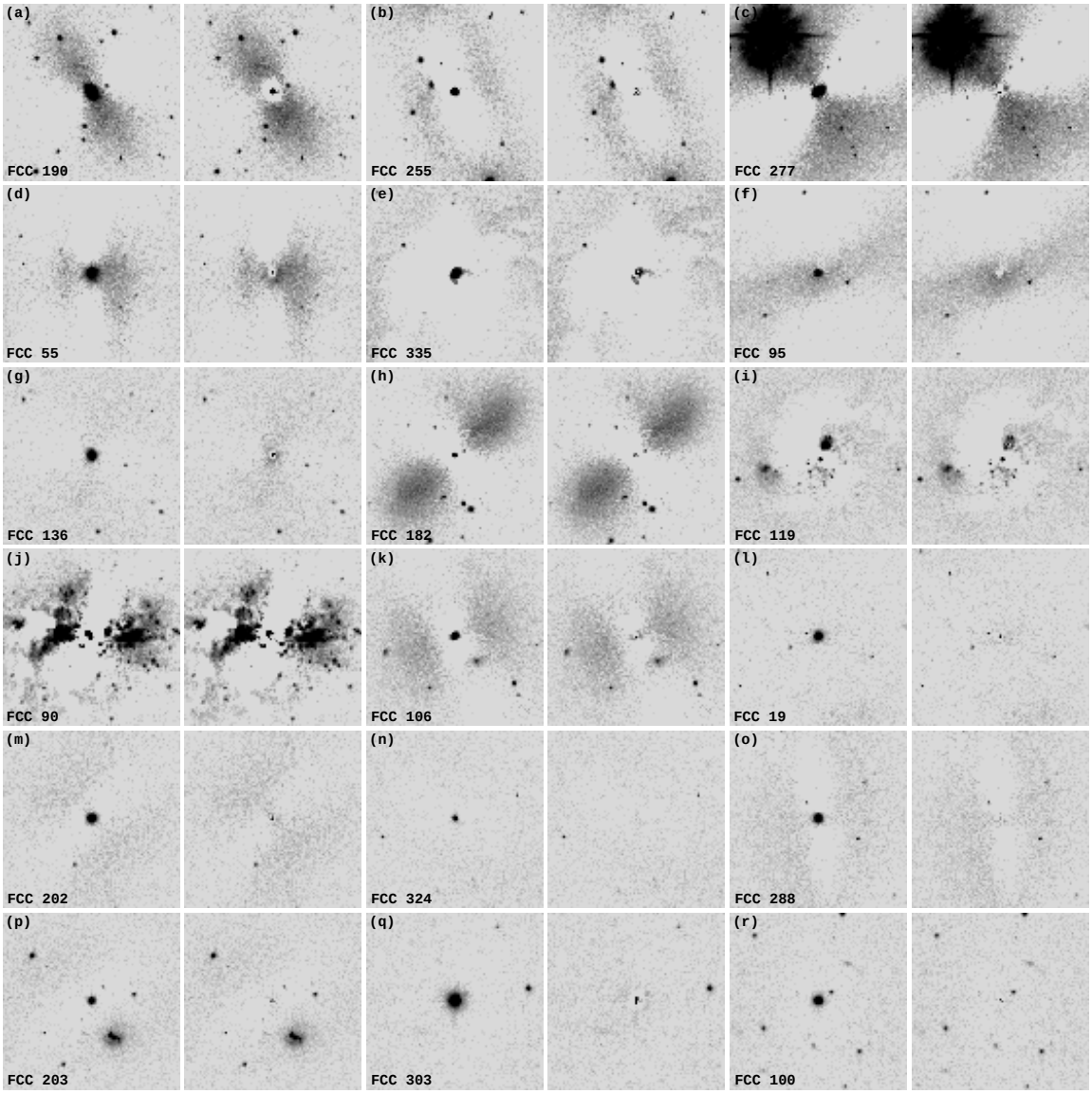

Figure 2.6 *(a)*: GALFIT residuals from an S1 (*left*) and S2 (*right*) profile fit for FCC 190, showing the inner $10'' \times 10''$ region. *(b)–(r)*: Same as for (a), but for the galaxy labelled. Galaxies are ordered in increasing blue magnitude from the FCC.

2.4.4 Nucleated Galaxies with Multiple Large-Scale Components (S>2)

There are six galaxies in our sample which we were unable to characterize as nucleated using an S2 profile, as the second Sérsic component will, even with its Sérsic index held fixed at some value, converge to fit a different portion of the underlying galaxy substructure. Thus, we need to include a second, or even third, Sérsic component to the main body in order to extract the nucleus parameters. A comparison of the 1D and 2D nucleus parameters for these six galaxies is given in Table 2.2.

FCC 43: A small ($< 10''$ diameter) round central component, seen in Figure 2.6a needs to be fitted before it is possible to recover the nucleus. When the nucleus is included, the outer and inner components have Sérsic indices of 1.06 and 1.55 respectively. However, because of the small size of the nucleus determined in 2D (i.e., an effective semi-major axis of 0.39 pixels), the value of the effective radius is deemed unreliable by GALFIT. The 2D nucleus is found to be 0.34 mag fainter than in 1D. It is possible that in 1D, the central disk might be contributing to nucleus component and causing the nucleus luminosity to be over-estimated.

FCC 310: After fitting with a single Sérsic profile, the bar and and outer envelope-like structure of this SB0 galaxy become apparent from the residuals, seen in Figure 2.6b. To fit the nucleus, we must first fit an n=2.38 bulge-like profile, an n=0.26 bar profile, and an n=0.20 outer envelope. After these three components are fit, the nucleus appears quite clearly in the residuals, and it can be fitted by adding a fourth Sérsic profile with its Sérsic index held fixed at 2.

FCC 249: A single-Sérsic fit reveals a peanut-shaped residual in the centre (Figure 2.6c), with a possible nucleus. After a second small component is added, a nucleus becomes apparent in the residuals. The nucleus can then be fitted with its Sérsic index held fixed at 2.

FCC 148: This galaxy shows a very boxy inner bulge, with X-shaped isophotes in intermediate regions (Figure 2.6d). Since we are unable to fit the host and nucleus with a double Sérsic profile, a second large-scale component with disk-like properties (n=1.04, and an axis ratio of 0.36) is introduced, after which GALFIT will converge on the nucleus. Although a nucleus is not very prominent in the two-component fit residual, the Sérsic index of the bulge-like component grows to 9.35 if a nucleus is not included in the fit. After a nucleus is included, the fitted bulge Sérsic index is 5.10. The disk-like component does not change significantly with the addition of the

Table 2.2. 1D and 2D nucleus parameters for S>2 galaxies

FCC	g'_{AB} (mag)		r_e (arcsec)		n	
	1D	2D	1D	2D	1D	2D
43	21.6	21.9	0.04	0.02	4.0	0.3
310	18.6	18.5	0.36	0.46	1.4	2.0
249	20.1	19.0	0.04	0.09	2.0	2.0
148	16.4	18.0	0.27	0.05	4.0	2.2
301	20.3	20.0	0.02	0.03	1.0	1.1
204	20.0	20.4	0.09	0.04	4.0	2.0

nucleus.

FCC 301: The complex structure of this galaxy, seen in the single Sérsic component fit residuals in Figure 2.6e, can be appreciated from the 1D surface brightness profile (Figure 2.2), where the intensity is over-subtracted at $1''$, and then under-subtracted out until $5''$. There are also bright outer wings, at $> 10''$ scales. After a single-Sérsic profile is fitted, a second component will converge on the larger bright central excess, and a third Sérsic profile will then fit the nucleus. However, the bright residuals show that the the main body of this complex galaxy is not well described even by two Sérsic profiles.

FCC 204: Similar to FCC 43, there appears to be an embedded disk in this galaxy, which can be seen in the residual of a single Sérsic fit, Figure 2.6f. The nucleus is also found to be brighter in the 2D fit than in 1D, as in the case of FCC 43.

In general, the 2D nucleus parameters from these more complex galaxies are in reasonable agreement with those found in the 1D fits. In magnitude, only FCC 148 and FCC 249 show differences of > 0.5 mag. However, all except for FCC 310 show discrepancies of $> 50\%$ in effective radius and Sérsic index. These differences do not appear to be systematic, in the sense that there does not seem to be consistent under- or over-estimation of a specific parameter in 1D or 2D. The nucleus parameters for these cases are likely to be more uncertain overall, and thus a larger difference between the extracted parameters might be expected.

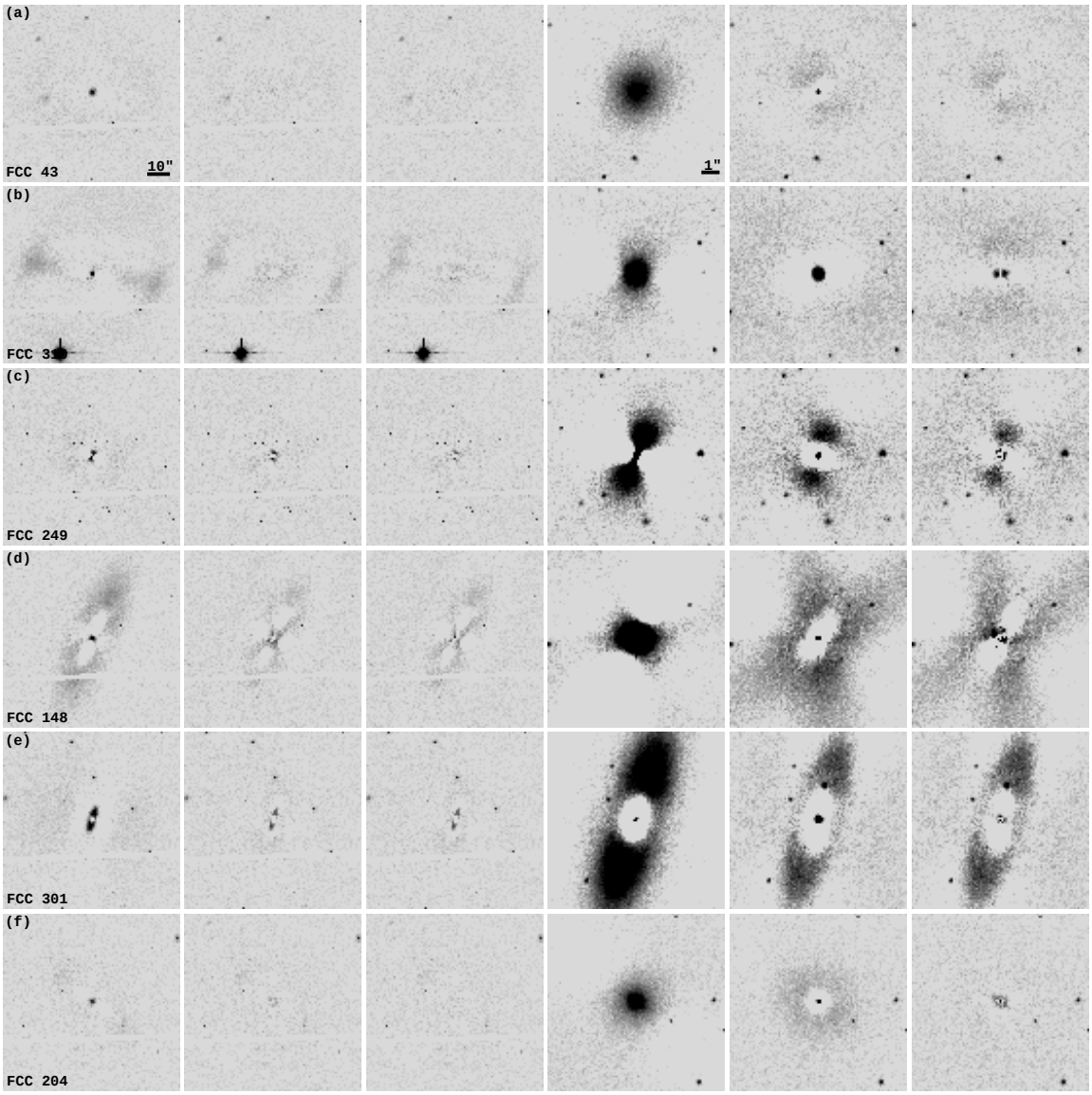

Figure 2.7 *(a)*: The first three panels, from left to right, show $80'' \times 80''$ sized regions of FCC 43 with GALFIT residuals from an S1 fit, a two-Sérsic profile fit, and a two-Sérsic profile plus Sérsic nucleus component fit,. The last three panels show the same, for the inner $10'' \times 10''$. *(b)–(f)*: The same as (a), but for the galaxies labelled. In the case of FCC 310 (b), the residuals are from three-Sérsic profile fits instead of two-Sérsic profile fits.

2.4.5 2D Analysis Conclusion

Overall, Figure 2.4 shows that we find reasonable agreement between the nuclei parameters measured in 1D and 2D. This comparison demonstrates that our 1D nucleus parameters are, for the most part, robust, although the brightest and most structurally complex galaxies — which typically have $\mu_g(1'') \lesssim 19$ mag arcsec^{-2} — present a challenge for measuring photometric and structural parameters for the nuclei using *either* approach.

Indeed, even in cases where adding a second or third profile to the main body is required to fit the nucleus in 2D, it is unclear how many components must be added until a "best" fit is actually achieved, and it is usually difficult to say whether one method produces parameters closer to that of the true nucleus. In our study of Fornax nuclei, we are primarily interested in extracting the nuclei parameters relative to the *average* outer profile. Although much of the power of GALFIT lies in its ability to fit multiple large-scale components, in galaxies that require more than one outer Sérsic profile, it becomes more difficult to perform a fully objective and homogenous comparison between the nuclei and galaxy parameters. We therefore proceed in our analysis using the results from our 1D fits. Nevertheless, the general consensus between methods indicates that the main conclusions in this work (particularly the results that depend on nucleus magnitude, such as the constant nucleus-to-galaxy luminosity ratio and nucleus colour-magnitude relation) are independent of the chosen approach to surface brightness profile fitting.

Chapter 3

Results

3.1 Frequency of Nucleation

In the FCC, only 12 out of our 43 programme galaxies were classified as nucleated, which sets the frequency of nucleation $f_n \approx 28\%$. Column 8 of Table 2.1 shows the classification as nucleated or non-nucleated in the FCC, which can be compared to our classification as in the ACSFCS, where the use of the double-Sérsic (S2) model indicates that we consider the galaxy to be nucleated. We find all galaxies previously classified as nucleated by Ferguson to be nucleated in our sample, as well as an additional 19, for a total of 31 out of the 43 galaxies, or $f_n \approx 72\%$.

The cause of this sharp rise in frequency of nucleation can be attributed to observational selection effects. In the top of Figure 3.1, the open histogram shows the luminosity of all of the programme galaxies, while the hatched and solid histograms denote those found to be nucleated in the ACSFCS and the FCC, respectively. The bottom of Figure 3.1 plots f_n as a function of luminosity for the two surveys. The ACSFCS uncovers many more nuclei in more luminous host galaxies, as the high resolution of the WFC allows us to resolve nuclei in their high surface brightness cores. This selection effect is explored further in Figures 3.2 and 3.3.

Galaxy surface brightness at a geometric mean radius of $R = 1''$ (≈ 97 pc) was calculated using spline interpolation, in the g- and z-bands. By measuring surface brightness at a large and constant radius (rather than at some function of the effective radius), the result is a model-independent measure of central surface brightness, at a distance large enough to avoid the contribution from a nucleus, if present. A histogram of these values is shown in Figure 3.2, in which the trend of nucleus iden-

tification based on galaxy surface brightness becomes much more pronounced.

To illustrate this point in another way, Figure 3.3 plots the integrated nucleus magnitude derived from the S2 fit against galaxy surface brightness measured at a geometric mean radius of $R = 1''$. The filled circles and open squares show the measurements for galaxies classified as nucleated in the ACSFCS and FCC, respectively. Clearly, the nuclei that went undetected in the earlier (photographic) survey come in two forms: bright nuclei that are embedded at the centres of luminous galaxies with steeply rising surface brightness profiles, and faint nuclei belonging to the lowest luminosity galaxies. Needless to say, we too may be missing some nuclei in our survey, so we take $f_n \approx 72\%$ as a lower limit to the frequency of nucleation in the ACSFCS sample.

3.2 Possible Offset Nuclei

The offset of each nucleus from the host galaxy photocentre was measured for 28 of our 31 nucleated galaxies. For FCC 335, FCC 119, and FCC 90, the elliptical isophote fitting was performed with the ellipse centres held fixed, as convergence could not be otherwise achieved due to large amount of dust in their central regions. Thus, offsets for these nuclei could not be measured using the following technique, although we did examine their offsets using our GALFIT analysis, as described below.

For the 28 remaining galaxies, an analysis similar to that used in C06 was performed. The galaxy photocentre was determined by averaging the centre pixel values of ellipses with geometric radii $1'' \leq R \leq R_e$, where the error on the position of the photocentre was taken to be the standard deviation of these values. The position and error of the centroid of the nucleus were taken from the smallest fitted ellipse. These errors were then added in quadrature to obtain the total error on the offset.

The results are presented in Figure 3.4. With the exception of FCC 288, which has an offset of $0\farcs116 \pm 0\farcs001$ in the z-band, we find that all of the galaxies in our sample have an offset of less than $0.1''$. FCC 288 is also the only galaxy with an offset greater than 1% of the host galaxy's effective radius.

A number of the fainter galaxies in Figure 3.4 have very small error bars. This is due to a non-varying ellipse centre for the range $1'' \leq r \leq r_e$. When the `ellipse` task is used to fit isophotes, if the radial surface-brightness gradient of the galaxy becomes too small, then `ellipse` holds the isophote centres fixed as it continues to grow them to larger radii. For brighter galaxies, the point at which the gradient

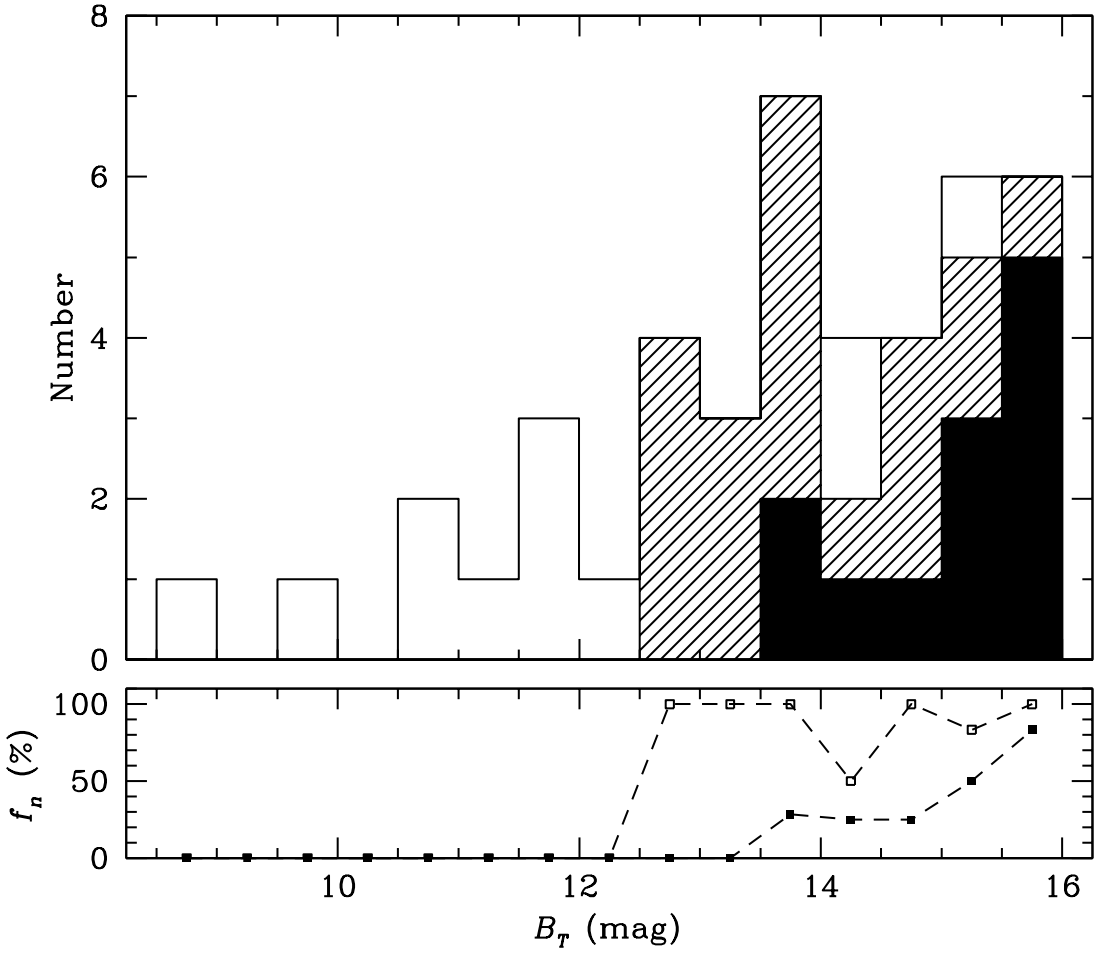

Figure 3.1 *Top*: Luminosity distribution of the 43 ACSFCS programme galaxies (open histogram). The overlaid hatched histogram shows the distribution of the 31 galaxies classified as nucleated in this study, while the solid histogram shows the distribution of the 12 nucleated galaxies according to the FCC. *Bottom*: The percentage of nucleated galaxies (f_n) in this study (open squares) and in the FCC (solid squares).

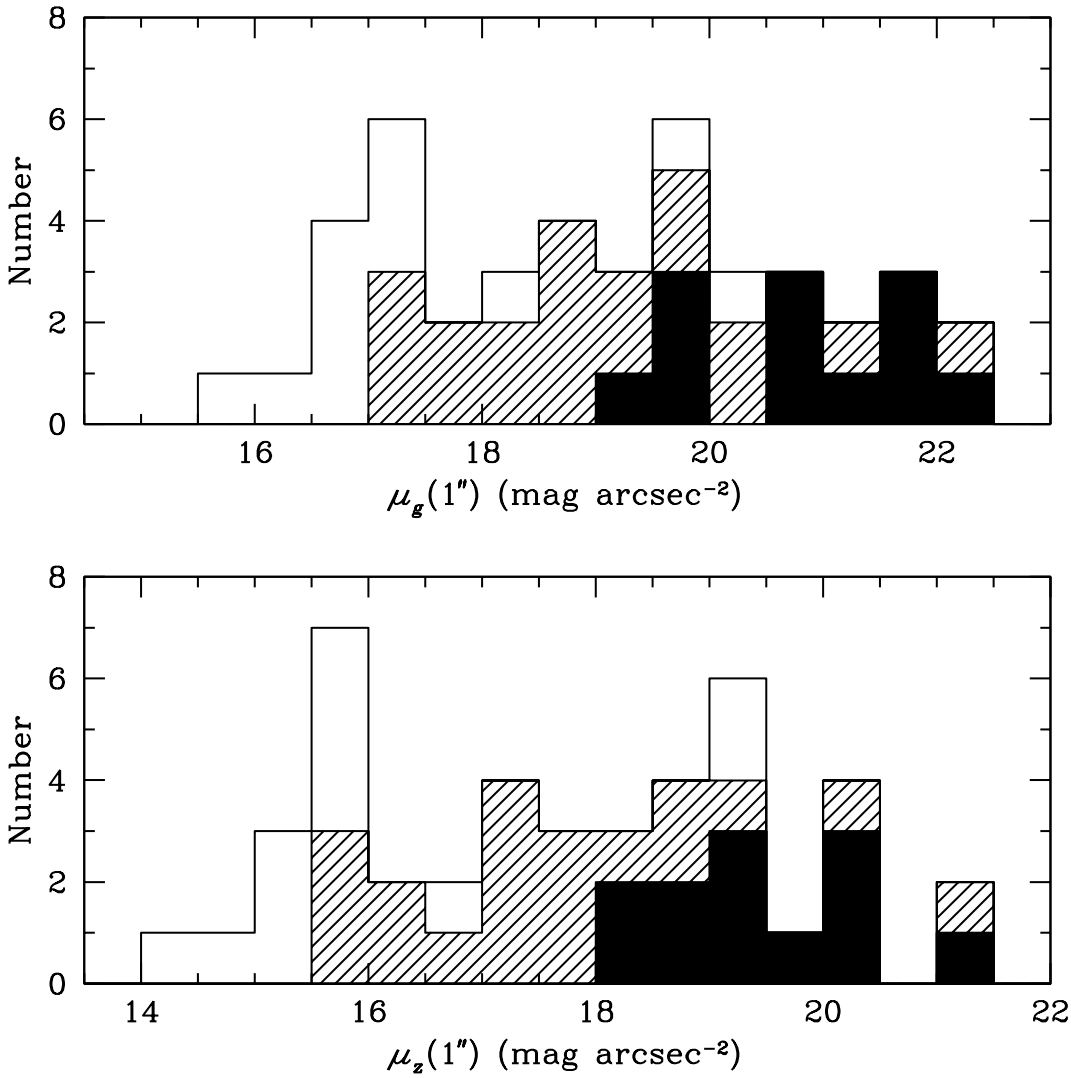

Figure 3.2 Distribution of g-band (*top*) and z-band (*bottom*) galaxy surface brightness measured at a mean radius of $1''$, for the 43 ACSFCS galaxies (*open histogram*). The hatched histogram shows the distribution of the 31 galaxies found to be nucleated by this study, while the solid histogram shows the distribution of the 12 galaxies classified as nucleated in the FCC.

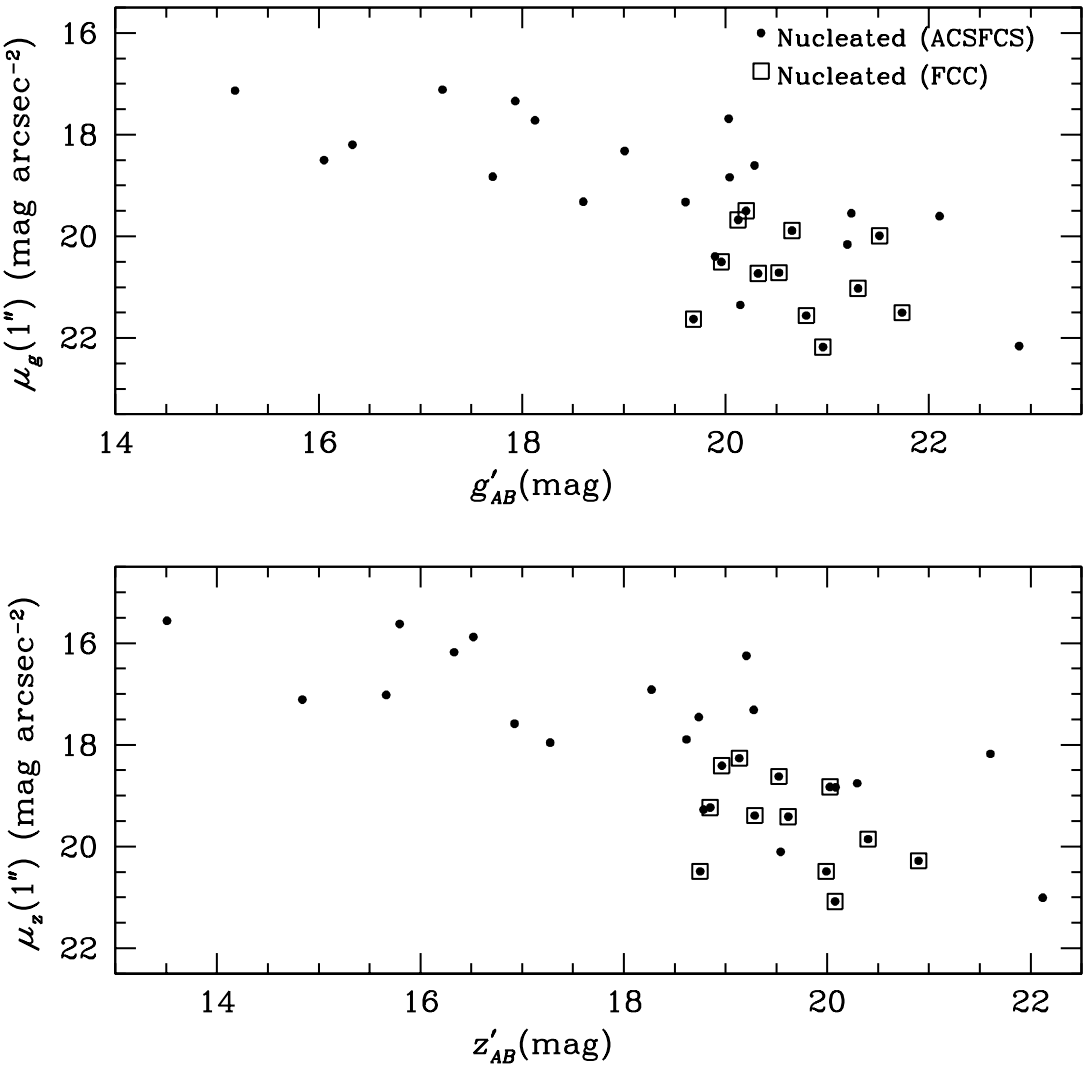

Figure 3.3 Galaxy surface brightness in the g-band (*top*) and z-band (*bottom*) measured at a mean radius of $1''$, plotted against the magnitude of the nucleus. The filled circles show the 31 galaxies found to be nucleated by this study, while the open squares show the 12 galaxies classified as nucleated in the FCC.

becomes too small for convergence typically occurs past the effective radius of the galaxy. However, for faint galaxies, or those with significant amounts of dust, this point can occur well inside R_e, so that the measurement of the "average" photocentre is not particularly meaningful. To illustrate this effect, we plot elliptical isophote offset as a function of geometric mean radius in Figure 3.5 for the galaxies that have the largest nucleus offsets in the z-band (where dust obscuration is minimized). A non-varying ellipse centre for most or all of the isophotes with mean geometric radii between $1'' \leq R \leq R_e$ is found for FCC 19, FCC 324, FCC 288, FCC 100, FCC 203, and FCC 303; this likely leads to a systematic underestimation of their nuclei offsets for these six galaxies. However, each of these galaxies was well fitted in our GALFIT analysis, so we can examine those results to further search for evidence of nucleus offset.

We generally find the offsets from our 2D analysis to be larger than those determined using our 1D method. This is due mainly to the fact that the 2D fitting procedure gives significant weight to the large numbers of pixels in the outer regions of the galaxy, whereas the 1D fit increases in radius logarithmically, giving more weight to the central regions in the determination of the photocentre. Thus, for our 2D analysis, we are not concerned with offsets $\lesssim 0\farcs5$, and only three galaxies are found to have offsets larger than this — FCC 119 ($0\farcs65$), FCC 324 ($0\farcs70$), and FCC 288 ($0\farcs62$). FCC 119 is fairly irregular, with large amounts of central dust. FCC 324 and FCC 288 are both low surface-brightness, highly flattened galaxies, with no obvious clusters near the photocentre that may have caused source confusion with what we consider to be the nucleus. We conclude that our sample contains at most 10% nuclei that are offset at the level of $0\farcs5$ or more, consistent with the findings of C06 for the Virgo cluster.

To measure any trend of offset with galaxy luminosity, we perform a least-squares fit to the data from Figure 3.4. All points are weighted equally since, as discussed in the previous paragraph, the errors may not be accurate for galaxies with ellipse centres fixed at some point within an effective radius. Using the offsets from our 1D analysis, we obtain

$$\begin{aligned} \log \delta r_g &= (0.081 \pm 0.060)\, B_T - (2.9 \pm 0.9) \\ \log \delta r_z &= (0.090 \pm 0.056)\, B_T - (3.0 \pm 0.8), \end{aligned} \tag{3.1}$$

which suggests a weak, but significant, trend of increasing offset with decreasing

galaxy luminosity. Moreover, as mentioned above, the measured offsets for some of the fainter galaxies may be underestimated, potentially suppressing the apparent strength of this relation. Indeed, a least-squares fit to the offsets measured in the 2D analysis gives a slope that is roughly twice this large:

$$\log \delta r_{2D} = (0.21 \pm 0.18)\, B_T - (4.1 \pm 2.7). \tag{3.2}$$

Finally, some of the galaxies in our sample which we do not find to be nucleated may, in fact, be dIrr/dE transition objects, where a nucleus could be in the process of formation. In particular, FCC 152 and FCC 26 are irregular in shape and contain many star clusters and large amounts of dust in their central regions. It is possible that one or more of these clusters could be nucleus progenitors that will migrate inwards through dynamical friction.

3.3 The Nucleus-to-Galaxy Luminosity Ratio

Previous studies of early-type dwarfs (Lotz et al., 2004; Grant et al., 2005), including C06, find that nucleus brightness increases with host galaxy brightness. Similar relations are known to exist for the nuclear clusters in late-type galaxies (see, e.g., Carollo et al., 1998; Böker et al., 2004). A plot of nucleus versus host galaxy magnitude, determined through the integration of the outer Sérsic profile over all radii, is shown at the top of Figure 3.6. Best-fit linear relations of the form:

$$\begin{aligned} g'_{\rm n} &= m g'_{\rm g} + b \\ z'_{\rm n} &= m z'_{\rm g} + b \end{aligned} \tag{3.3}$$

were fitted to the data, where $g'_{\rm n}$ and $z'_{\rm n}$ are nuclei magnitudes and $g'_{\rm g}$ and $z'_{\rm g}$ are the galaxy magnitudes. The best-fit parameters (m_1, b_1, b_2) are given in Table 3.1. Results are given for the two cases of fixing the slope at $m_2 \equiv 1$, and allowing it to vary freely (shown respectively as the solid and dashed lines in the upper panel of Figure 3.6).

Since the best-fit slope of the nucleus-galaxy luminosity relation is very nearly one, we explore the possibility of a constant nucleus-to-galaxy luminosity ratio, $\eta = \mathcal{L}_{\rm n}/\mathcal{L}_{\rm g}$, where $\mathcal{L}_{\rm n}$ and $\mathcal{L}_{\rm g}$ are nucleus and galaxy luminosity, respectively. In the bottom of Figure 3.6, η is is plotted as a function of host galaxy magnitude in the same band.

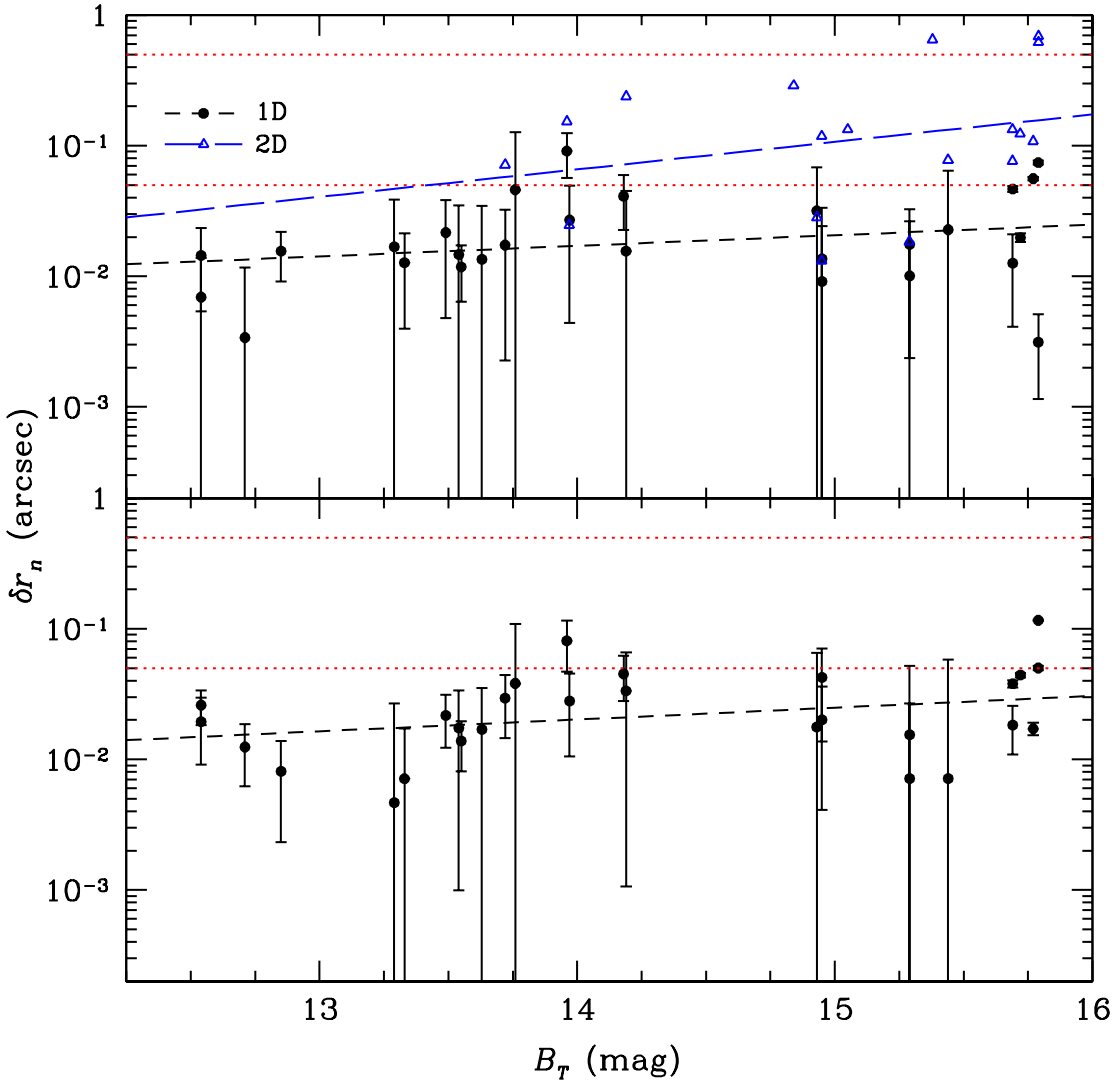

Figure 3.4 *Top*: Projected offset between the nucleus and the galaxy photocentre in the g-band, plotted against host galaxy magnitude. Offsets were calculated using our 1D (black circles) and 2D (blue triangles) analyses. The two dotted red lines show offsets one and ten ACS/WFC pixels (0.″05 and 0.″5). The black short-dashed line and blue long-dashed line represent the best-fit relation for 1D and 2D offsets, respectively. *Bottom*: Same as above, but for the z-band.

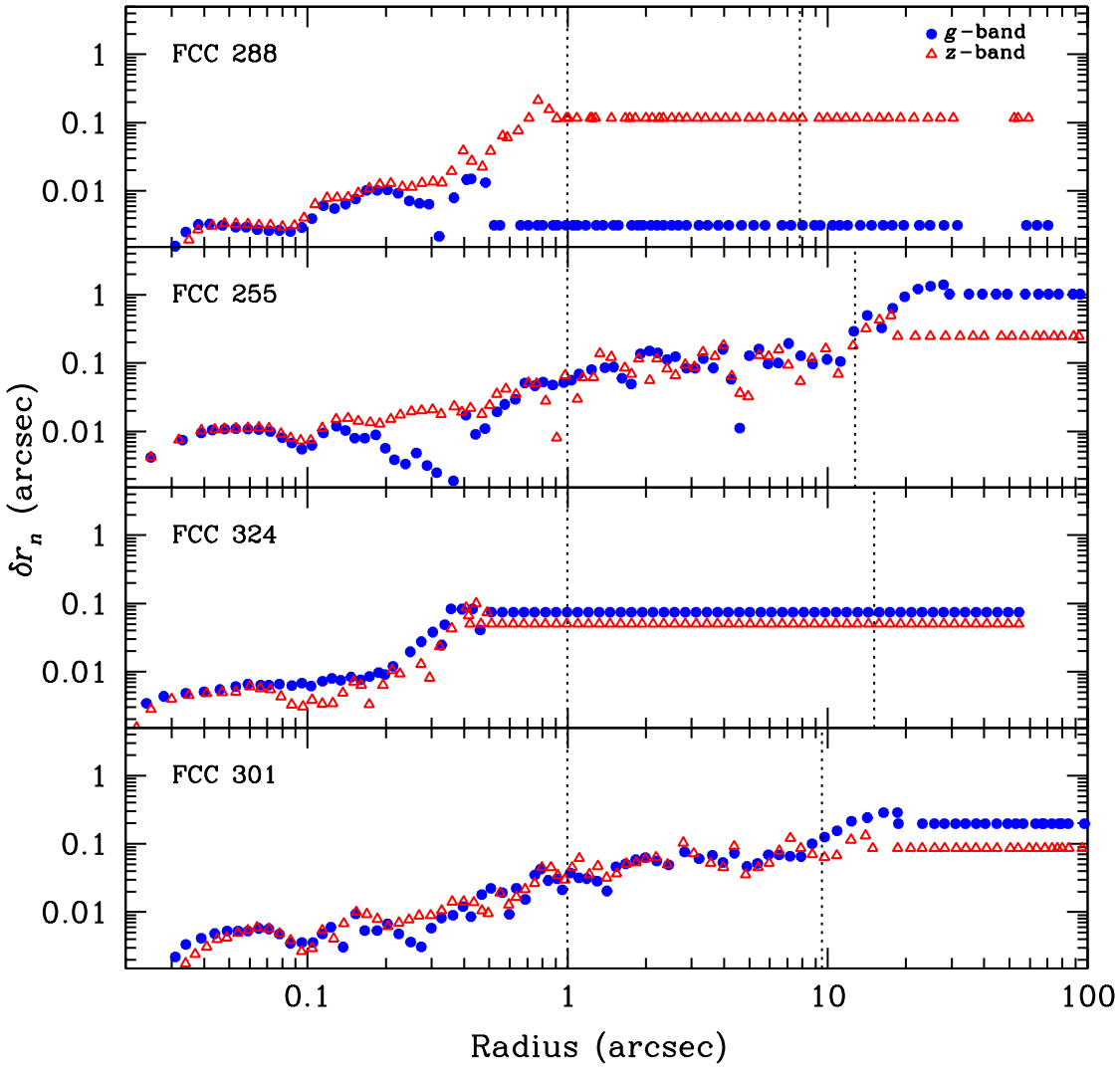

Figure 3.5 Offset of elliptical isophotes from the nucleus as a function of isophote geometric mean radius, for the four galaxies found to have the largest offsets in the z-band. The blue closed circles and red open triangles represent the offsets measured in the g-band and z-band, respectively. The left vertical dotted lines mark 1″, and the right lines indicate the galaxy's effective radius. The average value of the offset between these two lines is used to define the galaxy photocentre. Due to their very low gradients in surface brightness, the isophote centres were held fixed in this region for FCC 288 and FCC 324, possibly underestimating the true offset.

The values of the mean and standard deviations in both bands is given in Table 3.1, while the mean ratio and standard error on the mean from both bands is

$$\langle \eta \rangle = 0.43\% \pm 0.06\%. \tag{3.4}$$

This is 0.13% larger than the value of $\langle \eta \rangle = 0.30 \pm 0.04\%$ found in C06 (a 1.7σ discrepancy). At first glance, this might suggest that, at a given luminosity, early-type galaxies in Fornax were slightly more efficient in assembling their nuclei than those in Virgo; however, the difference is in fact due to the use of of Sérsic rather than King models in fitting the ACSFCS nuclei. As Sérsic profiles with even moderate n have somewhat extended wings, they increase the inferred luminosity of the nuclei relative to the King models (whose defining characteristic is a tidal truncation radius). Re-fitting the Virgo data with S2 profiles confirms this result – in § 4.1.2, where the new fits to Virgo are presented, we find agreement between η for both clusters.

Finally, we point out that there appears to be a weak trend with η and galaxy luminosity in the sense that brighter galaxies tend to have brighter nuclei relative to the magnitude of the host. The values from a least-squares fit (m_η, b_η) are given in Table 3.1. However, the F-statistic for these fits has p-values of 0.19 and 0.067 for the g- and z- band data respectively, so we do not reject the null hypothesis.

Table 3.1. Nucleus-to-Galaxy Luminosity Ratio Best-Fit Values

Data Set	m_1	b_1	b_2	$\langle\eta\rangle$	σ	m_η	b_η
Fornax, g	1.26 ± 0.20	2.13 ± 2.75	5.80 ± 0.22	-2.32	0.48	-0.105 ± 0.079	-0.851 ± 1.098
Fornax, z	1.36 ± 0.19	1.53 ± 2.39	6.04 ± 0.22	-2.42	0.49	-0.143 ± 0.075	-0.610 ± 0.952

3.4 Luminosity Functions

One mechanism for the formation of galaxy nuclei is through mergers of GCs that sink to the galaxy centre by dynamical friction (e.g., Tremaine, 1976; Capuzzo-Dolcetta, 1993; Capuzzo-Dolcetta & Tesseri, 1999; Lotz et al., 2001; Bekki et al., 2004). A comparison of the luminosity function of our nuclei with that of the GCs identified in the ACSFCS can offer some insight into this theory. In Figure 3.7, we performed a maximum-likelihood fit of our nuclei and the GC luminosities to a normalized Gaussian

$$\Phi(m_{\rm n}^0) \propto \exp\left[-(m_{\rm n}^0 - \bar{m}_{\rm n}^0)/2\sigma_{\rm n}^2\right]. \tag{3.5}$$

While this choice of parameterization is commonly used for GCs, there is no physical reason that the nuclei should have a Gaussian distribution. Nevertheless, it is useful for the purposes of comparison with the GC luminosity function.

Our GC sample consists of ≈ 2000 candidates with probability index $\mathcal{P}_{\rm gc} \geq 0.5$ (see Paper VIII for more details on GC probability index, and a detailed study of their luminosity functions). The best-fit parameters for both nuclei and GCs are given in Table 3.2. We find the luminosity function of the nuclei to be both brighter, and have a much greater spread than that of the GCs. The difference in the means is $\Delta g = 4.28$ mag and $\Delta z = 4.24$ mag; that is, on average the nuclei are $\sim 50\times$ brighter than a typical GC.

In reality, since we find the nucleus-to-galaxy luminosity ratio to be roughly constant, the nucleus luminosity function should reflect that of the host galaxies (albeit with more scatter), and is most likely parameterized by a Schechter function truncated on both ends – on the bright end because we don't find any bright galaxies to be nucleated, and on the faint end because our sample is magnitude-limited. To demonstrate this, we plot a full Schechter function over the B-band galaxy luminosity distribution of the FCC and the ACSFCS in Figure 3.8. We then make cutoffs at $B_T = 12.5$ and 16 mag (so that we are left with the magnitude range of the nucleated

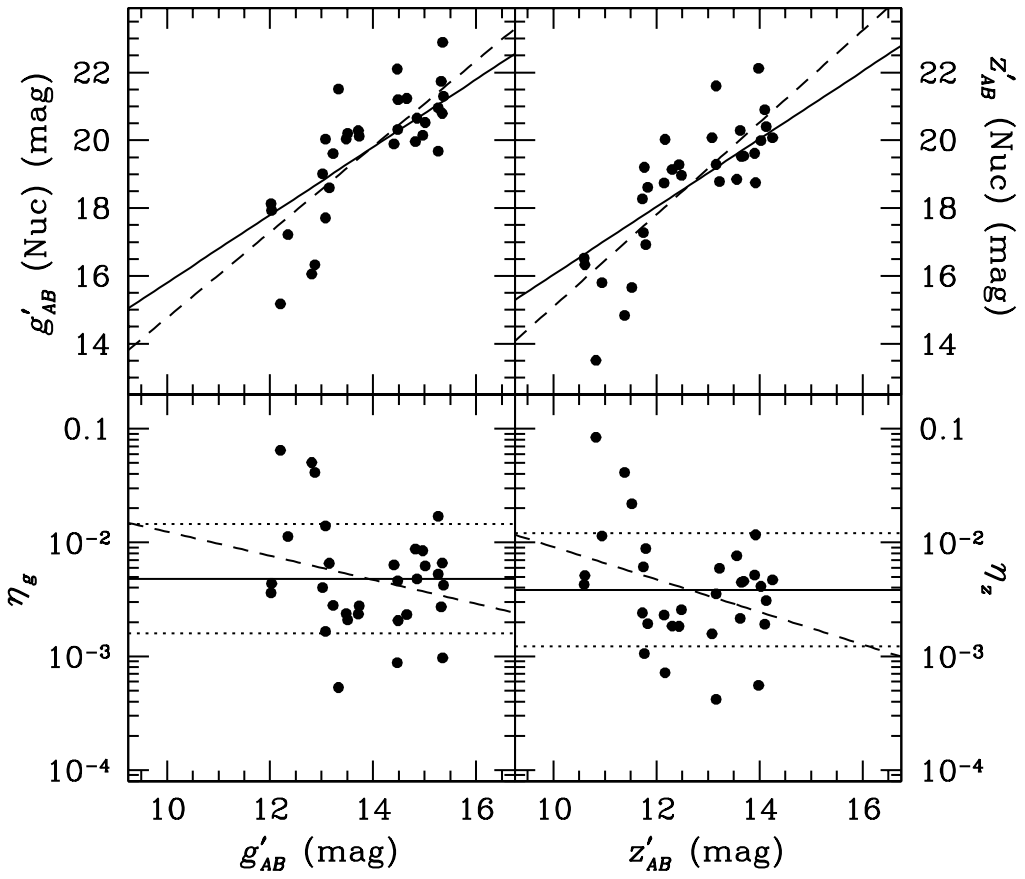

Figure 3.6 *Top*: Nucleus magnitude plotted against host galaxy magnitude for the 30 galaxies found to be nucleated; results for the g and z bands are shown on the left and right, respectively. The lines show the best fit relations, with the slope held fixed at unity (*solid*) and allowed to vary (*dashed*). *Bottom*: Nucleus-to-galaxy luminosity ratio η against host galaxy magnitude, for the g-band (*left*) and z-band (*right*). The solid and dotted lines show the mean and one standard deviation, respectively. The dashed line shows the best fit relation.

Table 3.2. Nucleus and Globular Cluster Luminosity Function Best-Fit Values

Data Set	$\bar{m}_n^0$	σ_n	$\bar{m}_{gc}^0$	σ_{gc}
Fornax, g	19.72 ± 0.32	1.79 ± 0.23	24.00 ± 0.01	1.08 ± 0.01
Fornax, z	18.67 ± 0.35	1.94 ± 0.25	22.91 ± 0.01	1.09 ± 0.01

galaxies in our sample), and scale it down by 91% (since we have 34 galaxies in this magnitude range, 31 of which are nucleated), and shift the Schechter function over by +5.8 mag (which corresponds to an η_g of 0.48%) and −0.4 mag (to convert from B to g). Finally, we convolve it with a Gaussian with $\sigma = 1.2$ mag, the standard deviation of η_g, to take the scatter around $\langle \eta_g \rangle$ into account. The resulting function plotted over the nucleus luminosities shows good agreement, although with a few bright outliers.

3.5 Structural Properties

Thanks to the excellent resolution of the ACS, it is possible to measure sizes for the nuclei (which appear unresolved in ground-based seeing; i.e., $1''$ corresponds to ≈100 pc at the distance of Fornax). In Figure 3.9, we present a comparison of sizes of the nuclei and the ACSFCS GC candidates. On average, the nuclei are larger in size and have a much larger spread in distribution than the GCs, although the overlap between the two distributions demonstrates that the most compact nuclei are very nearly the same size as typical GCs. The two most prominent outliers are the nuclei of FCC 63 and FCC 47; both of these galaxies both have complex central structure that may be contributing to their large size. Regardless, Figure 3.9 clearly demonstrates that the nuclei have a size distribution that peaks at compact sizes, and an extended tail populated by larger nuclei. The median sizes of the full sample are found to be $0\farcs073$ (7.1 pc) and $0\farcs071$ (6.8 pc) in the g- and z-bands, respectively.

Another comparison that can be made between the nuclei and GCs is their surface brightness. Figure 3.10 plots average surface brightness within the half-light radius:

$$\langle \mu_h' \rangle = m' + 0.72526 + 2.5 \log(\pi r_h^2) \tag{3.6}$$

against magnitude for the two types of objects. The lines in this figure are not

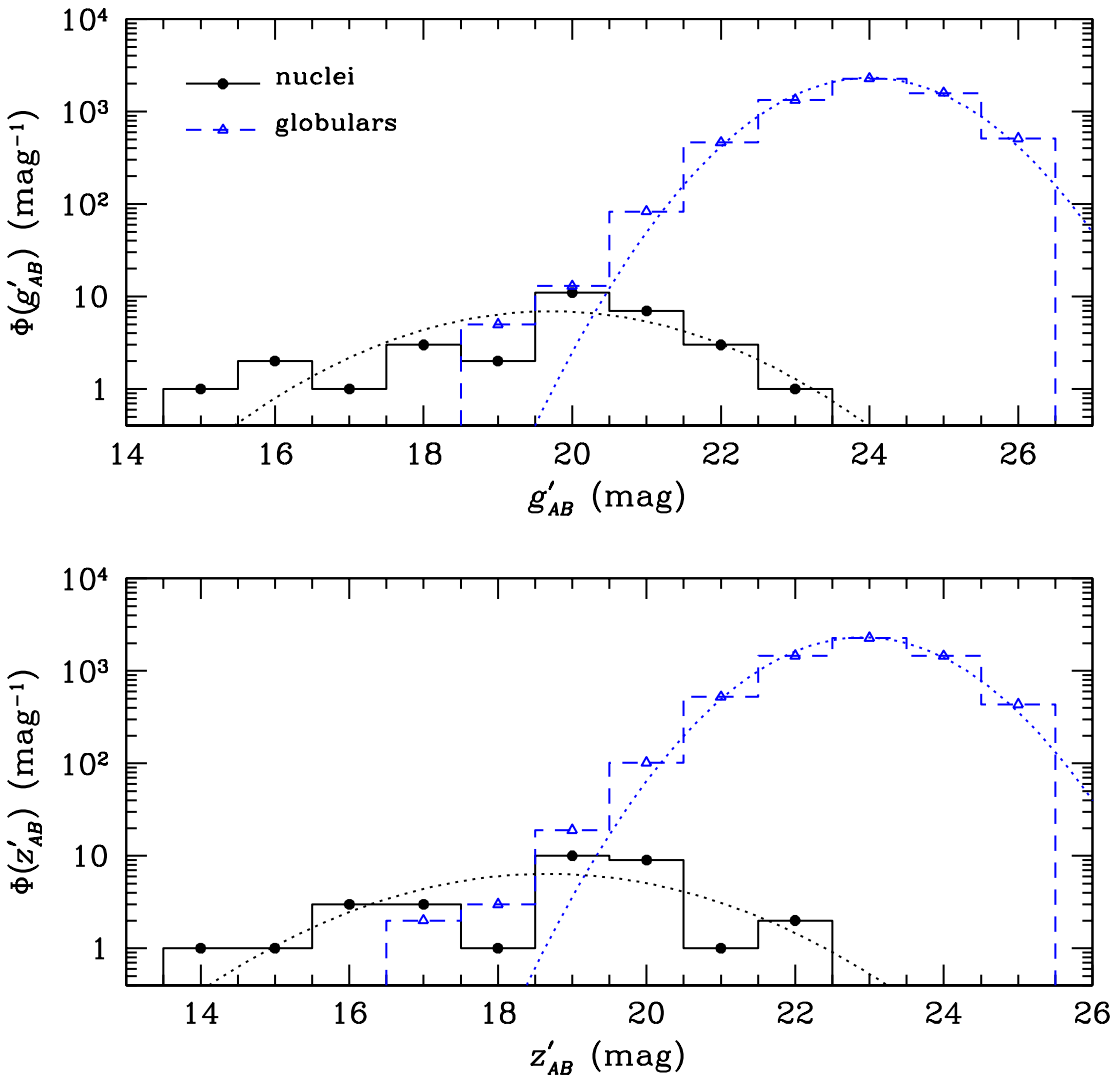

Figure 3.7 Luminosity function for the nuclei in the g- (*top*) and z-bands (*bottom*). The luminosity function for the GC candidates in the ACSFCS is plotted for comparison. Both data sets are fitted with a normalized Gaussian.

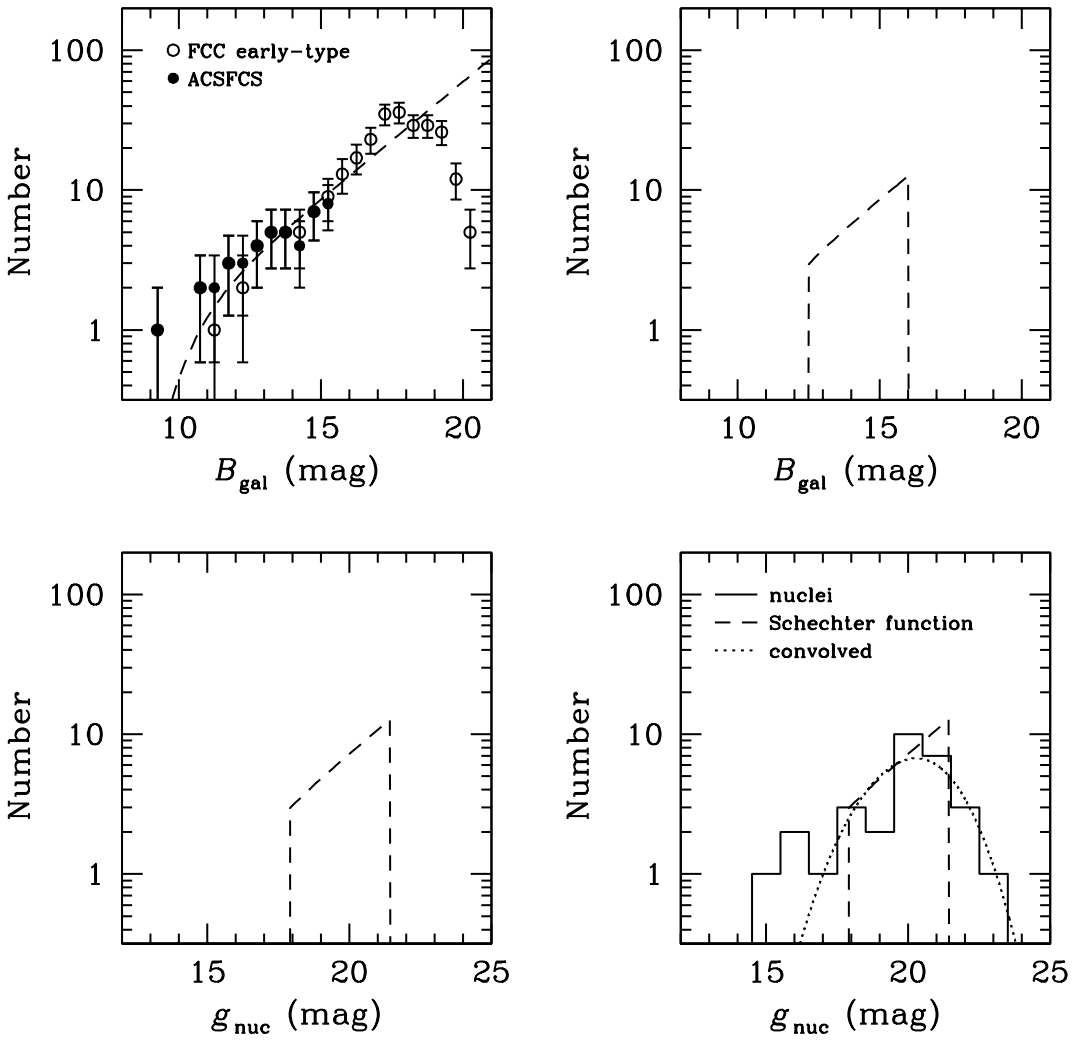

Figure 3.8 *Top left*: A Schechter function plotted over the B-band galaxy luminosity distribution for all early-type galaxies in the FCC (open circles) and the ACSFCS sample (filled circles). *Top right*: The previous Schechter function truncated at $B_T = 12.5$ and 16, and reduced by 91%, so that it represents the nucleated galaxies in our sample. *Bottom left*: The previous Schechter function shifted by +5.8 mag, corresponding to a constant η_g of 0.47%, and −0.4 mag to convert from B to g. It should now be roughly correspond to the nucleus luminosity distribution, although without taking into account the scatter. *Bottom right*: The luminosity distribution of the nuclei (solid line), the previous Schechter function (dashed line), and the same Schechter function convolved with a Gaussian of $\sigma = 1.2$ mag, the standard deviation of η_g (dotted line).

best-fit lines — rather, the dotted line is the expected scaling relation for nuclei formed through GC mergers (Bekki et al., 2004), while the dashed line is set to a constant half-light GC radius of 2.7 pc. We find the average surface brightness to be 16.3 mag arcsec^{-2} and 15.0 mag arcsec^{-2} in the g- and z-bands, respectively. The standard deviations were found to be 1.2 mag arcsec^{-2} in g and 1.4 mag arcsec^{-2} in z; the larger scatter in z possibly attributed to the greater difficulty of measuring the nucleus parameters in this band due to a slightly more complex PSF structure (see, e.g., Sirianni et al., 2005) and reduced contrast between the nuclei and their host galaxies.

3.6 Nuclei Colours

As in C06, we find a relation between nuclei colours and their host galaxies, as well as a nucleus colour-magnitude relation. Specifically, the brighter nuclei tend to have redder colours, and reside in more luminous host galaxies, as is shown in Figure 3.11. A great deal of scatter is seen for the brighter galaxies, which are labelled with their FCC number; this scatter was also seen in C06, but it seemed that the bright nuclei were preferentially red. Since the scatter seen here is seen in both the red and blue regimes, its cause may be attributed to difficulty in measuring the nucleus parameters in such high surface brightness regions, or, because these larger galaxies may have more complex formation and enrichment histories in their inner regions, perhaps fuelled by mergers, gas inflow, star formation, and GC accretion, leading to observed deviations from the general trend.

We plot the following line, which has been fitted only to the nuclei belonging to galaxies fainter than $B_T = 13.5$:

$$(g - z)'_{\rm AB} = -(0.048 \pm 0.043)\, g'_{\rm AB} + (2.0 \pm 0.9) \tag{3.7}$$

Figure 3.12 is the same as Figure 3.11, but with colours derived from a 4-pixel aperture instead of an integrated Sérsic profile. The same nuclei colours and trends are seen, including the locations of the outliers (save for FCC 43); thus indicating that our conclusions from the previous plot are model-independent. The line of best fit to galaxies fainter than $B_T = 13.5$ is given by,

$$(g - z)'_{\rm AB} = -(0.097 \pm 0.037)\, g'_{\rm AB} + (2.9 \pm 0.8). \tag{3.8}$$

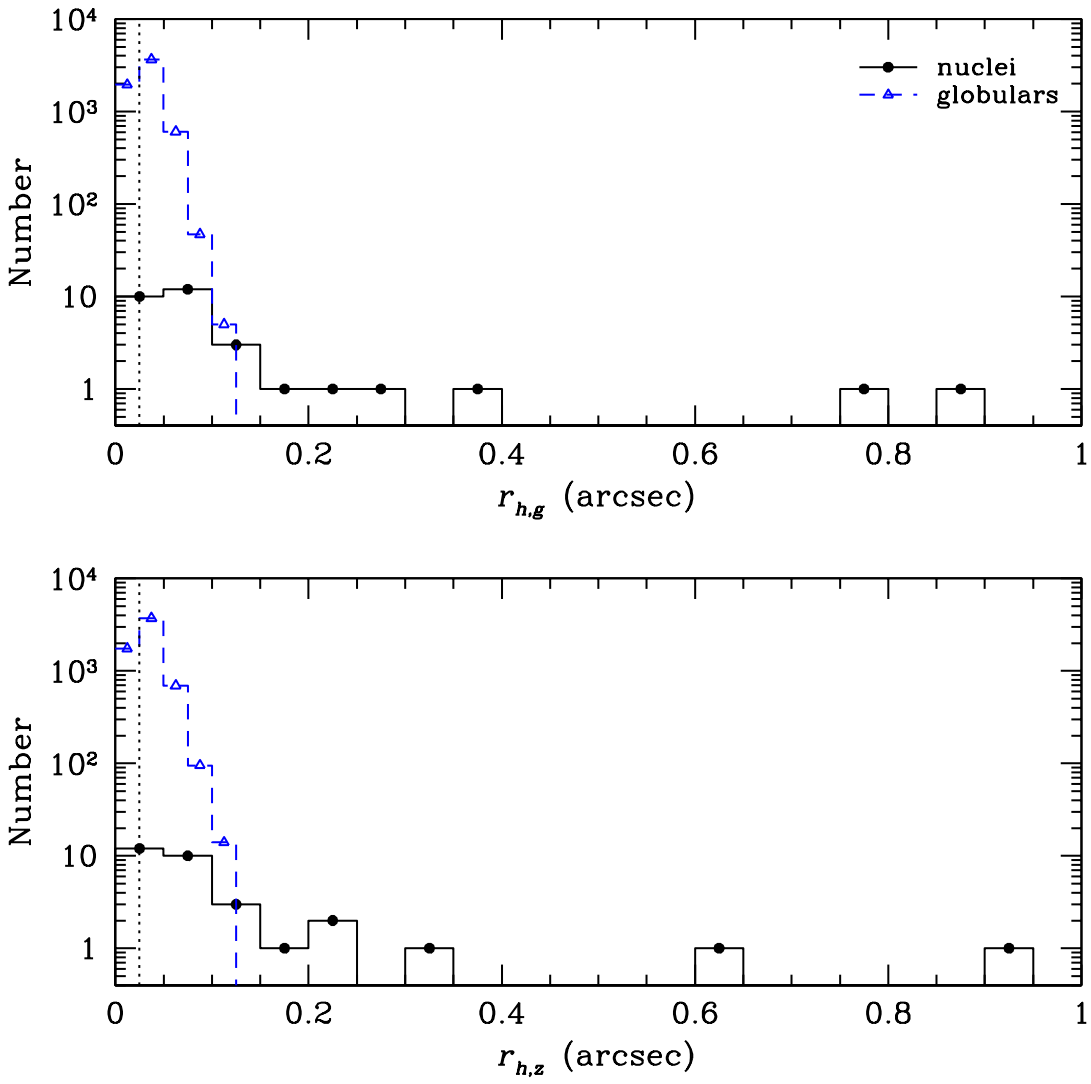

Figure 3.9 Distribution of half-light radii of the 31 nuclei identified in this study. The distribution of the of the candidate GC half-light radii is also shown. The vertical dotted lines indicate the adopted resolution limit of $\sim 0\farcs025$.

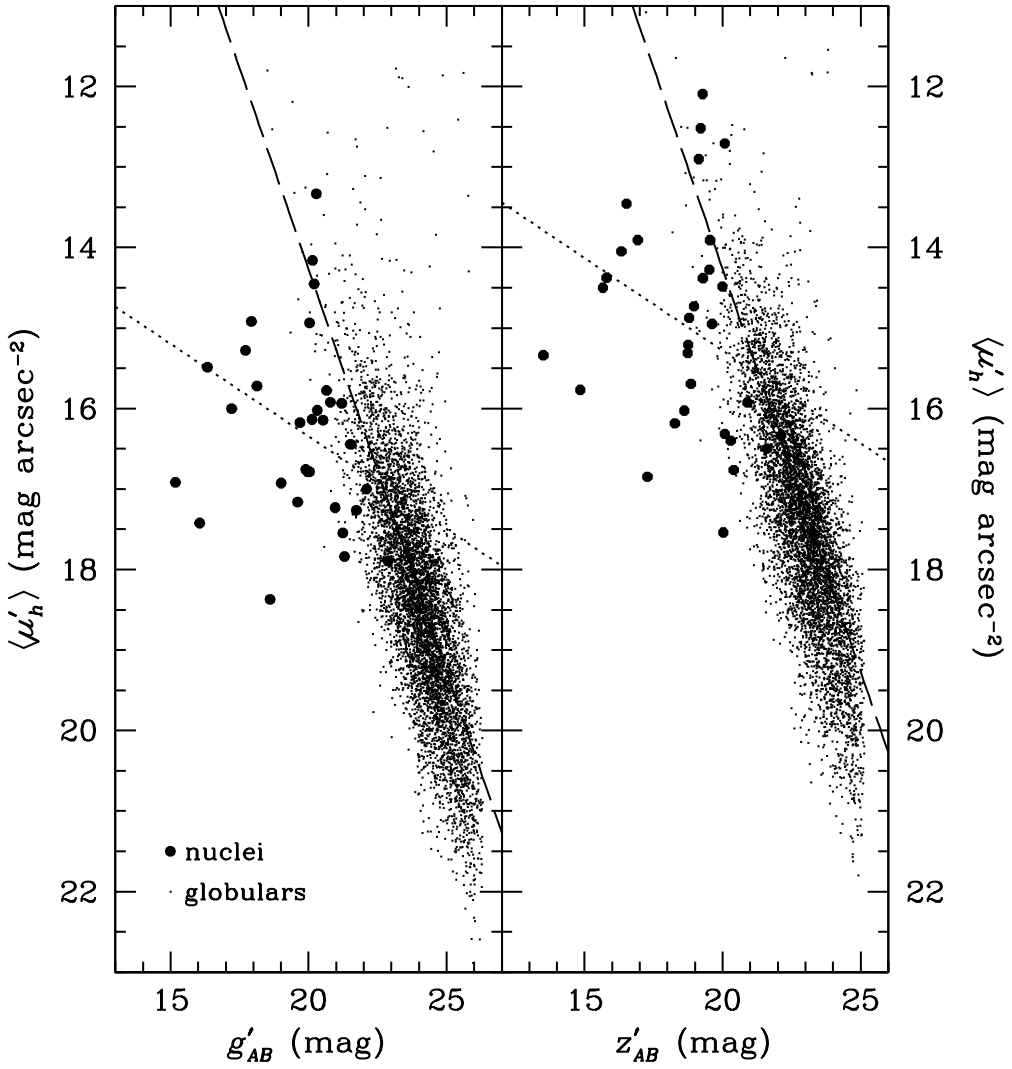

Figure 3.10 Average surface brightness within half-light radius plotted against magnitude for the 31 nuclei identified in this study, where both values are either in the g-band (*left*) or the z-band (*right*). The dotted line is the expected scaling relation for nuclei if they are formed through GC mergers (Bekki et al., 2004), $\langle \mu_h \rangle \propto \mathcal{L}^{0.23}$, where a least-squares fit to our data was used to determine the intercept. The dashed line is the scaling relation for GCs assuming a "universal" half-light radius of $\langle r_h \rangle \approx 2.7$ pc ($\sim 0''.28$ angular size in Fornax). (Paper VII).

We also examine how the colours of the nuclei compare to those of the host galaxies. In Figure 3.13, we show nucleus colour plotted against host galaxy colour. A least-squares fit gives the relation

$$(g-z)'_{\rm AB,nuc} = (1.8 \pm 0.4)\,(g-z)'_{\rm AB,gal} - (1.3 \pm 0.6), \tag{3.9}$$

which is indicative of a positive trend between galaxy and nucleus colour: i.e., bluer nuclei tend to lie in bluer host galaxies, and vice-versa. The nuclei are also found to have a larger range in colours, and are in most cases bluer than their host galaxy.

In Fig 3.14, we show galaxy and nucleus colours as a function of host galaxy luminosity. The colours of both the galaxies and the nuclei are found to become redder with increasing host luminosity, as indicated by the following least-squares fit relation,

$$\begin{aligned}(g-z)'_{\rm AB,nuc} &= -(0.072 \pm 0.010)\,B_T + (2.3 \pm 0.1)\\ (g-z)'_{\rm AB,gal} &= -(0.17 \pm 0.04)\,B_T + (3.4 \pm 0.6).\end{aligned} \tag{3.10}$$

We find that nucleus colours vary more steeply with host luminosity than those of the galaxies, due to their larger range of values. Examining the offset between galaxy and nucleus colours reveals that those nuclei found to be more red than their host lie predominantly in high-luminosity galaxies. The least-squares relation for the colour difference is given by

$$\delta_{(g-z)'_{\rm AB}} = (0.098 \pm 0.039)\,B_T - (1.1 \pm 0.6). \tag{3.11}$$

On average, we find the nuclei to be more blue than their hosts by 0.27 ± 0.25 mag. If we exclude the nuclei in galaxies with $B_T < 13$ (the regime in which the nuclei are systematically found to be more red than their hosts) we obtain a mean offset of 0.32 ± 0.22 mag.

3.7 Age and Metallicity Distributions

Given the well known age-metallicity degeneracy, we are severely limited in our ability to derive ages and metallicities for the nuclei from broadband colours alone. Nevertheless, the colours do allow us to place some broad constraints on the mix of stellar populations in the nuclei. In the top panel of Figure 3.15, we show the [Fe/H]-

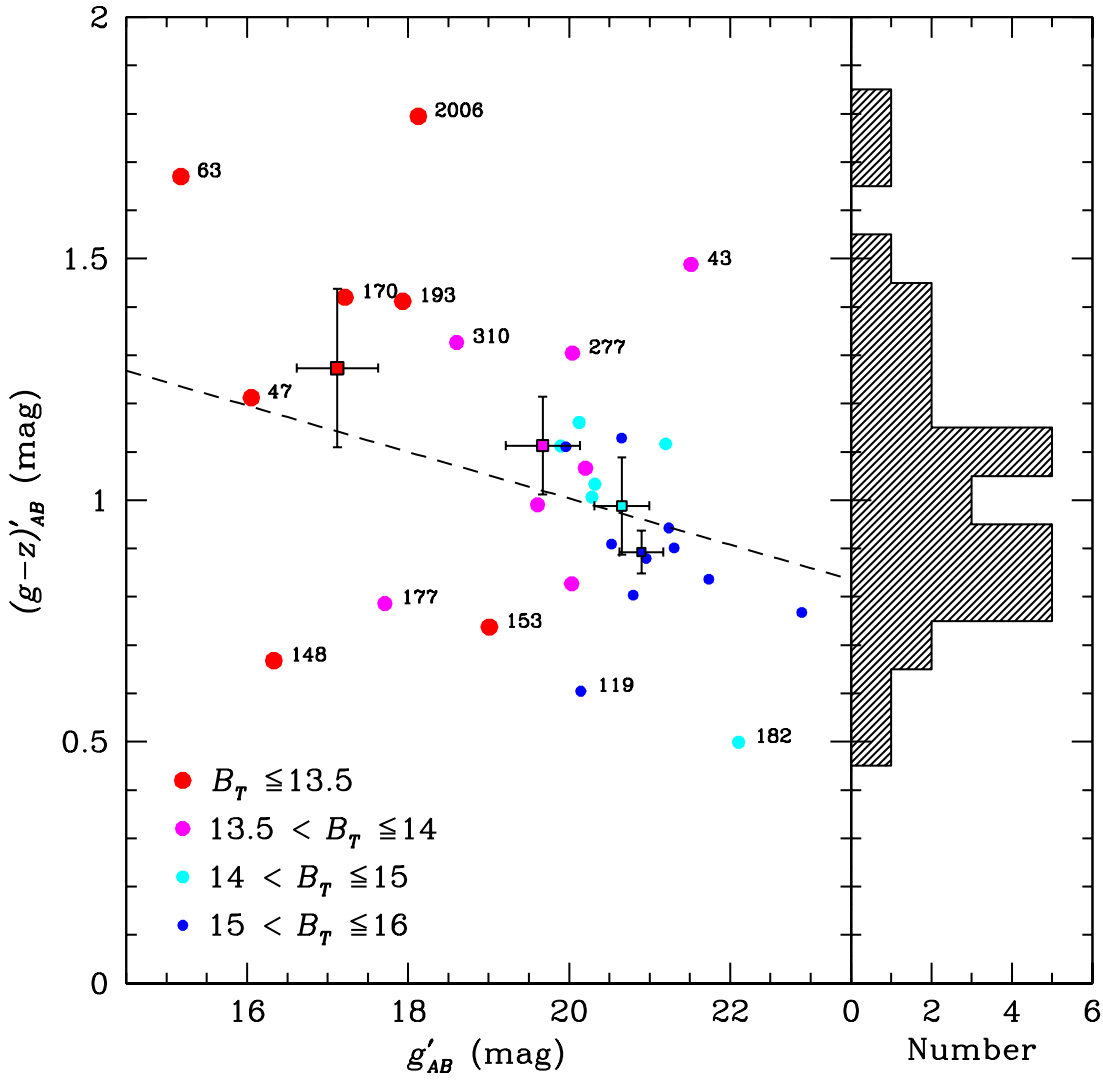

Figure 3.11 *Left*: Integrated colour-magnitude diagram for the 31 nuclei identified in this study. The sizes of the circles are proportional to the magnitude of the host galaxy. The dashed line is the best fit for galaxies fainter than $B_T = 13.5$. Galaxies with $B_T \leq 13.5$ or with unusually red or blue nuclei are labelled. The mean and standard error of the mean for each luminosity bin are indicated by the outlined squares. *Right*: Histogram of the nuclei colours showing a broad distribution that is skewed to blue colours.

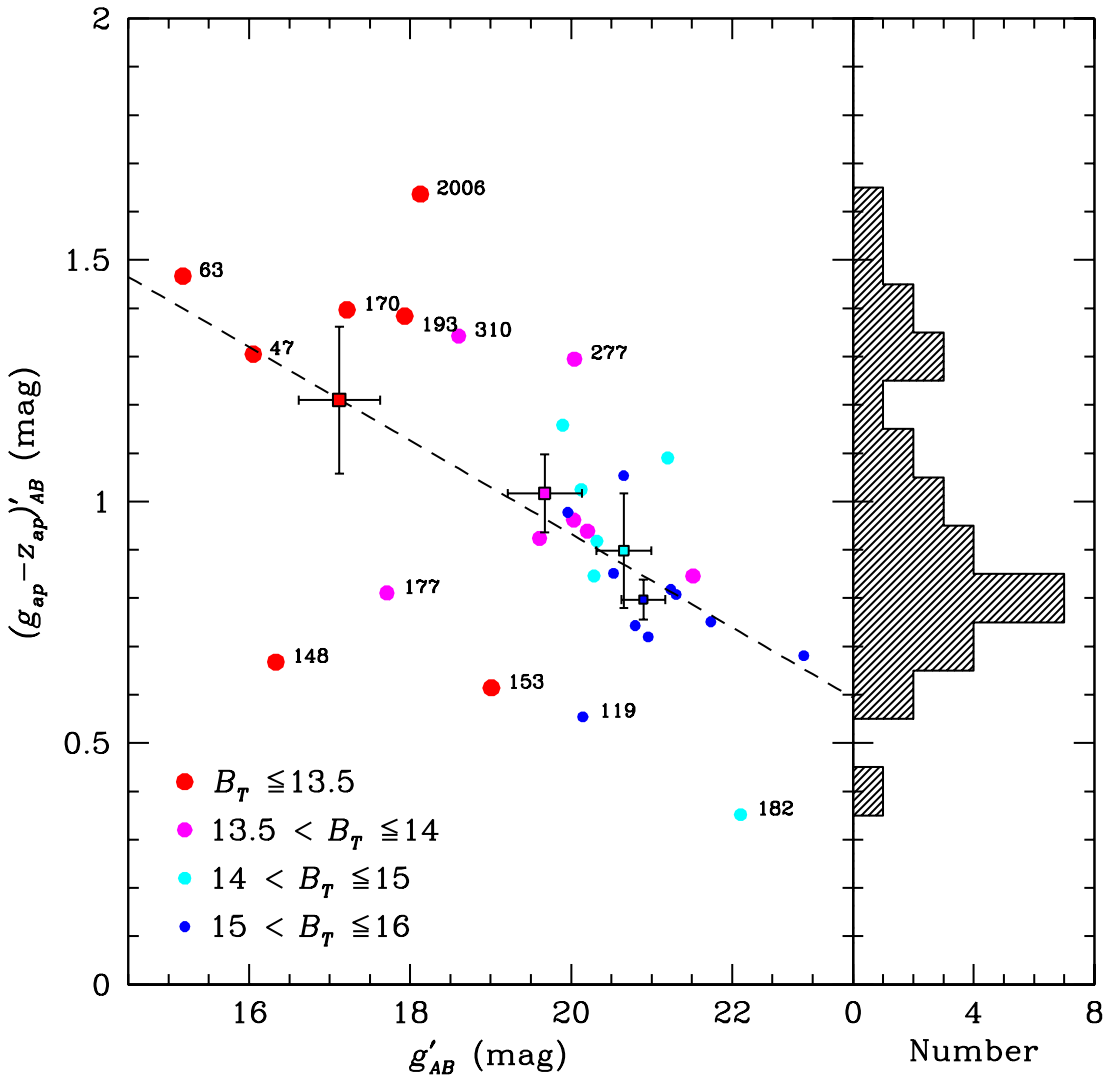

Figure 3.12 Same as Figure 3.11, but using aperture magnitudes instead of integrated models.

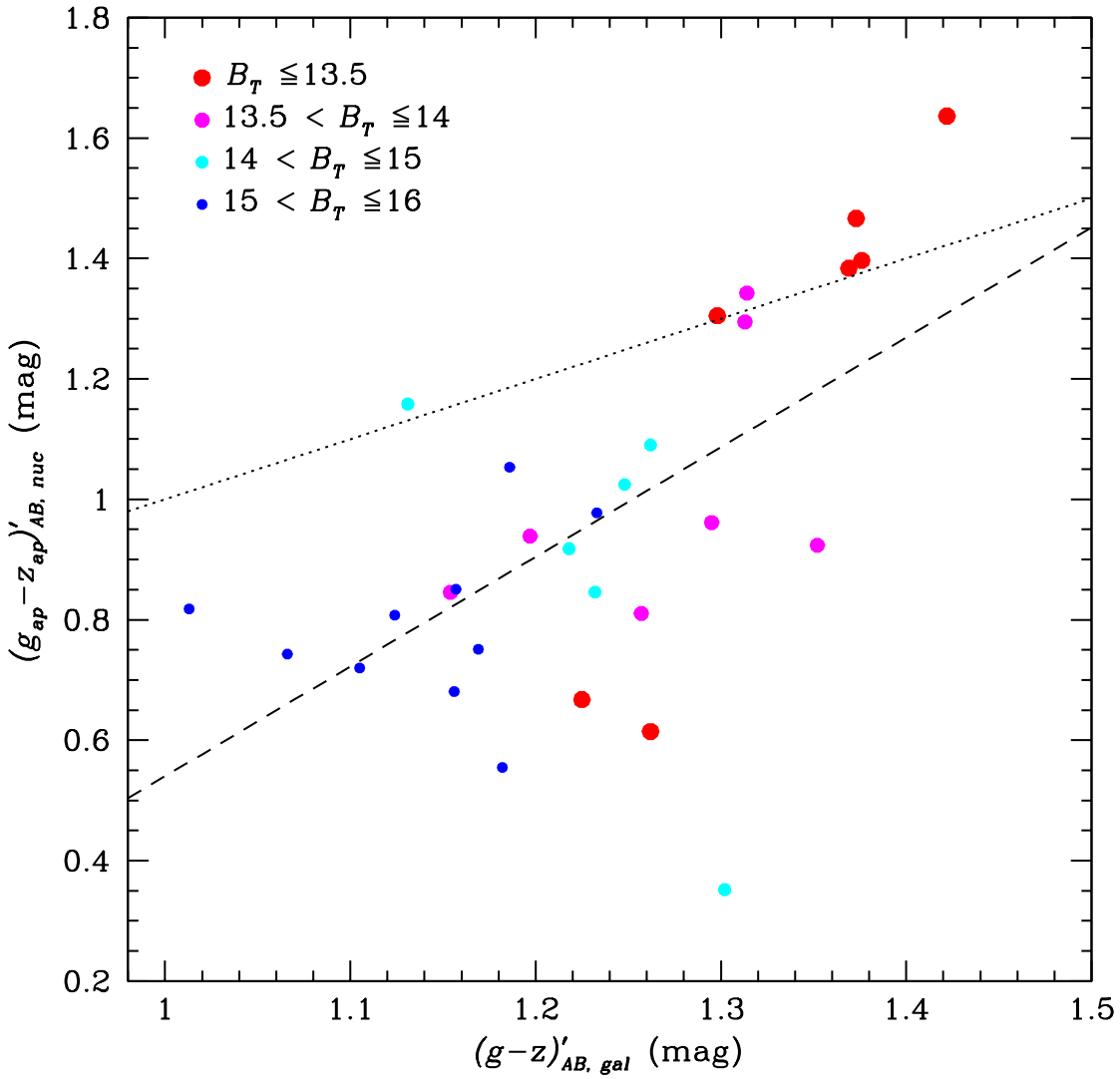

Figure 3.13 Aperture derived nucleus colours plotted against host galaxy colours from Paper V. The sizes of the circles are proportional to the magnitude of the host galaxy. The dotted line indicates equal colours, and the dashed line is the best fit for all plotted points. On average, nuclei are ≈ 0.3 mag bluer than their host galaxies (see text for details).

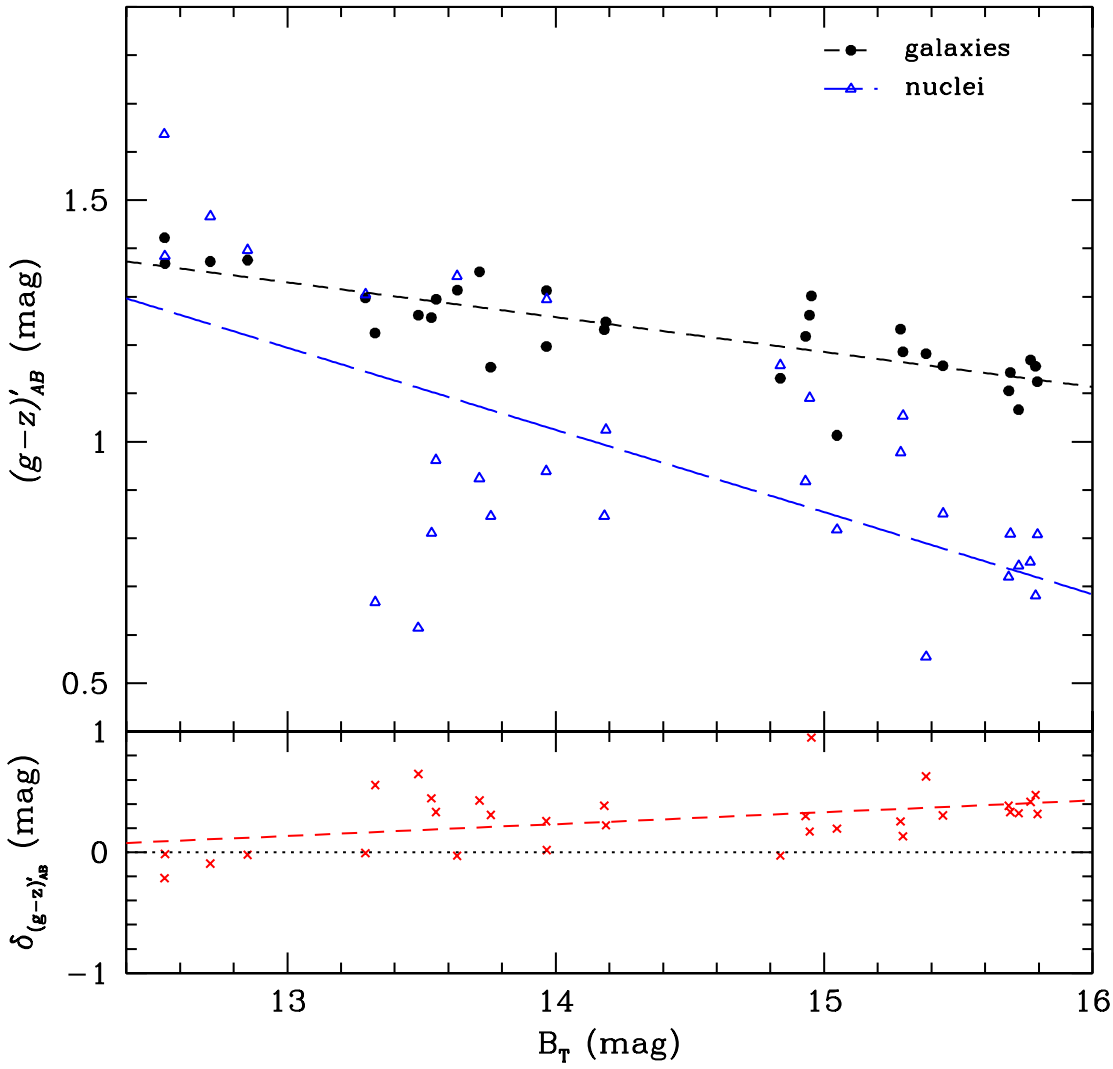

Figure 3.14 *Top*: Galaxy colours (black closed circles, from Paper V) and aperture determined nucleus colours (blue open triangles) plotted against host galaxy magnitude. Only galaxies that we find to be nucleated are shown. The black short-dashed and blue long-dashed lines are the best fit to the galaxies and nuclei, respectively. *Bottom*: Difference between galaxy and nucleus colour, as a function of host galaxy magnitude. The black dotted line marks a difference of zero, while the red short-dashed line shows the best fit to all points.

$(g-z)'_{AB}$ relations which will be used to estimate the nucleus metallacities. Assuming a Chabrier (2003) initial mass function, we plot the simple stellar population models from Bruzual & Charlot (2003) with ages of $\tau = 1$, 2, 5, and 10 Gyr. Of course, it is quite likely that the nuclei, as a population, show a distribution of ages. In addition, we are comparing the colours to the predictions of single-burst models, but it is quite possible that individual nuclei are composed of multiple populations that formed in discrete bursts (e.g., Bica et al., 1990; Sarzi et al., 2005; Seth et al., 2006; Rossa et al., 2006).

With these caveats in mind, the linear interpolation between the points from the models is plotted in Figure 3.15. The top panel also shows an empirical colour-metallicity relation from Peng et al. (2006), which was derived using 95 GCs from the Milky Way, M49, and M87. Histograms of the nuclei metallicities, determined from the above models using the nucleus colours, are plotted in the bottom panel of Figure 3.15, and the mean nuclei metallicities for each model are shown in Table 3.3. From this figure, it can be seen that using a single formation epoch to describe the full sample gives at least a few nuclei with unusually high or low metallicities (part of this scatter may be related to errors in the colours, which can be large for the nuclei in the brighter galaxies; see above). For assumed ages of 1 or 2 Gyr, many nuclei will have metallicities greater than several times solar. Conversely, for an age of 10 Gyr, or assuming the same relation as GCs, a handful of nuclei would have metallicities below ≈ -2.5. The true distribution of ages and metallicities is likely to lie somewhere between these extremes. For instance, with ages in the range 5 – 10 Gyr, the inferred metallicity distributions peak at [Fe/H] ~ -0.8 to -1.3 dex. Using the GCs colour-metallicity relation gives a comparable value of -0.9 dex. These numbers are consistent with those found in Virgo by C06, although slightly more metal-poor by ~ 0.3 dex.

Table 3.3. Nucleus Mean Metallicities for Assumed Model and Age

$(g-z)_{0^-}$ [Fe/H]	τ (Gyr)	$\langle$[Fe/H]$\rangle$ (dex)
Bruzual & Charlot (2003)	1	$+0.66 \pm 0.66$
	2	-0.22 ± 0.88
	5	-0.84 ± 0.92
	10	-1.3 ± 1.2
Peng et al. (2006)	...	-1.2 ± 1.0

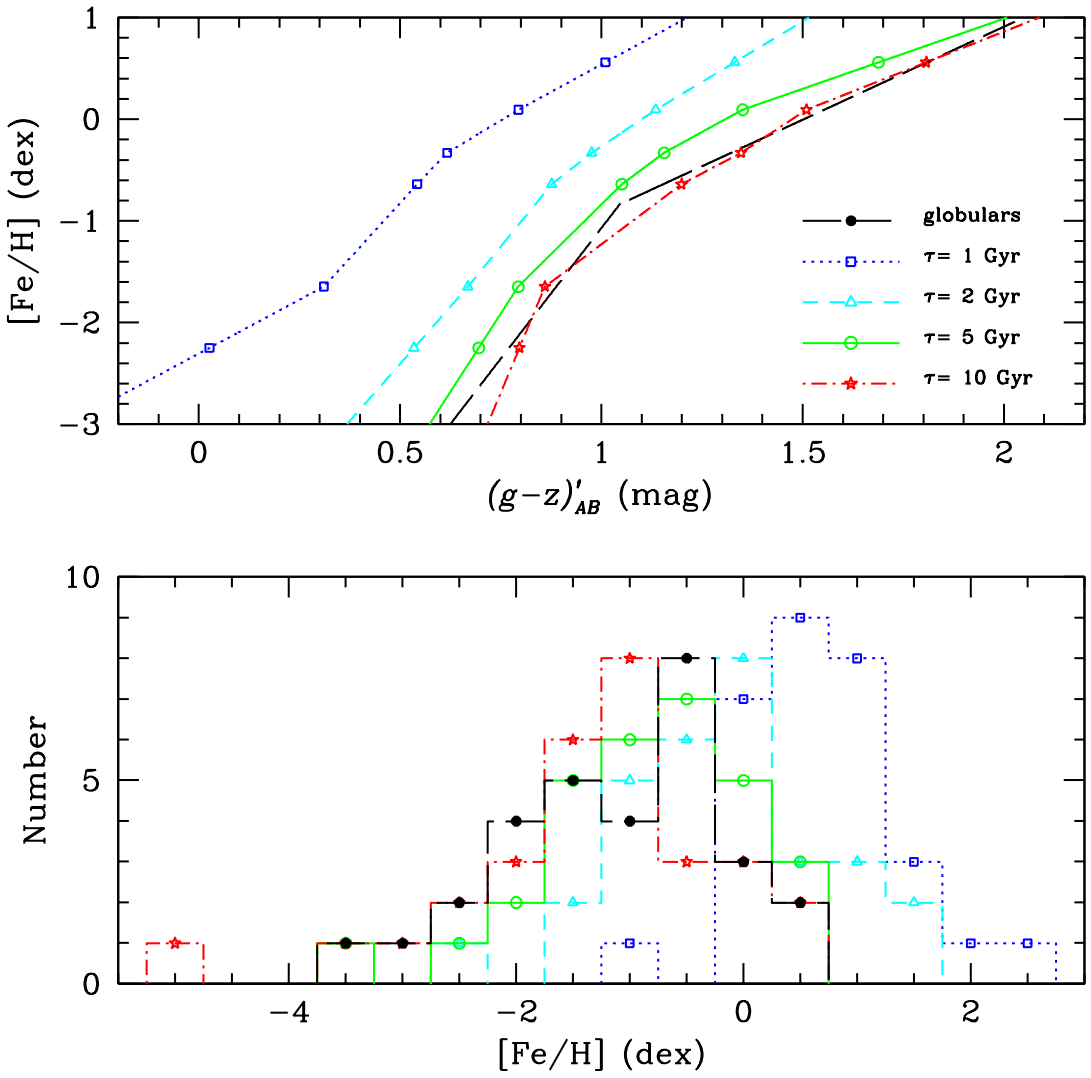

Figure 3.15 *Top*: Coloured lines show the theoretical colour-metallicity relations for Bruzual & Charlot (2003) simple stellar populations of ages τ = 1, 2, 5 and 10 Gyr, with Chabrier (2003) initial mass functions. The black line shows the empirical colour-metallicity relation for 95 GCs from Peng et al. (2006). *Bottom*: Histogram of the derived nucleus metallicities based on the above models.

Chapter 4

Discussion

4.1 Comparison to the ACSVCS

As described in Chapter 1, this survey was preceded by a similar study of 100 early-type galaxies in Virgo, known as the ACSVCS. An analogous investigation into the properties of the nuclei in Virgo galaxies for the ACSVCS was performed by C06. The motivation for undertaking a methodologically similar analysis of the nuclei in both Virgo and Fornax was to enables us to perform a uniform comparison of nucleus properties in two very different cluster environments. This in turn allows us to assess the extent to which environment plays a role in nucleus formation and evolution.

In the following section, we will directly compare results from the two surveys. The Virgo sample presented here only has 99 members, since VCC 575 has since been omitted due to extreme dust in the central regions that cause difficulty with the fit. While C06 used King profiles for the nuclei in their paper, they have updated their results with fits to the nuclei using Sérsic profiles, in order to allow a fair comparison of properties between the two studies. Although 67 galaxies from the Virgo sample are found to be nucleated, we only present photometric properties for 63, as the revised fitting procedure using Sérsic profiles is still in progress. To calculate absolute magnitudes and sizes, distances from Mei et al. (2005) for Virgo galaxies and Paper V for the Fornax galaxies were used. We note that the two surveys have slightly different cutoff magnitudes from the VCC and FCC ($B_T \sim 16$ and ~ 15.5 for Virgo and Fornax, respectively) and that the distance modulus of Fornax is ~ 0.5 mag larger than that of Virgo (Paper V). Therefore, the Virgo galaxies can reach absolute magnitudes ~ 1 mag fainter than those in Fornax.

4.1.1 Frequency of Nucleation

In Fig 4.1, we plot the frequency of nucleation of the Virgo and Fornax programme galaxies, as a function of their absolute blue magnitude. The Virgo galaxies appear in red, and the Fornax galaxies are denoted in blue. In the top plot, we show overlaid histograms of all galaxies (hatched) and nucleated galaxies (solid). This figure visualizes how the Virgo galaxy magnitudes extend to ~ 1 mag below those of Fornax, as explained above. Our Virgo sample contains 99 galaxies, 67 of which are found to be nucleated, so we obtain a total frequency of nucleation, $f_n = 68\%$, which is in good agreement with $f_n = 72\%$ that we found for our full Fornax sample.

The bottom plot shows frequency of nucleation (f_n) for each luminosity bin. Both clusters exhibit very similar f_n properties, with $f_n = 0$ for the bright galaxies, while fainter than galaxy magnitudes of $M_B \sim -19.5$, f_n continuously stays above $\sim 70\%$. Since our Virgo sample has 83 galaxies below $M_B = -19.5$, and our Fornax sample has 35, we find the total frequency of nucleation for galaxies fainter than $M_B = -19.5$ to be 81% for Virgo and 89% for Fornax.

Both C06 and this study have demonstrated that this sharp increase in frequency of nucleation compared to previous ground based studies (the VCC and FCC) is due mainly to surface brightness selection (see Figure 7 and 8 in C06 and Figure 3.2 and 3.3 in this work), and to a lesser extent, to the improved resolution and depth offered by the ACS imaging. That is, the excellent angular resolution of HST has allowed us to uncover previously undetected nuclei in both very high surface brightness galaxies, where the nuclei are difficult to distinguish from the main body, and low luminosity galaxies, in which the nuclei may lie below the magnitude limit of the older photographic surveys.

4.1.2 Nucleus-to-Galaxy Luminosity Ratio

As in § 3.3 and Figure 3.6, absolute nucleus magnitude has been plotted against absolute galaxy magnitude in the top panels of Figure 4.2. Lines given by Eq. 3.3 have been fitted using least squares to the Virgo and Fornax samples separately as well as together, and the parameters are given in Table 4.1. These results are in agreement to within error for both galaxy samples, although we note that the lines fit to the Fornax sample show a stronger deviation away from a unity slope.

We also plot nucleus-to-galaxy luminosity ratio η as a function of absolute galaxy magnitude, in the bottom panel of Figure 3.6. The values for the mean and standard

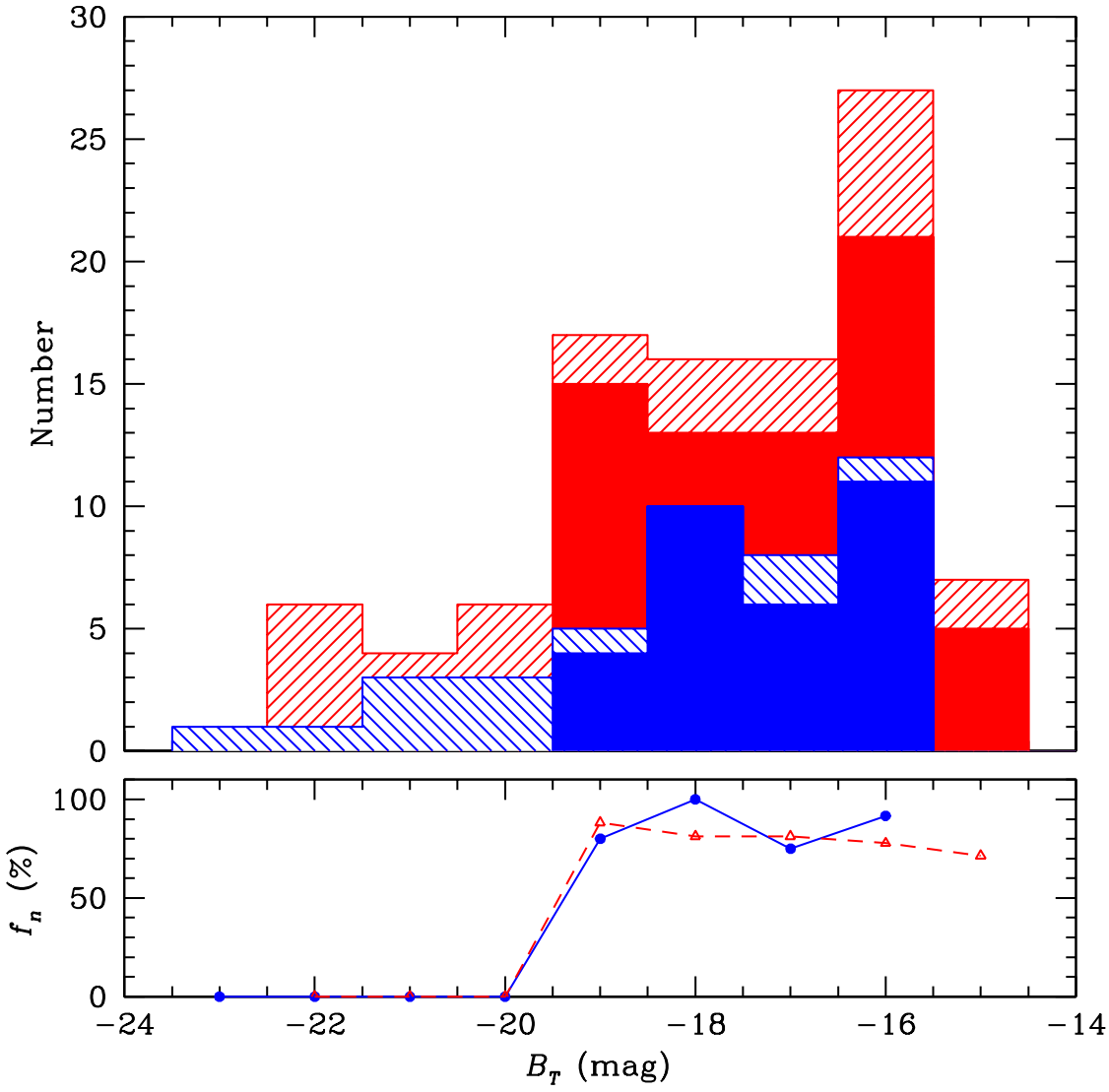

Figure 4.1 Same as Figure 3.1, but using absolute magnitudes and including the 99 ACSVCS and 43 ACSFCS programme galaxies. *Top*: Luminosity distribution of the programme galaxies for Virgo (red and hatched in the upwards-right direction) and Fornax (blue and hatched in the downwards-right direction). The overlaid solid histograms show the distribution of the 67 Virgo and 31 Fornax galaxies found to be nucleated by the ACSVCS and ACSFCS. *Bottom*: The percentage of galaxies found to be nucleated (f_n) for Virgo (red open triangles) and Fornax (blue filled circles).

Table 4.1. Virgo and Fornax Nucleus-to-Galaxy Luminosity Ratio Best-Fit Values

Data Set	m_1	b_1	b_2	$\langle\eta\rangle$	σ	m_η	b_η
Fornax, g	1.24 ± 0.20	9.96 ± 3.4	5.80 ± 0.22	-2.32	0.48	-0.0950 ± 0.0782	-3.98 ± 1.38
Virgo, g	1.01 ± 0.15	6.22 ± 2.66	6.07 ± 0.20	-2.43	0.64	-0.0033 ± 0.0606	-2.49 ± 1.06
Both, g	1.07 ± 0.12	7.21 ± 2.12	5.98 ± 0.15	-2.39	0.59	-0.0280 ± 0.0484	-2.88 ± 0.85
Fornax, z	1.33 ± 0.19	12.3 ± 3.5	6.04 ± 0.22	-2.42	0.50	-0.132 ± 0.075	-4.91 ± 1.42
Virgo, z	1.17 ± 0.15	9.28 ± 2.88	6.14 ± 0.22	-2.38	0.78	-0.0424 ± 0.0708	-3.17 ± 1.33
Both, z	1.21 ± 0.12	10.0 ± 2.3	6.10 ± 0.16	-2.39	0.70	-0.0639 ± 0.0542	-3.59 ± 1.02

deviation of η, as well as those from a least-squares fit line to η versus galaxy magnitude, are given in Table 4.1. Taking the mean nucleus-to-galaxy luminosity ratio of both data sets combined, we obtain the following values for each band:

$$\begin{aligned} \langle\eta_g\rangle &= 0.40\% \pm 0.06\% \\ \langle\eta_z\rangle &= 0.41\% \pm 0.07\%, \end{aligned} \tag{4.1}$$

which gives a mean value for both bands of

$$\langle\eta\rangle = 0.41\% \pm 0.04\%, \tag{4.2}$$

where the errors quoted are the standard error on the mean.

Although η is roughly constant, in § 3.3 we noted that there is a possible trend of increasing nucleus-to-galaxy luminosity ratio with decreasing galaxy magnitude. Figure 4.2 shows that this effect is more prominent in the Fornax sample than in Virgo. However, we do not reject the null hypothesis, as the F-statistic for these fits has a p-value > 0.05 in all cases.

4.1.3 Nucleus Luminosity Function

In Figure 4.3, histograms of the nucleus luminosities for both our Virgo and Fornax sample are plotted. The parameters of the maximum-likelihood fit of a normalized Gaussian to each sample are given in Table 4.2. Although we find that the Fornax nuclei have a higher $\bar{m}_n^0$ value by ~ 0.4 mag, this can be attributed to the difference in the absolute magnitude limit of the surveys. A constant nucleus-to-galaxy luminosity ratio is equivalent to constant magnitude difference between a nucleus and its host galaxy. Therefore, because the Virgo programme galaxies extend to magnitudes $\sim$ 1 mag fainter than Fornax, we expect the luminosity function of the nuclei to

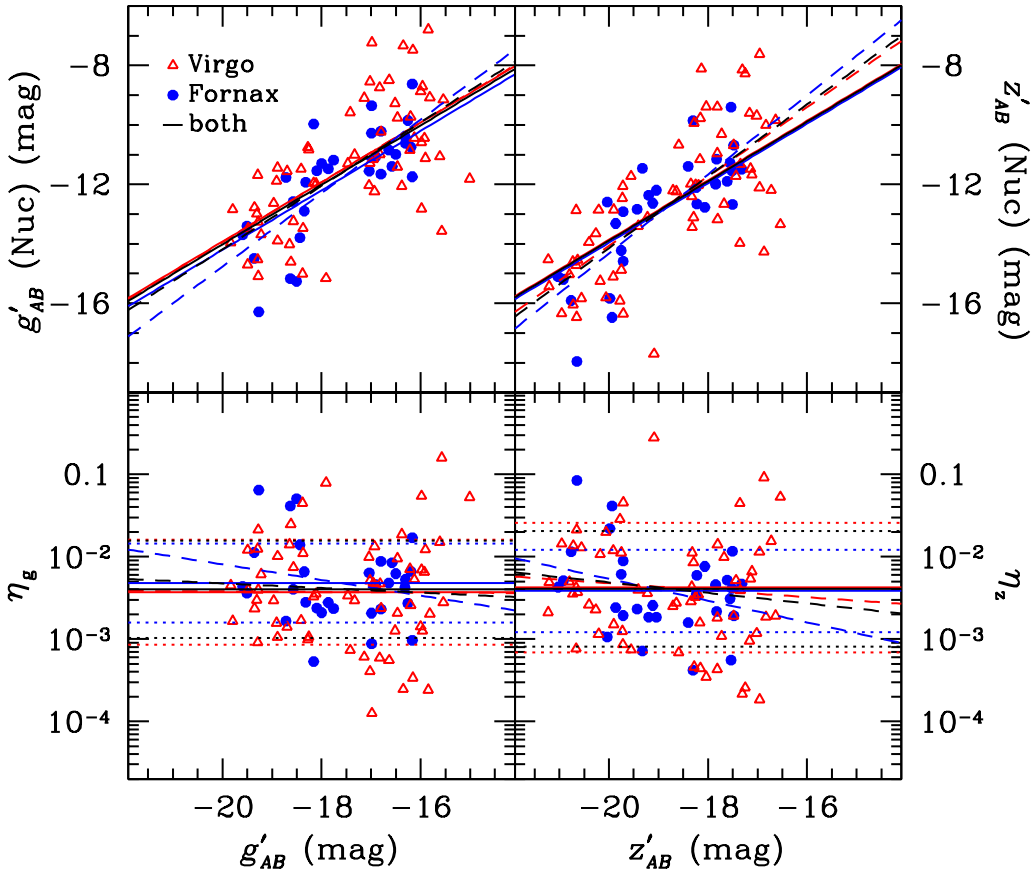

Figure 4.2 Same as Figure 3.6, but using absolute magnitudes and including 63 ACSVCS and 31 ACSFCS nuclei. *Top*: Nucleus magnitude plotted against host galaxy magnitude, for the Virgo (red open triangles) and Fornax (blue filled circles) galaxies found to be nucleated, in the g-band (*left*) and z-band(*right*). The lines show the best fit relations, with the slope held fixed at unity (*solid*) and allowed to vary (*dashed*). The red and blue lines correspond to fits to the Virgo and Fornax samples respectively, while the black lines show the fits to the combined sample. *Bottom*: Nucleus-to-galaxy luminosity ratio η against host galaxy magnitude, for the g-band (*left*) and z-band (*right*). The solid and dotted lines show the mean and one standard deviation, respectively. The dashed line shows the best fit relation.

Table 4.2. Virgo and Fornax Nucleus Luminosity Function Best-Fit Values

Data Set	$\bar{m}_n^0$	σ_n
Fornax, g	-11.81 ± 0.32	1.78 ± 0.23
Virgo, g	-11.40 ± 0.26	2.08 ± 0.19
Fornax, z	-12.86 ± 0.35	1.93 ± 0.25
Virgo, z	-12.61 ± 0.30	2.35 ± 0.21

reproduce this trend, although possibly with more scatter. Since the Fornax sample is missing faint galaxies (and thus faint nuclei) relative to Virgo, it is not surprising that the mean nucleus luminosity of Fornax would be slightly brighter.

In Figure 15 of C06 and Figure 3.7 of this work, the nucleus luminosity function is compared to that of the GCs. The mean of the Virgo nucleus luminosity function was found to be ~ 3.6 times brighter than that of the GCs, while the analogous value for Fornax was found to be ~ 4.3. This difference may be due to the King profiles used in the C06 fits, which caused the nuclei magnitudes to be fainter and closer to those of the GCs. The important point to note is that in both samples, we expect the nuclei to be significantly ($\sim$ 25–50) times brighter than an average globular cluster.

4.1.4 Nucleus Sizes

We plot a histogram of nucleus sizes in Figure 4.4 for both our Virgo and Fornax samples. Although there is a large range in size (the very large Virgo nucleus belonging to VCC 1178), most nuclei appear to have radii < 10 pc. The typical sizes of both samples are in good agreement, with median values of 5.6 pc and 5.8 pc in the g-band, and 7.2 pc and 7.1 pc in the z-band, for Virgo and Fornax respectively.

4.1.5 Other Properties

In addition to the above shared characteristics, we find agreement in all other measured parameters. Both studies find that the programme galaxies exhibit a trend along the luminosity function where their central surface brightness profiles gradually change from having a luminosity "deficit" to an "excess" (see Figures 3 and 4 in C06, Figure 1 of Côté et al. (2007), Figures 2.1 and 2.2 here, as well as a discussion of

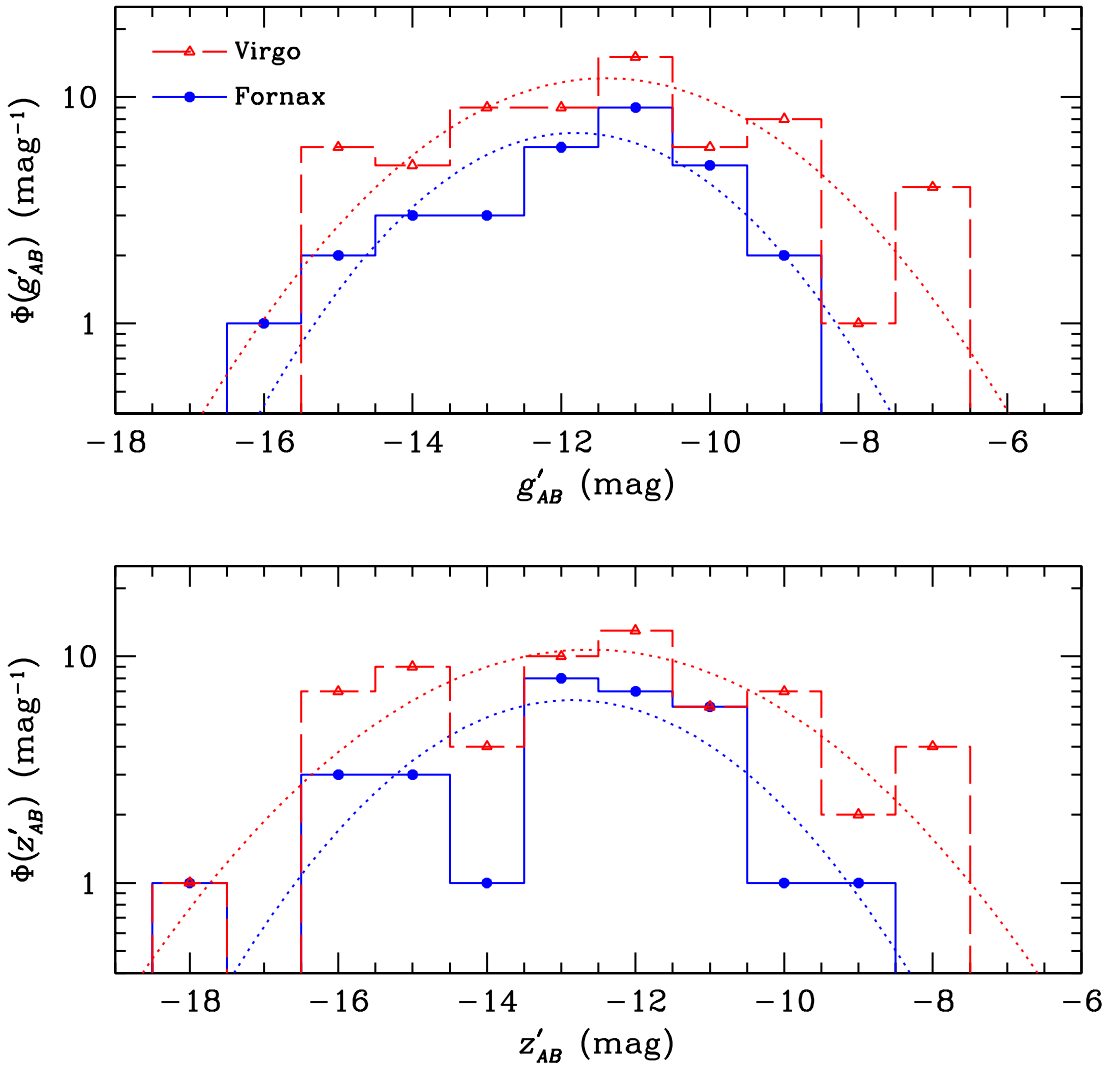

Figure 4.3 Same as Figure 3.7, but using absolute magnitudes and including 63 ACSVCS and 31 ACSFCS nuclei. The luminosity functions for both the Virgo (red open triangles) and Fornax (blue filled circles) nuclei are shown, in the g-band (*top*) and z-band (*bottom*). Both data sets are fit with a normalized Gaussian.

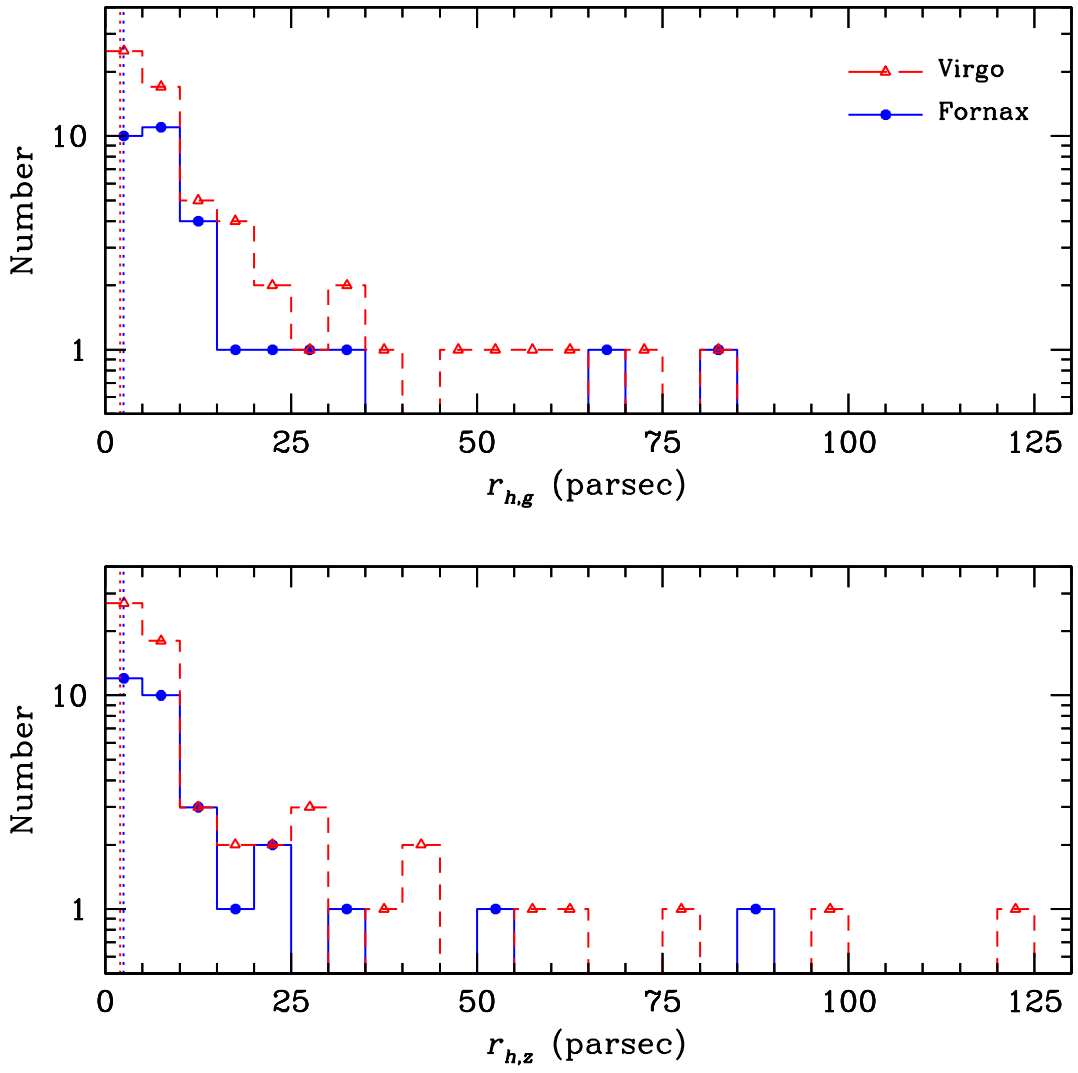

Figure 4.4 Same as Figure 3.9, but using parsecs and including 63 ACSVCS and 31 ACSFCS nuclei. The distribution of half-light radii for both Virgo (red open triangles) and Fornax (blue filled circles) nuclei are shown. The red and blue vertical dotted lines indicate the adopted resolution limit of $\sim 0\farcs025$, which corresponds to 2.0 pc in the ACSVCS and 2.4 pc in the ACSFCS.

this trend in Paper IV). Plotting surface brightness against magnitude, the nuclei are found to have different scaling relations than the GCs (see Figure 18 in C06 and Figure 3.10 here). The best-fit line parameters outlining the integrated colour-magnitude relation for the nuclei with $B_T \leq 13.5$, given by Eq. 13 in C06 and Eq. 3.7 in this work, are consistent to within errors. However, even better agreement is achieved when using our aperture determined colour-magnitude relation (Eq. 3.8), which may be a more appropriate comparison to the King profiles used in the C06 fits. Finally, no major differences are found in the distribution of nucleus ages and metallicities (Figure 24 and Table 6 in C06, Figure 3.15 and Table 3.3 here).

Overall, we find a striking similarity between the nuclei of Virgo and Fornax, despite the strong environmental differences between the two clusters. The results of this study therefore indicate that characteristics of the galaxy clusters (such as density) or processes that depend on them (such as ram pressure stripping efficiency) may not play a major role in the formation and evolution of nuclei that reside in early-type galaxies, and we can consider the nucleus properties derived here as being fairly generic of early-type galaxies.

4.2 Spectroscopic Studies

Studies of nucleus stellar populations can offer insight into their formation mechanisms, by determining their ages and metallicities. However, to our knowledge, the only spectroscopic studies of early-type galaxy nuclei are by Paudel & Lisker (2009) (7 Virgo members) and Paudel et al. (2011) (26 Virgo members). There are also a handful of papers which have spectroscopically examined the radial gradients and the light of central versus outer regions in early-type galaxies; however, these studies must be interpreted with caution in respect to the nucleus characteristics, as the nucleus and underlying galaxy light have not been separated, and not all objects in their samples necessarily contain a nucleus.

In general, the central regions of early-type dwarfs (Chilingarian, 2009; Koleva et al., 2009; Spolaor et al., 2010; Koleva et al., 2011), as well their nuclei (Paudel & Lisker, 2009; Paudel et al., 2011), were found to be younger and more metal rich than the outer regions or host. Specifically, Chilingarian (2009) found that central regions could be up to 7 Gyr younger than outer regions, while Paudel et al. (2011) observed that nuclei were younger than their hosts by a median age difference of 3.5 Gyr, and with differences of up to > 10 Gyr. They also reported a median increase of nucleus

to host [Z/H] by 0.07 dex, with metallicities ranging from -1.22 to 0.18 dex.

In addition, Paudel et al. (2011) examined age and metallicity trends with galaxy host magnitude. They found that nuclei in bright hosts were young and metal rich, with ages that increased and metallicities that decreased as their hosts became less luminous. However, the parameters of nuclei in faint hosts were found to have a significant amount of scatter, with nuclei in these galaxies spanning the full range of metallicities and ages. The hosts themselves were not found to follow any obvious relation with age, although they were observed to have increasing metallicity with luminosity. The authors noted an apparent division at $M_B \sim -17$ mag, where some nuclei in galaxies fainter than this magnitude were found to be older and more metal poor than their hosts. Other studies have also found metallicity gradients with central depressions (Koleva et al., 2009, 2011).

The metallicity in central regions of early-type galaxies was found to exhibit trends with galaxy magnitude and velocity dispersion (Spolaor et al., 2010; Koleva et al., 2011) that agree with the results of Paudel et al. (2011). These results could imply that both hosts and their nuclei follow the known luminosity-metallicity relation (Poggianti et al., 2001) and mass-metallicity relation (e.g. Henry & Worthey, 1999).

The luminosity-metallicity trends from these studies are consistent with our Figure 3.14, where we observe that both nuclei and galaxies become increasingly red when moving up the luminosity function, and that nuclei in the brightest galaxies are more red than their hosts. Paudel et al. (2011) and Spolaor et al. (2010) both find that the increase in central or nucleus metallicity with host luminosity or mass is steeper than that of the outer regions, which may be what is reflected in our observed colours. Of course, interpretation of the galaxy and nucleus colours is not straightforward, due to the degeneracy of colours with metallicity and age. Because colours are also indicative of ages, we would expect nucleus colours to become more red going down the luminosity function, since the study of Paudel et al. (2011) found older nuclei reside only in faint hosts. We speculate that this disagreement could be reconciled if the colours of the nuclei reflect their metallicities more than their age, but we have no reason to believe that this is necessarily the case. Therefore, although we are limited in our ability to draw conclusions from our nucleus and galaxy colours alone, we simply note that the observed colours imply the possibility of an age and/or metallicity relation with host magnitude.

4.3 Formation and Evolution Models

The formation and evolution of central galactic nuclei remains an open theoretical problem. There are two main avenues of nucleus creation that are currently considered viable mechanisms. The first suggests that a galaxy's star clusters will experience orbital decay due to dynamical friction and spiral inwards, eventually coalescing in the centre of the galaxy. An alternative formation mode may be due to gas accretion into the centre, followed by star formation. Additionally, shared scaling relations between nuclei and black holes have prompted models that consider the development of both objects in a shared context. In this section, we discuss theoretical works on the two main formation scenarios, as well as models that connect nuclei and black holes.

4.3.1 Dissipationless Infall of Star Clusters

Tremaine et al. (1975) first suggested that the nucleus of M31 was formed from GCs spiralling to the centre of the galaxy via dynamical friction from background stars. However, not all clusters that reach the centre of the galaxy may contribute to nucleus formation – Capuzzo-Dolcetta (1993) showed that the dynamical friction and tidal stripping are competitive processes, where clusters are more readily destroyed by larger nuclei, thus limiting nucleus growth.

Evidence for this formation scenario was described in Capuzzo-Dolcetta & Tesseri (1999), who pointed out that the radial distribution of GCs in galaxies is less concentrated to the centre than the halo stars, and that the "missing" clusters may have contributed to nucleus formation. Monte Carlo simulations based on this premise by Lotz et al. (2001) predicted nucleus luminosities which were consistent with observations for bright galaxies, although they were overestimated for less luminous ones. They noted that this result could be attributed to dynamical friction timescales being much shorter in low-mass galaxies, thus nuclei are able to form more efficiently, in spite of the fact that these galaxies have relatively few star clusters.

Numerical simulations by Oh & Lin (2000) and similar, higher resolution N-body simulations by Capuzzo-Dolcetta & Miocchi (2008a,b) were able to successfully reproduce observed surface brightness profiles of known nucleated galaxies. A dependence on local tidal field was found in the Oh & Lin (2000) model, where disruptive tidal forces on the outskirts of galaxy clusters would alter the globular cluster orbits, increasing dynamical friction timescales and decreasing nucleation frequency.

The Capuzzo-Dolcetta & Miocchi (2008a,b) models determined that if linear scaling is assumed, observed nuclei could be formed from the infall of tens to hundreds of GCs. Both simulations found that nuclei may begin to coalesce away from the galaxy photocentre, although to quite different extents: i.e., up to ~ 0.3 kpc and settling within ~ 1 Gyr in Oh & Lin (2000), and ~ 4 pc away in Capuzzo-Dolcetta & Miocchi (2008a,b).

Other simulations by Bekki et al. (2004) noted that the scaling relations of nuclei formed through mergers of GCs would be notably different than those of the GCs. More recent work by Bekki (2010) investigated simulations of star cluster infall due to dynamical friction in disk galaxies. He found that the effectiveness of dynamical friction did not depend strongly on bulge mass, but increased with smaller disk mass, and with larger disk mass fraction, galaxy surface brightness, and star cluster mass. The ratio of nucleus mass to disk mass was found to decrease as a function of increasing disk mass, with a mass ratio of $\gtrsim 0.4\%$ for smaller disks, and $\lesssim 0.1\%$ for disks with masses $M \gtrsim 10^9 M_\odot$.

A general characteristic found in the above models is that dissipationless cluster infall is more effective in smaller galaxies, due to shorter dynamical friction timescales. In addition, Capuzzo-Dolcetta (1993) noted that infalling clusters could be destroyed by larger nuclei. These ideas suggest that this method may be an important avenue for nucleus formation in lower-mass galaxies, a result would at first seem at odds with our finding of constant nucleus-to-galaxy luminosity ratio (which implies that the nucleus-to-galaxy mass ratio should also be approximately constant).

Observational evidence for dissipationless formation is exhibited in Paudel et al. (2011), who found that nuclei in the faint galaxies were older and more metal poor than their hosts, which is certainly suggestive of a relation to GCs. Some cluster infall models find that the nucleus remnant could be initially offset from the galaxy centre, possibly for extended periods (Oh & Lin, 2000), which is consistent with our observation that nuclei in fainter galaxies are more offset from their hosts. In fact, FCC 288, which we found to have one of the most offset nuclei, was observed to be more metal poor and possibly older (although within the errors) in the central $1''$ than in outer regions (Koleva et al., 2009). (To our knowledge, there have been no studies of the metallicity and age parameters for our other offset nuclei (FCC 119 and FCC 324)). However, formation of observed young and metal rich nuclei in low-mass galaxies (Paudel et al., 2011) through star cluster infall cannot be ruled out, since our observations and many others have shown that some low-mass galaxies exhibit

ongoing star cluster formation throughout the galaxy potential (e.g., Anders et al., 2004; Kyeong et al., 2010).

4.3.2 Dissipational Infall of Gas

The notion that nuclei might form through central gas accretion was first proposed by van den Bergh (1986), based on the observation that nucleated spheroidals tend to be rounder than non-nucleated ones. The author noted that it is easier for gas to collect in the central regions of round slow-rotators, and thus the prevalence of nuclei in round galaxies could be explained if the nuclei originated from infalling gas.

A number of models suggest that the gas could originate from the local environment outside the galaxy. Davies & Phillipps (1988) proposed that dwarfs may be formed from fading stellar populations in dwarf irregulars, where accretion from infalling primordial HI gas induced starbursts, the final one occurring in the centre and forming the nucleus. Silk et al. (1987) predicted that the inter-galactic medium (IGM) could fall into dwarf galaxies when it is cooled and compressed during group formation. This model notes that dwarfs closer to large galaxies may not be able to form nuclei as efficiently, since the large galaxy's tidal field makes it difficult for the dwarf to capture the gas. Babul & Rees (1992) found the opposite trend with environment for nucleus formation. They noted that nucleus evolution may depend on local IGM density, because this determines whether supernova-driven gas outflows are able to escape. Dwarfs in low pressure regions would have their gas ejected and fade away, while those in dense environments have their winds restricted to the starburst region by the IGM. This confinement could cause gas to cool and re-collapse, creating two short or one prolonged starburst. One prediction of this model is that there not be a colour gradient between the nucleus and its stellar envelope, since these components formed simultaneously.

Gas could also be funnelled to the centres of galaxies which have disks and axisymmetric features Milosavljević (2004) suggested that in spiral galaxies, magneto-rotational instability in the disk transports gas to the centre. Bekki et al. (2006) and Bekki (2007) performed chemodynamic simulations of the inner 1 kpc of dwarf galaxies, to explore the remnant created through dissipative merging of stellar and gaseous clumps formed from nuclear gaseous spiral arms in a gas disk. The simulations produced nuclei which were rotating and flattened, consisting of stars with varying ages and metallicities. Although the initial clump was found to form off-centre (about

200 pc by visual inspection of the simulation data), it would fall into the centre within 100 Myr. They found that overall, the nuclei were characteristically younger and more metal rich than the host, with more massive hosts creating more metal-rich nuclei. Dynamical friction timescales increased with decreasing dwarf mass (due to feedback being more effective in smaller galaxies), so low mass dwarfs were found to have younger and bluer nuclei. More massive and dense nuclei were formed in more massive dwarfs with deeper central potentials, and both the mass and mass fraction of the nucleus were found to increase with spheroid mass. Nuclei in high surface brightness galaxies should also have higher surface brightness, owing to the increased dynamical friction due to higher stellar densities. The nucleus surface brightness was strongly dependent on the gas fraction of the host, and thus may be more likely to form in this manner in high gas-fraction late-type galaxies. Finally, the addition of a central black hole to the simulation had little effect on the properties of the remnant nucleus.

Galaxy mergers can also induce the dissipative infall of gas to the galaxy centre. Mihos & Hernquist (1994) perform N-body simulations of disk galaxy mergers, where they found that gas dissipation and the star formation that followed created dense stellar cores in the remnant. Similar higher resolution simulations by Hopkins et al. (2008, 2009), showed that gravitational torques during gas-rich mergers removed the angular momentum of the gas, which would then undergo gravitational collapse. The amount of gas infall was found to largely depend on the progenitor galaxy gas fraction. These results of these simulations were found to not significantly change with the presence of a central black hole. However, these models did not have high enough resolution to study individual nuclei.

The simulations of Bekki et al. (2006) and Bekki (2007) are in good agreement with observations. In particular, their simulated nuclei were found to be younger and more metal rich than their hosts, with nucleus metallicity increasing with host mass, a trend that was seen in Paudel et al. (2011). Their finding that low mass dwarfs have younger and bluer nuclei is consistent with some of the nuclei from Paudel et al. (2011), as well as with the nucleus colours observed in our study.

They also found that the mass fraction of the nucleus increased with host spheroid mass, and that their modelled surface brightness profiles showed nuclei which become more prominent with increasing dwarf mass, where in low-mass dwarfs the nuclei were barely distinguishable. It is therefore possible that nucleus formation through gas infall may be most significant for intermediate mass galaxies. This is supported

by the increased likelihood of mergers for more massive galaxies, and the fact that such mergers cause central gas inflows. In addition, such a result can be reconciled with our observed constant nucleus-to-galaxy luminosity ratio (as a potential tracer of nucleus-to-galaxy mass ratio) if dissipationless cluster infall can account for nucleus build up in lower-mass galaxies.

One difficulty with the gas inflow model is that it obviously requires the presence of gas and stellar features, which are not consistent with the classical picture of elliptical galaxies. However, intermediate- and low-mass ellipticals are now recognized to be quite complex, having been found to contain spiral arms, embedded disks, and bars (Jerjen et al., 2000; Barazza et al., 2002; De Rijcke et al., 2003a; Lisker et al., 2006b; Ferrarese et al., 2006b), as well as counter rotating and kinematically decoupled cores (De Rijcke et al., 2004; Thomas et al., 2006), and ongoing star formation (e.g., De Rijcke et al., 2003b; Lisker et al., 2006a; Côté et al., 2006; Michielsen et al., 2007).

It is also possible that the nuclei formed in late-type progenitors. A recent finding by Emsellem & van de Ven (2008) noted that galaxies with deprojected Sérsic indices of $n \lesssim 3.5$ have compressive tidal forces in their central regions, with the size of the compressive region increasing with decreasing Sérsic index. Assuming a constant Sérsic index of 1, the amplitude of the tidal forces is found to scale linearly with galaxy mass, and form a central massive object (CMO) with a constant host mass fraction of $\sim 0.5\%$. A CMO growing through gas accretion in this way will eventually reach a critical density and luminosity, altering the galaxy profile such that it no longer has central compressive forces. Comparison of this theoretical threshold nucleus luminosity C06 nuclei reveals that many observed nuclei are much more luminous than would be predicted by this model. This suggests that the nuclei in early-type galaxies formed in low Sérsic index gas-rich progenitors, which have since morphologically evolved.

4.3.3 Connection with Black Hole Formation

Early-type nucleus masses have recently been found to have a linear relation with their host galaxy mass, which extends down from an analogous black hole to host mass relation (Côté et al., 2006; Ferrarese et al., 2006a; Wehner & Harris, 2006). Further studies of spiral galaxies found that CMOs correlate linearly with host bulge luminosity (Rossa et al., 2006). Balcells et al. (2007) found a CMO to bulge mass relation for spirals, however, they determined that nuclei and black holes had varying

slope, and suggested that their estimated masses might be lower then previous studies because they used bulge-disk decomposition before determining the virial mass of disk galaxies. Combining both ellipticals and disk galaxies, (Graham & Driver, 2007) found a log-quadratic relation between CMOs and host bulge Sérsic index.

These relations have lead to two main avenues of nucleus formation related to black holes: either black holes and nuclei form via the same mechanisms and share scaling relations, or nuclei form first and become seeds for black hole formation. The former model was suggested by Wehner & Harris (2006), who noted that the rapidity of gas infall rate to the centre of a galaxy, governed by the depth of the galaxy's potential well, could determine the fate of the central object. In massive bulges, gas falls in very rapidly, fuelling the fast growth of a black hole. In smaller bulges, gas falls in more slowly, and could create stars which would stop further dissipation and gas infall, regulating the nucleus size.

A shared formation mechanism for both nuclei and black holes was explored in the 3D smoothed particle hydrodynamic simulations of isolated and merging galaxies were performed by Li et al. (2007). They assumed that the CMOs formed dynamically in bulgeless disk galaxies through gravitational collapse of gas to the centre. They did not set an *a priori* M-σ relation, and were still able to reproduce a correlation between CMO and host mass in both isolated disk galaxies and ellipticals formed through mergers, the latter of which was found to be in agreement with the observations of Ferrarese et al. (2006a). In lower-mass galaxies, the central gas clump could fragment and result in a star cluster, while black holes in the high-mass galaxies could be formed from cluster collisions during mergers, or directly if the gas clump undergoes rapid core collapse due to the deep potential.

Ferrarese et al. (2006a) noted that nuclei could, in principle, form in all galaxies, but in massive galaxies they might either collapse or be destroyed (or altered) by the presence of binary black holes. Devecchi & Volonteri (2009); Devecchi et al. (2010) find that nuclei could form at high redshifts, as possible black hole seeds. Early protogalactic disks accrete mass from the halo and become gravitationally unstable, which causes gas to be funnelled to the centre from angular momentum redistribution, forming a star cluster. If the collapse time of the cluster is $\lesssim 3$ Myr (before the first supernova explosion), a very massive star can build up in the centre of the cluster, which eventually collapses to a black hole seed.

Evidence for such a scenario is supported by recent observations that have found nuclei and black holes to co-exist in some intermediate mass galaxies (González Del-

gado et al., 2008). AGN signatures have been observed in nucleated galaxies of all Hubble types, with host masses 10^8 – 10^{11} $M_\odot$ (Graham & Spitler, 2009) and host magnitudes as faint as $M_B \sim -16$ (Seth et al., 2008). Graham & Spitler (2009) found that the ratio of black hole to total CMO mass increased with host spheroid mass, as black holes begin dominating the CMO mass in larger galaxies. However, they determined that the CMO-to-galaxy mass ratio increased from 0.1% in large ellipticals with supermassive black holes to several % in low stellar mass spheroids (10^8 $M_\odot$), where the CMO is dominated by a nucleus.

If both nuclei and black holes form simultaneously, then it is possible that momentum feedback determines which object will eventually dominate the CMO mass. McLaughlin et al. (2006) noted that the same momentum flux that drives out gas from black holes (King, 2003, 2005) could also regulate the growth of nuclear star clusters. Nayakshin et al. (2009) use this result to explain why nuclei instead of black holes are likely to form in less massive hosts. Both objects can form simultaneously as gas is driven to the centre of a galaxy through an event such as a merger, but it is the mass of the host bulge that sets the individual formation rates. The growth of a black hole is limited by the Salpeter time, which determines the Eddington accretion rate; while star formation dictates nucleus growth, and is set by the free-fall or dynamical time. A small bulge with short dynamical times would quickly regain dynamical equilibrium after a merger, making it efficient for gas to cool in the centre and form a nucleus. In contrast, large bulges have Saltpeter times much shorter than dynamical times, and a black hole will be able to grow much more quickly than a nucleus. If both objects experience self-regulation from momentum flux, then the CMO will have a maximum mass, and the dominating object will be the one that reaches this mass first.

The co-existence of nuclei and black holes in intermediate mass galaxies may also have implications for the evolution of central regions in mergers. Bekki & Graham (2010) simulated a merger of two nuclei containing black holes, and found the dynamical heating of the cluster from the black hole binary expelled stars from the centre, with the final stellar density of the remnant decreased with increasing black hole mass fraction. This type of merger could produce observed "core" galaxies with larger black holes, and create the region of intermediate luminosity galaxies in which a nuclear cluster is difficult to distinguish observationally. Their simulation found that if only one nucleus had a black hole, the decrease in stellar density of the nucleus was less pronounced, as most of the heating comes from the black hole binary. In

mergers where neither nucleus had a black hole, the stellar density of the nucleus increased.

If black holes become increasingly common in intermediate-luminosity galaxies, they could either hinder nucleus growth, or lower the density of the nucleus through mergers until it is destroyed by black hole binary feedback. These effects could create the trends in intermediate-mass galaxy surface brightness profiles observed in this study, where the galaxies transition from having central light excess to deficit as they become more luminous.

Chapter 5

Conclusion

This HST study examined 43 early-type galaxies in the Fornax cluster, imaged in the ACS F475W and F850LP bands. Our analysis — performed in both one- and two-dimensions — extracted photometric and structural parameters for 31 compact central nuclei in these early-type galaxies. The main results are summarized as follows:

1. We have compared our results to those obtained by using 2D surface brightness profile fitting techniques, and found the extracted nucleus structural parameters to be in agreement for both methods. Although 2D fitting potentially allows for full structural decomposition of a galaxy, 1D methods enable characterization the outer regions with a single surface brightness profile. We conclude that 1D fits are more appropriate for our study, since they allow us to easily compare nucleus and galaxy parameters in a homogeneous way.

2. We find that 72% of the galaxies in our sample are nucleated, which is a significant increase from ground-based studies. The nuclei are observed to reside in galaxies with $M_B \gtrsim -19.5$, and the frequency of nucleation for galaxies fainter than this magnitude is 89%. As was found previously in the Virgo cluster, nuclei are exceedingly common among faint, early-type galaxies in the Fornax cluster.

3. Although most nuclei are not significantly offset from their host photocentre (only three are offset by $> 0.5''$), we find that the magnitude of the offset increases slightly with decreasing galaxy luminosity. This implies different timescales and/or pathways of nucleus formation for fainter galaxies.

4. We find a constant nucleus-to-galaxy luminosity ratio of ≈0.4%. The observed nucleus luminosity function can be understood therefore in terms of the galaxy selection function (and the fact that galaxies brighter than $M_B = -19.5$ do not contain nuclei). If we parameterize the nucleus luminosity function as a normalized Gaussian, we find peaks at $\langle M_g \rangle = -11.8 \pm 0.3$ and $\langle M_z \rangle = -12.9 \pm 0.4$ mag, which is ~ 50 times more luminous than the peak of the GC luminosity function. The nuclei are also found to have larger sizes and different half-light surface brightness scaling relations than the GCs.

5. The colours of the nuclei in hosts with $B_T < 13.5$ were found to correlate with galaxy colours, as well as with galaxy and nucleus luminosities. In particular, both the galaxies and the nuclei were observed to become increasingly red with increasing galaxy luminosity, with the trend being steeper for the nuclei. This leads to a relation between nucleus-and-host colour difference and host magnitude, where nuclei that are more red than their hosts are found predominantly in brighter galaxies, and vice versa. However, on average most of the nuclei are bluer than their hosts by 0.17 ± 0.26 mag.

6. A comparison to C06, which examined the nuclei of early-type galaxies in Virgo, yields many similarities. Both studies find similar frequencies of nucleation, surface brightness selection effects, nucleus-to-galaxy luminosity ratios, and nucleus luminosity functions, sizes, and colour-magnitude relations. The trend along the luminosity function where the galaxy central surface brightness profiles gradually change from having a luminosity "deficit" to an "excess" is shared by both samples, which suggests that generic formation and evolution processes largely independent of the galaxy environment are involved in shaping the central regions of galaxies. Rather, nucleus creation may be more contingent on local factors, particularly host galaxy mass, as is suggested by the constant nucleus-to-galaxy luminosity ratio (which implies that nucleus mass increases with that of its host) found in both galaxy clusters environments.

Although differing formation processes for the nuclei have been proposed, it is possible that more than one of them may be at work, with the importance of each process varying along the luminosity function. In fainter low-mass galaxies, it may be that the dominant mechanism for nucleus growth is through the infall of star clusters via dynamical friction, while gas accretion may be more important as galaxies

become more massive. Since simulations have found that star cluster infall is more effective in low-mass galaxies, while central gas collection produces more massive nuclei with increasing galaxy mass, a combination of both processes could explain the observed constant nucleus-to-galaxy luminosity ratio. The presence of black holes in intermediate-luminosity galaxies might then quench nucleus formation through competitive feedback, or destroy nuclei after a black hole binary forms in mergers, creating galaxies with depleted cores at the bright end of the luminosity function, and giving rise to the observed transition of surface brightness profiles from having a central light deficit to excess. Simulations that simultaneously take into account multiple formation mechanisms, such as star cluster infall in addition to gas accretion, may shed some light on what the dominant processes are at various scales.

Both dissipationless cluster infall and gas accretion models make predictions that nucleus formation would depend on local density (Oh & Lin, 2000; Babul & Rees, 1992). Although the fact that we do not find any major differences between the nuclei of Virgo and Fornax suggests that local density may not be a dominant factor in their formation, observations that examine the entire volume of a galaxy cluster (and that have the sensitivity necessary to detect the nuclei) may help determine the role density plays in shaping the nuclei and their hosts. In addition, acquiring complementary spectroscopic data for the nuclei would greatly aid in detangling the age-metallicity degeneracy, and help uncover the origin of the colour-luminosity relations observed in this study.

Bibliography

Anders, P., de Grijs, R., Fritze-v. Alvensleben, U., & Bissantz, N. 2004, Monthly Notices of the RAS, 347, 17

Anderson, J. & King, I. R. 2006, PSFs, Photometry, and Astronomy for the ACS/WFC, Tech. rep.

Babul, A. & Rees, M. J. 1992, Monthly Notices of the RAS, 255, 346

Balcells, M., Graham, A. W., & Peletier, R. F. 2007, Astrophysical Journal, 665, 1084

Bandara, K., Crampton, D., & Simard, L. 2009, Astrophysical Journal, 704, 1135

Barazza, F. D., Binggeli, B., & Jerjen, H. 2002, Astronomy and Astrophysics, 391, 823

Barth, A. J., Ho, L. C., Rutledge, R. E., & Sargent, W. L. W. 2004, Astrophysical Journal, 607, 90

Bekki, K. 2007, PASA, 24, 77

— 2010, Monthly Notices of the RAS, 401, 2753

Bekki, K., Couch, W. J., Drinkwater, M. J., & Shioya, Y. 2004, Astrophysical Journal, Letters to the Editor, 610, L13

Bekki, K., Couch, W. J., & Shioya, Y. 2006, Astrophysical Journal, Letters to the Editor, 642, L133

Bekki, K. & Graham, A. W. 2010, Astrophysical Journal, Letters to the Editor, 714, L313

Bell, E. F., McIntosh, D. H., Katz, N., & Weinberg, M. D. 2003, Astrophysical Journal, Supplement Series, 149, 289

Bender, R. & Moellenhoff, C. 1987, Astronomy and Astrophysics, 177, 71

Bica, E., Alloin, D., & Schmidt, A. A. 1990, Astronomy and Astrophysics, 228, 23

Binggeli, B., Tammann, G. A., & Sandage, A. 1987, Astronomical Journal, 94, 251

Blakeslee, J. P. et al. 2009, Astrophysical Journal, 694, 556

Böker, T., Sarzi, M., McLaughlin, D. E., van der Marel, R. P., Rix, H., Ho, L. C., & Shields, J. C. 2004, Astronomical Journal, 127, 105

Bower, R. G., Benson, A. J., Malbon, R., Helly, J. C., Frenk, C. S., Baugh, C. M., Cole, S., & Lacey, C. G. 2006, Monthly Notices of the RAS, 370, 645

Bower, R. G., Lucey, J. R., & Ellis, R. S. 1992, Monthly Notices of the RAS, 254, 601

Bruzual, G. & Charlot, S. 2003, Monthly Notices of the RAS, 344, 1000

Byun, Y. et al. 1996, Astronomical Journal, 111, 1889

Capuzzo-Dolcetta, R. 1993, Astrophysical Journal, 415, 616

Capuzzo-Dolcetta, R. & Miocchi, P. 2008a, Astrophysical Journal, 681, 1136

— 2008b, Monthly Notices of the RAS, 388, L69

Capuzzo-Dolcetta, R. & Tesseri, A. 1999, Monthly Notices of the RAS, 308, 961

Carollo, C. M., Stiavelli, M., & Mack, J. 1998, Astronomical Journal, 116, 68

Chabrier, G. 2003, Publications of the ASP, 115, 763

Chen, C.-W., Côté, P., West, A. A., Peng, E. W., & Ferrarese, L. 2010, Astrophysical Journal, Supplement Series, 191, 1

Chilingarian, I. V. 2009, Monthly Notices of the RAS, 394, 1229

Ciotti, L. 1991, Astronomy and Astrophysics, 249, 99

Cole, S., Lacey, C. G., Baugh, C. M., & Frenk, C. S. 2000, Monthly Notices of the RAS, 319, 168

Combes, F., Debbasch, F., Friedli, D., & Pfenniger, D. 1990, Astronomy and Astrophysics, 233, 82

Côté, P. et al. 2007, Astrophysical Journal, 671, 1456

— 2006, Astrophysical Journal, Supplement Series, 165, 57

Davies, J. I. & Phillipps, S. 1988, Monthly Notices of the RAS, 233, 553

De Rijcke, S., Dejonghe, H., Zeilinger, W. W., & Hau, G. K. T. 2003a, Astronomy and Astrophysics, 400, 119

— 2004, Astronomy and Astrophysics, 426, 53

De Rijcke, S., Zeilinger, W. W., Dejonghe, H., & Hau, G. K. T. 2003b, Monthly Notices of the RAS, 339, 225

Devecchi, B. & Volonteri, M. 2009, Astrophysical Journal, 694, 302

Devecchi, B., Volonteri, M., Colpi, M., & Haardt, F. 2010, Monthly Notices of the RAS, 1399

Djorgovski, S. G., Volonteri, M., Springel, V., Bromm, V., & Meylan, G. 2008, ArXiv e-prints

Emsellem, E. & van de Ven, G. 2008, Astrophysical Journal, 674, 653

Fabian, A. C., Celotti, A., & Erlund, M. C. 2006, Monthly Notices of the RAS, 373, L16

Ferguson, H. C. 1989, Astronomical Journal, 98, 367

Ferrarese, L. et al. 2006a, Astrophysical Journal, Letters to the Editor, 644, L21

— 2006b, Astrophysical Journal, Supplement Series, 164, 334

Ferrarese, L. & Merritt, D. 2000, Astrophysical Journal, Letters to the Editor, 539, L9

Filippenko, A. V. & Ho, L. C. 2003, Astrophysical Journal, Letters to the Editor, 588, L13

Franx, M. 1993, Publications of the ASP, 105, 1058

Fukugita, M., Ichikawa, T., Gunn, J. E., Doi, M., Shimasaku, K., & Schneider, D. P. 1996, Astronomical Journal, 111, 1748

Gavazzi, G., Donati, A., Cucciati, O., Sabatini, S., Boselli, A., Davies, J., & Zibetti, S. 2005, Astronomy and Astrophysics, 430, 411

Gebhardt, K. et al. 2000, Astrophysical Journal, Letters to the Editor, 539, L13

Glass, L. et al. 2011, Astrophysical Journal, 726, 31

González Delgado, R. M., Pérez, E., Cid Fernandes, R., & Schmitt, H. 2008, Astronomical Journal, 135, 747

Graham, A. W. & Driver, S. P. 2007, Astrophysical Journal, 655, 77

Graham, A. W., Erwin, P., Caon, N., & Trujillo, I. 2001, Astrophysical Journal, Letters to the Editor, 563, L11

Graham, A. W., Erwin, P., Trujillo, I., & Asensio Ramos, A. 2003, Astronomical Journal, 125, 2951

Graham, A. W. & Guzmán, R. 2003, Astronomical Journal, 125, 2936

Graham, A. W. & Spitler, L. R. 2009, Monthly Notices of the RAS, 397, 2148

Grant, N. I., Kuipers, J. A., & Phillipps, S. 2005, Monthly Notices of the RAS, 363, 1019

Gültekin, K. et al. 2009, Astrophysical Journal, 698, 198

Häring, N. & Rix, H. 2004, Astrophysical Journal, Letters to the Editor, 604, L89

Henry, R. B. C. & Worthey, G. 1999, Publications of the ASP, 111, 919

Hopkins, P. F., Cox, T. J., Dutta, S. N., Hernquist, L., Kormendy, J., & Lauer, T. R. 2009, Astrophysical Journal, Supplement Series, 181, 135

Hopkins, P. F., Hernquist, L., Cox, T. J., Dutta, S. N., & Rothberg, B. 2008, Astrophysical Journal, 679, 156

Jedrzejewski, R. I. 1987, Monthly Notices of the RAS, 226, 747

Jerjen, H., Kalnajs, A., & Binggeli, B. 2000, Astronomy and Astrophysics, 358, 845

Jordán, A. et al. 2007, Astrophysical Journal, Supplement Series, 169, 213

— 2005, Astrophysical Journal, 634, 1002

Kauffmann, G. & Haehnelt, M. 2000, Monthly Notices of the RAS, 311, 576

King, A. 2003, Astrophysical Journal, Letters to the Editor, 596, L27

— 2005, Astrophysical Journal, Letters to the Editor, 635, L121

King, I. R. 1966, Astronomical Journal, 71, 64

Koleva, M., de Rijcke, S., Prugniel, P., Zeilinger, W. W., & Michielsen, D. 2009, Monthly Notices of the RAS, 396, 2133

Koleva, M., Prugniel, P., De Rijcke, S., & Zeilinger, W. W. 2011, ArXiv e-prints

Kormendy, J. & Richstone, D. 1995, Annual Review of Astronomy and Astrophysics, 33, 581

Krajnovic, D. et al. 2011, ArXiv e-prints

Kyeong, J., Sung, E.-C., Kim, S. C., & Chaboyer, B. 2010, Journal of Korean Astronomical Society, 43, 1

Li, Y., Haiman, Z., & Mac Low, M.-M. 2007, Astrophysical Journal, 663, 61

Lisker, T., Glatt, K., Westera, P., & Grebel, E. K. 2006a, Astronomical Journal, 132, 2432

Lisker, T., Grebel, E. K., & Binggeli, B. 2006b, Astronomical Journal, 132, 497

Lisker, T., Grebel, E. K., Binggeli, B., & Glatt, K. 2007, Astrophysical Journal, 660, 1186

Liu, C., Peng, E. W., Jordán, A., Ferrarese, L., Blakeslee, J. P., Côté, P., & Mei, S. 2011, Astrophysical Journal, 728, 116

Lotz, J. M., Miller, B. W., & Ferguson, H. C. 2004, Astrophysical Journal, 613, 262

Lotz, J. M., Telford, R., Ferguson, H. C., Miller, B. W., Stiavelli, M., & Mack, J. 2001, Astrophysical Journal, 552, 572

Magorrian, J. et al. 1998, Astronomical Journal, 115, 2285

Marconi, A. & Hunt, L. K. 2003, Astrophysical Journal, Letters to the Editor, 589, L21

Masters, K. L. et al. 2010, Astrophysical Journal, 715, 1419

Matthews, L. D. et al. 1999, Astronomical Journal, 118, 208

McLaughlin, D. E., King, A. R., & Nayakshin, S. 2006, Astrophysical Journal, Letters to the Editor, 650, L37

Mei, S. et al. 2007, Astrophysical Journal, 655, 144

— 2005, Astrophysical Journal, 625, 121

Michie, R. W. 1963, Monthly Notices of the RAS, 125, 127

Michielsen, D. et al. 2007, Astrophysical Journal, Letters to the Editor, 670, L101

Mieske, S. et al. 2010, Astrophysical Journal, 710, 1672

Mihos, J. C. & Hernquist, L. 1994, Astrophysical Journal, Letters to the Editor, 437, L47

Milosavljević, M. 2004, Astrophysical Journal, Letters to the Editor, 605, L13

Murray, N., Quataert, E., & Thompson, T. A. 2005, Astrophysical Journal, 618, 569

Nayakshin, S., Wilkinson, M. I., & King, A. 2009, Monthly Notices of the RAS, 398, L54

Nieto, J.-L., Bender, R., Poulain, P., & Surma, P. 1992, Astronomy and Astrophysics, 257, 97

Oh, K. S. & Lin, D. N. C. 2000, Astrophysical Journal, 543, 620

Paudel, S. & Lisker, T. 2009, Astronomische Nachrichten, 330, 969

Paudel, S., Lisker, T., & Kuntschner, H. 2011, Monthly Notices of the RAS, 413, 1764

Peng, C. Y., Ho, L. C., Impey, C. D., & Rix, H. 2002, Astronomical Journal, 124, 266

— 2010, Astronomical Journal, 139, 2097

Peng, E. W. et al. 2006, Astrophysical Journal, 639, 95

Poggianti, B. M. et al. 2001, Astrophysical Journal, 562, 689

Reines, A. E., Sivakoff, G. R., Johnson, K. E., & Brogan, C. L. 2011, Nature, 470, 66

Robertson, B., Hernquist, L., Cox, T. J., Di Matteo, T., Hopkins, P. F., Martini, P., & Springel, V. 2006, Astrophysical Journal, 641, 90

Rossa, J., van der Marel, R. P., Böker, T., Gerssen, J., Ho, L. C., Rix, H., Shields, J. C., & Walcher, C. 2006, Astronomical Journal, 132, 1074

Sandage, A. & Binggeli, B. 1984, Astronomical Journal, 89, 919

Sarzi, M., Rix, H.-W., Shields, J. C., Ho, L. C., Barth, A. J., Rudnick, G., Filippenko, A. V., & Sargent, W. L. W. 2005, Astrophysical Journal, 628, 169

Schlegel, D. J., Finkbeiner, D. P., & Davis, M. 1998, Astrophysical Journal, 500, 525

Scorza, C., Bender, R., Winkelmann, C., Capaccioli, M., & Macchetto, D. F. 1998, Astronomy and Astrophysics, Supplement Series, 131, 265

Searle, L. & Zinn, R. 1978, Astrophysical Journal, 225, 357

Sersic, J. L. 1968, Atlas de galaxias australes, ed. Sersic, J. L.

Seth, A., Agüeros, M., Lee, D., & Basu-Zych, A. 2008, Astrophysical Journal, 678, 116

Seth, A. C., Dalcanton, J. J., Hodge, P. W., & Debattista, V. P. 2006, Astronomical Journal, 132, 2539

Silk, J. & Rees, M. J. 1998, Astronomy and Astrophysics, 331, L1

Silk, J., Wyse, R. F. G., & Shields, G. A. 1987, Astrophysical Journal, Letters to the Editor, 322, L59

Sirianni, M. et al. 2005, Publications of the ASP, 117, 1049

Spolaor, M., Kobayashi, C., Forbes, D. A., Couch, W. J., & Hau, G. K. T. 2010, Monthly Notices of the RAS, 408, 272

Springel, V. et al. 2005, Nature, 435, 629

Thomas, D., Brimioulle, F., Bender, R., Hopp, U., Greggio, L., Maraston, C., & Saglia, R. P. 2006, Astronomy and Astrophysics, 445, L19

Thomas, D., Greggio, L., & Bender, R. 1999, Monthly Notices of the RAS, 302, 537

Trager, S. C., Faber, S. M., Worthey, G., & González, J. J. 2000, Astronomical Journal, 120, 165

Tremaine, S. D. 1976, Astrophysical Journal, 203, 345

Tremaine, S. D., Ostriker, J. P., & Spitzer, Jr., L. 1975, Astrophysical Journal, 196, 407

van den Bergh, S. 1986, Astronomical Journal, 91, 271

Villegas, D. et al. 2010, Astrophysical Journal, 717, 603

Wake, D. A. et al. 2006, Monthly Notices of the RAS, 372, 537

Walcher, C. J. et al. 2005, Astrophysical Journal, 618, 237

Wehner, E. H. & Harris, W. E. 2006, Astrophysical Journal, Letters to the Editor, 644, L17

White, S. D. M. & Frenk, C. S. 1991, Astrophysical Journal, 379, 52

White, S. D. M. & Rees, M. J. 1978, Monthly Notices of the RAS, 183, 341

York, D. G. et al. 2000, Astronomical Journal, 120, 1579